DOI: 10.31891/2079-1372

THE INTERNATIONAL SCIENTIFIC JOURNAL

PROBLEMS OF TRIBOLOGY

Volume 27 ***No 4/106-2022***

МІЖНАРОДНИЙ НАУКОВИЙ ЖУРНАЛ

ПРОБЛЕМИ ТРИБОЛОГІЇ

PROBLEMS OF TRIBOLOGY

INTERNATIONAL SCIENTIFIC JOURNAL

Published since 1996, four time a year

Volume 27 No 4/106-2022

Establishers:
Khmelnitskiy National University (Ukraine)
Lublin University of Technology (Poland)

Associated establisher:
Vytautas Magnus University (Lithuania)

Editorial board address:
International scientific journal "Problems of Tribology",
Khmelnitsky National University,
Institutskaia str. 11, Khmelnitsky, 29016, Ukraine
phone +380975546925

Indexed: CrossRef, DOAJ, Ulrichsweb, Google Scholar, Index Copernicus

E-mail: tribosenator@gmail.com

Internet: http://tribology.khnu.km.ua

ПРОБЛЕМИ ТРИБОЛОГІЇ

МІЖНАРОДНИЙ НАУКОВИЙ ЖУРНАЛ

Видається з 1996 р. ***Виходить 4 рази на рік***

Том 27 **№ 4/106-2022**

Співзасновники:
Хмельницький національний університет (Україна)
Університет Люблінська Політехніка (Польща)

Асоційований співзасновник:

Університет Вітовта Великого (Литва)

Адреса редакції:
Україна, 29016, м. Хмельницький, вул. Інститутська 11, к. 4-401
Хмельницький національний університет, редакція журналу "Проблеми трибології"
тел. +380975546925, **E-mail**: tribosenator@gmail.com

Internet: http://tribology.khnu.km.ua

Зареєстровано Міністерством юстиції України
Свідоцтво про держреєстрацію друкованого ЗМІ: Серія КВ № 1917 від 14.03. 1996 р.
(перереєстрація № 24271-14111ПР від 22.10.2019 року)

Входить до переліку наукових фахових видань України
(Наказ Міністерства освіти і науки України № 612/07.05.19. Категорія Б.)

Індексується в МНБ: CrossRef, DOAJ, Ulrichsweb, Google Scholar, Index Copernicus

Рекомендовано до друку рішенням вченої ради ХНУ, протокол № 6 від 29.11.2022 р.

Problems of Tribology, *V. 27, No 4/106-2022*

Problems of Tribology

Website: http://tribology.khnu.km.ua/index.php/ProbTrib
E-mail: tribosenator@gmail.com

CONTENTS

***Problems of Tribology**, V. 27, No 4/106-2022*

Problems of Tribology

Website: http://tribology.khnu.km.ua/index.php/ProbTrib

E-mail: tribosenator@gmail.com

ЗМІСТ

Problems of Tribology, *V. 27, No 4/106-2022,6-12*

Problems of Tribology
Website: http://tribology.khnu.km.ua/index.php/ProbTrib
E-mail: tribosenator@gmail.com

DOI: https://doi.org/10.31891/2079-1372-2022-106-4-6-12

Nanostructural glasscomposite self-lubricant coatings

N.M. Fialko [1], V.V. Shchepetov [2], S.D. Kharchenko [2], S.I. Kovtun [2], Ya.N. Hladkyi [3], S.S. Bys [3*]

[1] Institute of Technical Thermophysics of the National Academy of Sciences of Ukraine, Ukraine, Kyiv
[2] Institute of General Energy of the National Academy of Sciences of Ukraine, Ukraine, Kyiv
[3] Khmelnitsky National University, Ukraine, Khmelnitsky
**E-mail: serhiibys@gmail.com*

Received: 30 July 2022: Revised:31 August 2022: Accept:28 September 2022

Abstract

The results of the study of glass-composite nanostructured self-lubricating coatings are presented. The structural components of these coatings significantly affect the graphitization process and provide an antifriction surface layer of α-graphite. The formation of this layer makes it possible to significantly minimize the contact parameters in the friction region.

A significant effect of aluminoborosilicate in the form of a glass phase on the tribological properties of coatings is noted. An increase in adhesive strength is achieved by forming a surface layer of glassy sodium silicate. The presence of near-surface particles in the graphite layer does not affect the tribotechnical characteristics of the coatings. The developed glass-composite nanostructured self-lubricating coatings have high antifriction characteristics throughout the entire load-speed range.

Key words: nanostructured coatings, wear intensity, glass composite, glass phase, graphitization.

Introduction

Preservation of operational characteristics limited by friction and wear, both of individual units and technical systems as a whole, can be ensured by modern surface engineering tools that implement the basic principle of minimum costs with maximum results. Structural engineering methods that use modification through the use of solid lubricants have taken a leading position in recent years in providing anti-friction contact interfaces. Coatings containing solid lubricants are among the innovative and most promising antifriction materials, the high quality of which is especially noticeable in conditions where traditional liquid lubricants are ineffective [1, 2]. They are used in various fields of technology from lubrication of precision aircraft mechanisms to preventing jamming of threaded joints [3,4].

The development of antifriction nanostructured glass-composite self-lubricating coatings meets the modern priorities of tribotechnical materials science aimed at increasing the wear resistance of friction-loaded movable interfaces and, on their basis, the development of scientific and applied solutions in the interests of improving the efficiency of using high-quality production technologies [5,6].

Objective

Ensuring high quality antifriction properties of nanostructured glass-composite self-lubricating coatings with increased adhesive strength due to the presence of aluminoborosilicate and structurally free magnesium carbide in the composition of the glass phase, as well as the selection of structural components that promote graphitization.

Materials and methods of research

As is known from the comparative characteristics of gas-thermal coatings, which are similar in their structural-phase composition, detonation-gas coatings have maximum operational properties [7]. On this basis, for the deposition of the coatings under study, the detonation method was used using nanostructured powders obtained by the mechanochemical method, the composition of SiC-Ni-Cu-Al-Si-Cwith a uniform distribution of

the aluminoborosilicate glass phase (SiO_2-Al_2O_3-B_2O_3). According to the developed technology, structurally free magnesium nanocarbide (MgC_2) was added to the resulting nanoglass composition, after which it was mixed, ensuring its uniform distribution in the powder mixture ready for spraying. All powder materials used in the work are obtained from the mineral resource base of the country.

The antifriction properties of the coatings were evaluated during friction of the ring samples along the end scheme under conditions of distributed contact in the continuous sliding mode at a load of 10.0 MPa. The influence of the environment, speed, load, implemented during the tests, were selected taking into account the maximum approximation of the processes of physicochemical friction mechanics to the real conditions of contact interaction, in addition, the program for studying nanostructured glass-composite coatings provided for a comparative analysis of their antifriction characteristics with similar values obtained during tests of tungsten-containing coatings of the VK15 type and coatings sprayed with alloyed nichrome powder.

The study of contact interfaces, in which activation processes occur during friction, which determine the intensity of surface reactions and tribophysical phenomena, was carried out using modern methods of physical analysis, involving metallography (an optical microscope of the typeNeofot-32 with an attachment), an X-ray electronic microanalyzer of the Camscan 4 DW type with a program for the distribution of chemical elements. The determination of the phase composition of the surface layers was carried out on a general-purpose X-ray diffractometer of the DRON-3 type with monochromatic CuKα radiation.

Increasing the adhesive strength, as a criterion for the performance of glass composite coatings, was carried out by preliminary deposition on the working surface of a sublayer of glassy sodium silicate $Na_2O(SiO_2)_2$. The exclusion of unproductive losses and adherence to the measurement technology using the conical pin method determined the correctness of the obtained results of the adhesion strength, which amounted to 145-150 MPa[8].

Research results

The contact interaction of surfaces is a complex sequence of cooperative influence of both external factors and internal transformations, the qualitative agreement of which reflects the commonality of quantitative patterns and determines their ordered causal relationship. According to the results of interactions of coatings under friction loading, Fig. 1 shows experimental values representing the averaged functional dependences of the wear intensity and friction coefficients, which change with time and stabilize after running in, in the field of sliding velocities at a constant load of 10.0 MPa. As can be seen from the graph, in the entire range of tests with a monotonically increasing sliding speed, the minimum values of wear rates and the corresponding friction coefficients correspond to nanostructured glass-composite coatings (curves 1 and 1'). The structure of nanoglass composites, which determines their properties, practically consists of a finely dispersed mixture representing both solid solutions and, mainly, intermetallic compounds with a significant presence of a glass phase. The invariance of the chemical composition and the constancy of the parameters of technological deposition determine the stability of the coating structure, the relative density of which was up to 99%. The cross section of the nanocomposite coating is shown in Fig.2. Metallographic analysis has established that the deposited layer has a quasi-ordered lamella-like appearance, which closely adheres to the base material, completely copying the surface topography, while accumulations of component oxides, as well as slag contamination, are practically absent, and defects in the form of pores and cracks are not detected.

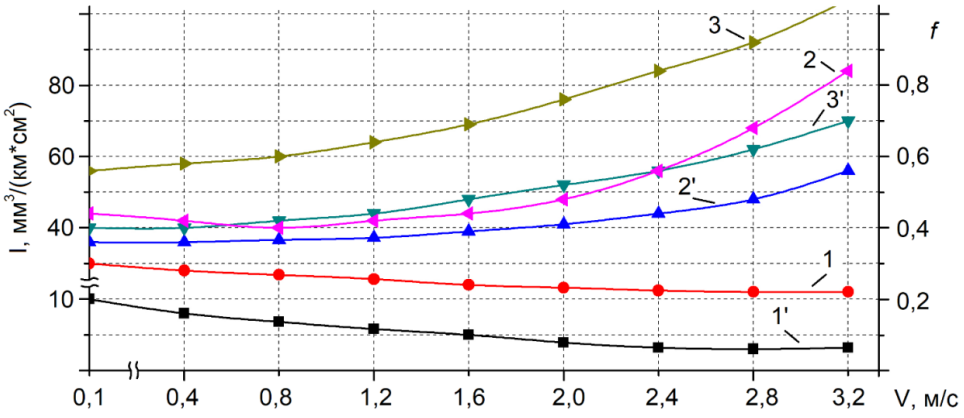

Fig.1. Dependence of wear intensity (1,2,3) and friction coefficient (1',2',3') on sliding speed of coatings SiC-Ni-Cu-Al-Si-C+glass phase+MgC2 (1,1'), WC-Co (2.2') and Ni-Cr-Al-B (3,3') on sliding speed (P=10.0 MPa).

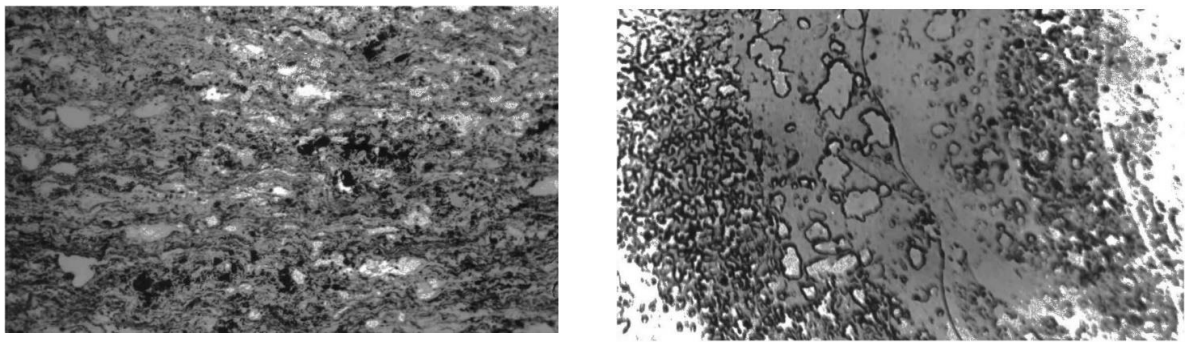

a) **b)**

Fig.2. Coating structure: a) x120; b) x5000

The synthesis and study of solid solutions based on refractory compounds, in particular silicon carbide, are being carried out quite intensively, but the capabilities of the latter and its complex of tribological properties are far from the expected results.

The developed glass composite is an antifriction material with an ultrafine structure. It is generally accepted that elastoplastic deformation is the main factor determining the development of the process of external friction, and in addition, in our opinion, the formation of a gradient structure is a derivative of it. It can be said that the evolution of the structure during contact interactions has pronounced scale levels, and the processes occurring at different scale levels are interdependent. The layer-by-layer picture of plastic deformation obtained by the diffraction method reveals the main regularities of the formation of a scale structure and makes it possible to establish uniform transitions from a dispersed polycrystalline fragmented structure on the surface through intermediate textured layers to the original crystalline, inherent in deep material. As can be seen from Fig. 3, in the coating under study, as it approaches the friction surface and the contact pressure increases, and the intensity of deformation, the structure is gradually replaced by an ultrafine one. In this case, high contact compressive and shear stresses create conditions for the implementation of significant plastic deformations in the near-surface layer of the coating material, which cause the formation of ultrafine structures.

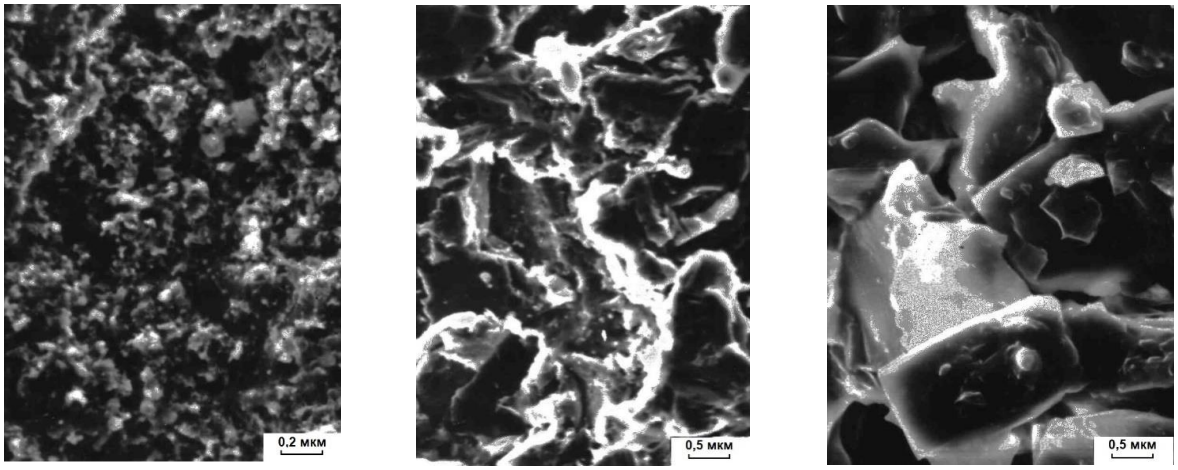

a) **b)** **c)**

Fig.3. Changes in the structure of the nanoglass-composite coating with increasing distance from the friction surface in a layer ~6 μm thick: a) near-surface zone; b) intermediate layer; c) undeformed structure.

This gives grounds to single out in a structure subjected to tribotechnical loads a near-surface zone, in which deformation processes that develop inhomogeneously in microvolumes form a specific layer at the near-surface level, in which structural-thermal activation causes a complex of physico-chemical interactions that determine the concomitant and leading type of wear. The surface zone is a structurally heterogeneous finely dispersed composition.

As evidenced by the results of X-ray microanalysis (MRSA) performed on the "Camebax SX", the basis of the nanoglass composition is silicon carbide of non-stoichiometric composition, along the grain boundaries of which silicate compounds are located, among which inclusions corresponding to the composition of silicon dioxide predominate, also in the carbide structure the role of dispersion-strengthened components is performed by Al_2O_3 oxides distributed along the boundariesand intermetallic inclusions in the form of spherical nanograins.However, the high thermomechanical properties of SiC carbide are discredited by significant brittleness.We noted that the substitutional solid solution that forms Al and SiC causes a slight distortion of the crystal lattice of the carbide, since the differences in the masses of Al atoms and Si are extremely small, as a

result of which the microhardness does not change, while plasticity increases. A similar effect on the composition of SiC, forming substitutional solid solutions by replacing Si atoms, is exerted by Cu and Ni. The formation of phases in the coating, as tests have shown, is determined not only by the ratio of components, temperature, dispersion, but also depends on their defectiveness and external conditions. Undoubtedly, as an axiom, tribochemical interaction takes place when the molecules receive the necessary activation energy. Endothermic reactions generally do not proceed without activation. The interaction of SiC with Mg, which is formed during the thermal decomposition of structurally free magnesium carbide under running-in conditions and depends on the process temperature, is accompanied by the formation of magnesium silicide and acetylenidemagnesium, the latter, under the influence of thermomechanical action, promotes the formation of graphite through the intermediate dimagnesium tricarbide ($2SiC + 5Mg \rightarrow 2Mg_2Si + MgC_2$, $MgC_2 \rightarrow Mg_2C_3 \rightarrow Mg + C$). It should be noted that, under thermodynamic action, the presence of a catalyst in the form of Al promotes the decomposition of magnesium carbide. The basis of physical phenomena that initiate the mechanism of decomposition of carbide graphite are structural transformations in the solid phase, caused by thermal effects. The factors that determine the qualitative level of thermomechanical carbide graphitization include both the degree of dispersion of structural components, specific pressure, operating temperature, and temperature in the contact zone, the presence of elements that initiate decomposition processes, as well as the influence of the environment (in vacuum, the probability of the amount of graphite increases), in addition, internal factors associated with the composition of the material, its structure, the presence of defects, etc. Figure 4 shows the topography of the friction surface obtained at sliding velocities equal to 0.8 m/s and 0.15 m/s. The antifriction layer of graphite, as can be seen, covers almost the working surface, providing an increase in the actual contact area, contributing to a decrease in the specific load due to an increase in the support length due to filling and leveling of microroughnesses and fixing graphite microparticles in microcavities. The contact zone constituting the near-surface layer (initial scale level) separating the coating material from the antifriction film consisting of polydisperse graphite particles is a deformed zone, which, according to the results of X-ray microanalysis performed on MAR-3 (probe diameter 1 μm), represents finely dispersed heterogeneous structural -phase compounds of the components that make up the coating. Among which, the presence of Ni, as a structural component, is due to its distinctive properties, so, on actual contact spots, when a temperature of about 450-500 ^{o} C is reached, depending on the dispersion and external influences in a local high-temperature field, Ni interacts with SiC, forming nickel silicides with a predominance of metal-enriched Ni_2Si. As a result, carbon is reduced, which is transformed in the form of a solid phase of elementary polydisperse graphite colonies combined into surface structures.

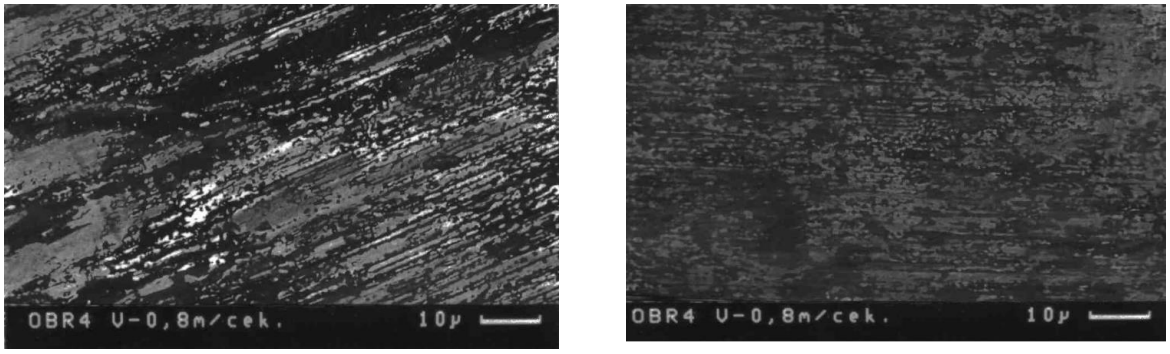

a) **b)**

Fig.4. Topography of the friction surface during the formation of a graphite film: a – V=0.8 m/s; b – V=1.5 m/s.

However, magnesium carbide remains the main component of the antifriction surface layer, consisting of a carbonaceous product - graphite. The value of the specific wear work characteristic of the initial running-in moment, as shown by calculations, is up to 10 kJ/mm^3, which is both a necessary and sufficient condition for initiating the thermal decomposition of MgC_2, which causes the formation of carbon in the form of a solid phase.

Using the natural ability of chemical elements to graphitize through the formation of carbide graphite, a high-quality, thickened anti-friction layer was obtained, which determines the operational properties of coatings.

In the structural-phase study of glass composite coatings, the presence of intermetallic compounds based on Al and Ni such as NiAl and Ni_2Al_3 was noted, while monoaluminide, being a high-temperature phase, has a significant hardness, as shown by measurements, most likely about 3.8 GPa. The presence of an ordered solid solution based on nickel monoaluminide with a reduced Al content (~20–25 wt %) was also found, which leads to increased ductility. According to the results of elemental and X-ray phase analyzes, the presence of a solid solution of Ni in Cu was noted, but their compounds were not found. Solid solutions of Ni in Si and Si in Ni, as well as their intermetallic compounds Ni_2Si, Ni_3Si_2, and $NiSi_2$, have been revealed. In addition, the presence of small amounts of colonies of solid solutions of Si in Cu was established, and the formation of their chemical compounds such as copper silicates is also likely, since the microhardness increases significantly. However, it was difficult to identify them accurately.

Powders of aluminoborosilicate glasses, the dispersion of which was 25–30 μm, in the process of mechanochemical treatment and thermomechanical action, being products of inorganic synthesis, caused, along with the preservation of the original components, the formation of new stable compounds, as was found, from

solid solutions of Al_2O_3 and SiO_2 obtained rhombic syngony, close to the structure of sillamanite, most likely it is the lowest mullite obtained by reaction as a result of the interaction of the oxidation products of the original components. From the point of view of glass-ceramic technologies, the greatest interest, in our opinion, is the presence of components that form refractory metal oxides, primarily Al and Si oxides. The presence of B_2O_3 was also established, which, as a result of partial oxidation, formed a solid solution of Al_2O_3 - B_2O_3.

From the point of view of condensed matter physics, the addition of a glassy component affects the quality of the coating material through the structural state and, as practice shows, interest in these technical products is steadily increasing. When studying glass composites, their optimal composition was established experimentally, in which the rational use of glass structures contributes to an increase in heat resistance and chemical resistance, in addition, the manifestation of high cohesive strength, an increase in the density of nanocomponents, crack resistance with significant corrosion resistance and ensures high adhesion (more than 127 MPa) with materials different chemical nature, in addition, the formation of a silicate barrier layer prevents the mutual diffusion of structure-forming particles of the coating and substrate.

The surface zone directly adjacent to the friction surface and separating the coating material from the antifriction layer consisting of polydisperse graphite particles is the thinnest film several micrometers thick. Studies have shown that the pressure in it is uneven, and the areas of tensile and compressive stresses, which are inevitable under the conditions of deformation of heterogeneous phases, are close in structure to a conglomerate of finely dispersed (quasi-amorphous) structures, having dimensions in the range of 5-15 nm, and representing mechanical mixtures, oxygen-free and oxide compounds of structure-forming components. The influence of plastic deformation is associated not only with the dispersion of the surface zone, but also with the accumulation of defects that change its physicochemical properties, including reactivity, and affect the intensity of chemical reactions in the solid phase.

At the same time, the thermal conductivity of a finely dispersed conglomerate having an increased porosity and forming a near-surface zone is lower than that of a solid material, therefore, the heating temperature of the finely dispersed fragments of the zone is higher than the temperature of the surface areas.

The temperature factor stimulates physicochemical processes, in particular, the reactive diffusion of structure-forming particles at the atomic-molecular level, which contributes to the introduction of kinetically active components of the dispersed zone through the weakening of the bond between the polyarene planes into the interlayer space of graphite and thus the formation of intercalated graphite.

Using X-ray phase analysis, it was established that the intercalating elements in the subsurface zone-graphite system at the initial stage of the process were Mg^{2+}, Al^{3+}, Cu^{2+} ions, which randomly intruded into the interlayer space of the graphite matrix. At sliding speeds of more than 3.0 m/s, intercalates of binary molecular compounds of these elements with oxygen were found in the layered system of graphite. Their intercalation is accompanied by a sequence of repetitive stages, which are reversible with a change in tribological parameters and are characterized by a specific transformation of the structure and, above all, by an increase in the distance between layers due to the influence of various types of interlayer defects and the introduction of intercalants. Note that today there is no general intercalation model that explains the electrochemical mechanism of the synthesis of layered systems. From the energy point of view, the intercalation process, which represents reversible topo-taxial chemical reactions, can be considered as an adequate way of self-organization of surface layers in the process of structural adaptability of the friction system.

We have found that quantitative changes during the intercalation of the graphite layer, which causes a high level of antifriction, does not affect the expected degree on the qualitative values of tribological parameters during testing for related characteristics associated with the electromagnetic properties of intercalated graphite, judging by the analysis of literature data, it has a significant effect.

The developed antifriction nanostructured glass-ceramic self-lubricating coatings containing magnesium carbide and structural components that promote surface graphitization do not contain expensive and scarce components, meet environmental safety requirements, and have high performance characteristics. The most effective use of nanostructured glass-ceramic self-lubricating coatings is to improve the operational reliability of friction units during their hardening and restoration of moving parts of control mechanisms, sliding bearings, lever parts, high-speed and thermally loaded interfaces, in which the use of traditional lubricants is not desirable.

The development of nanostructured glass-ceramic self-lubricating anti-friction coatings, the substantiation of their structural components, the results of applied tests and the ability to work in production conditions can significantly expand the arsenal of achievements of modern tribotechnics.

It should be noted that the developed nanostructured glass-composite powder can be used for strengthening and restoring worn parts by any technological methods used in powder materials.

The presented work continues the cycle of research on the creation of promising nanomaterials designed to reduce the coefficient of friction and increase the wear resistance of friction units of machine and equipment parts.

Conclusions

1. By means of theoretical prerequisites and experimental studies, the optimal structural-phase composition of nanostructured glass-composite coatings of the SiC-Ni-Cu-Al-Si-Csystem containing a glass phase of the SiO_2-Al_2O3-B_2O_3typeand structurally free magnesium carbide was realized. To improve the adhesion strength, a sublayer of glassy sodium silicate was applied to the substrate. The role of the glass phase in the formation of glass composites is disclosed, which contributes to an increase in the cohesive component, continuity and strength of the nanostructure, and an increase in the anticorrosion properties and chemical resistance of coatings.

2. It is noted that the assessment of the quality of the coatings under study is inextricably linked with the problem of the reproducibility of their technological process. By controlling the deposition of nanostructured glass-composite powders, it turned out to be possible to provide not only the desired chemical composition, but also to obtain a given nanostructure as a result, optimizing a set of properties that contribute to the stable manifestation of minimization of tribotechnical characteristics.

3. The physical mechanism and the main factors that determine the level of thermomechanical graphitization are considered, the nature and chemical interactions of the structural components of the friction system are noted, in ensuring high anti-friction properties of glass-composite coatings.

4. The synthesis of layered graphite compounds as a result of topo-taxial reactions has been studied. The nature of intercalants in a graphite matrix is established and it is noted that reversible topo-taxial chemical reactions in the solid phase represent one of the mechanisms of self-organization of the surface layers of a friction system under conditions of structural adaptability.

5. Fundamental ideas about the formation and structure of antifriction surface structures based on polydisperse carbide graphite were supplemented, which made it possible to expand the arsenal of achievements of modern tribotechnics.

6. Structural engineering, driven by the analysis and innovative provision of the functional properties of the developed materials, opens up promising opportunities associated with the modernization of friction surfaces.

References

1. Sahar Ghatrehsamania, SalehAkbarzadeha, M.M.KhonsariExperimentally verified prediction of friction coefficient and wear rate during running-in dry contact. //Tribology InternationalVol. 170 (2022). doi.org/10.1016/j.triboint.2022.107508.

2. Aleksandr V. Antsupov, Artem A. Fedulov, Alexey V. Antsupov and Victor P. Antsupov An Application of Antifriction Coatings to Increase the Lifetime of Friction Units. Mechanical Engineering. MATEC Web of Conferences 346, 03024 (2021).doi.org/101051/matecconf/202134603024.

3. I. Justin Antonyraj D. Lenin Singaravelu Tribological characterization of various solid lubricants based copper-free brake friction materials – A comprehensive study. materials today. Volume 27, Part 3 , 2020, Pages 2650-2656. doi.org/10.1016/j.matpr.2019.11.088.

4. Maciej Matuszewski, Małgorzata Słomion, Adam Mazurkiewicz and Andrzej Wojciechowski Mass wear application of cooperated elements for evaluation of friction pair components condition. mechanical engineering. MATEC Web of Conferences 351, 01006 (2021). doi.org/10.1051/matecconf/202135101006.

5. Babak, VP , Shchepetov, VV , Nedaiborshch, SD (2016). Wear resistance of nanocomposite coatings with dry lubricant under vacuum. Naukovyi Visnyk Natsionalnoho Hirnychoho Universytetuthis link is disabled , 2016, (1), nbuv.gov.ua/UJRN/Nvngu_2016_1_9.

6. Babak VP, Shchepetov VV, Harchenko SD Antifriction Nanocomposite Coatings that Contain Magnesium Carbide. J. Journal of Friction and Wear, 40 (6), Pp.593–598 (2019). doi.org/10.3103/S1068366619060035.

7. Vilhena, L.; Ferreira, F.; Oliveira, JC; Ramalho, A. Rapid and Easy Assessment of Friction and Load-Bearing Capacity in Thin Coatings. Electronics 2022, 11, 296. doi.org/10.3390/electronics11030296.

8. Zaytsev AN , Aleksandrova YP , Yagopolskiy AG Comparative Analysis of Methods for Assessing Adhesion Strength of Thermal Spray Coatings. BMSTU Journal of Mechanical Engineering. 5(734)/2021 -p48-59. DOI: 10.18698/0536-1044-2021-5-48-59 .

Фіалко Н.М., Щепетов В.В., Харченко С.Д., Ковтун І.І., Гладкий Я.М. , Бись С.С. Наноструктурні склокомпозитні самозмащувальні покриття

Досліджено характеристики тертя та зношування розроблених наноструктурних склокомпозиційних самозмащувальних покриттів, структурні складові яких мають якісний вплив на процес графітизації та забезпечують отримання поверхневого шару α-графіту, що мінімізує контактні параметри.

Встановлено позитивну роль склофази у вигляді алюмоборосилікату, що впливає на триботехнічні властивості покриттів. Відзначено, що підвищення адгезійної міцності досягається за рахунок формування при напилюванні поверхневого шару зі склоподібного силікату натрію. Констатовано, що інтеркаляція графітового шару частинками підповерхневої зони суттєво не впливає на триботехнічні характеристики. Розроблені наноструктурнісклокомпозиційні покриття показали високі антифрикційні характеристики у всьому навантажувально-швидкісному діапазоні випробувань.

Ключові слова: наноструктурні покриття, інтенсивність зношування, склокомпозит, склофаза, графітизація

***Problems of Tribology**, V. 27, No 4/106-2022,13-18*

Problems of Tribology
Website: http://tribology.khnu.km.ua/index.php/ProbTrib
E-mail: tribosenator@gmail.com

DOI: https://doi.org/10.31891/2079-1372-2022-106-4-13-18

Features of ion nitriding technology multicriteria optimization

E.K. Solovykh, I.V. Shepelenko*, A.E. Solovuch, S.E. Katerynych

Central Ukrainian National Technical University, Kropyvnytsky, Ukraine
**E-mail: kntucpfzk@gmail.com*

Received: 11 August 2022: Revised: 20 September 2022: Accept:02 October 2022

Abstract

In this work, the technology of 30HGSA steel ion nitriding was optimized in terms of tribotechnical characteristics – wear intensity and friction coefficient. When choosing controlled factors, the influence of all existing groups of factors that can affect the process of ion nitriding is taken into account: structural, technological and operational. Friction and wear tests were carried out under conditions that are as close as possible to the actual operating conditions of aircraft parts made of 30HGSA steel. As a result of experiments on friction and wear, tribotechnical characteristics of coatings were obtained depending on structural, technological and operational factors, respectively, to the matrix. The conducted studies showed the presence of three clearly defined zones in the dependences of wear intensity and friction coefficient on specific load at different sliding speeds and technological parameters of ion nitriding: run-in zones, uniform and catastrophic wear. The nature of samples dependences hardened by ion nitriding and heat-treated samples is similar and coincides with modern views on the laws of friction and wear processes. Analysis of tribotechnical characteristics showed the effectiveness of ion nitriding technology in comparison with traditional heat treatment. The optimal processing modes for the studied steel and triboconjugation have been established.

Key words: ion nitriding, optimization, wear intensity, friction coefficient, processing modes, operational factors.

Introduction

In the world mechanical engineering, a priority direction has developed – the technology of surface hardening and the application of multifunctional coatings. The possibility of creating products with a unique combination of the base material properties and the surface layer causes the growing interest of engineering enterprises and other industries in the wider use of this potential. The use of multifunctional hardening coatings makes it possible to repeatedly increase the durability of machines, operating temperatures and speeds, while reducing fuel consumption and providing the possibility of intensifying many production processes [1, 2].

In the theory and practice of the use of hardening coatings, the need to optimize the technology for such an important characteristic as the reproducibility of properties is noted [3]. The development of any technological process (TP) is inevitably associated with the solution of optimization problems, and in the field of creating functional coatings, optimization issues occupy a key place. This is because a large number of application methods, combined with an extensive nomenclature of materials from which the coating is formed, as well as many influencing factors, provide technologists with a wide range of alternative options.

Today in world practice there are more than 200 surface hardening technologies. Most of them are alternatives. The acceptance of optimal decisions on the choice of alternative technologies at the stage of designing new equipment, manufacturing, operation and repair should be carried out according to the criteria of the maximum strength and durability of the hardened part achieved with minimal energy and other material costs, as well as with minimal environmental damage [1-3].

Glow discharge chemical-thermal treatment is the most progressive and energy-saving in a wide range of alternative technologies. Ion nitriding (IN), which is traditionally used to improve wear resistance, corrosion resistance, and endurance limit, has received the widest industrial application and rapid development [3]. The

great technological possibilities of IN technology pose the need to solve optimization problems, taking into account structural, technological and operational factors.

Literature review

Compared to traditional gas saturation, glow discharge treatment provides reduction in energy consumption by an order of magnitude, and also reduces the duration of the technological cycle by an order of magnitude. The advantages are also controllability, stability and predictability of processing results. When hardening steels and cast irons, there are no changes in the size and shape of parts, as well as changes in surface roughness. Nitriding in a glow discharge is the finishing operation. This eliminates the need for final mechanical processing. All these characteristics confidently place IN technology as an alternative to classical carburizing followed by hardening [4].

In world practice, IN uses ammonia as a working gas. This creates environmental problems as well as explosive problems. However, the main disadvantage regarding the use of hydrogen-containing media is hydrogen embrittlement of applied coatings and substrates. V.G. Kaplun and his collaborators developed the technology and equipment for IN in hydrogen-free media [5]. This technology preserves the bulk initial strength of the products, the process becomes absolutely environmentally friendly, the consumption of working gas is reduced, and the design of the equipment is simplified by eliminating dissociators that are very difficult to operate. At the same time, the surface layer has greater plasticity, which is especially important for gear parts and parts operating under shock loads.

During the period of reconstruction and renewal of equipment technological park for applying protective coatings, it is the IN technology that is in especially high demand. In the practice of aircraft engine building, traditional carburizing and nitrocarburizing have been switched to IN of gear wheels. This process reduces the complexity of manufacturing by 1.5-2 times, because parts are processed at a low hardness of the material and are sent for hardening in the finished form. IN technology is mainly used to improve wear resistance. This also increases the corrosion resistance and endurance limit [6].

In this regard, it is extremely important to search for optimal conditions for the implementation of IN technology for individual indicators that can affect the process: structural, technological and operational.

Purpose

The aim of the work is to search for optimal solutions and establishing a connection between the technological regimes of IN and the tribotechnical characteristics of the studied material.

Research Methodology

When choosing material for research, we proceeded from the following considerations. An analysis of statistical data shows that of all parts of the airframe and power plant rejected during the overhaul of the aircraft, approximately 45% are products made of steels of various grades. Of this amount, the largest percentage of rejection falls on parts made of 30HGSA steel – 30%, and about 50% of them cannot be restored [3]. That is why the optimization of the IN technology was carried out on steel 30HGSA, the chemical composition of which is presented in Table 1.

Table 1

The chemical composition of steel 30HGSA, % [7]

C	Si	Mn	Ni	Cr	S	P	Cu
0.28 – 0.34	0.9 – 0.12	0.8 – 1.1	≤ 0.3	0.8 – 1.1	≤ 0.025	≤ 0.025	≤ 0.3

Using peer review methods and a series of screening experiments, we obtained an average a priori ranked number of factors that affect the IN technology (Fig. 1).

Thus, a planning matrix was compiled, which included the first six technological factors (Fig. 1), as well as operational factors: sliding speed and specific load in triboconjugations. As optimization criteria, the main tribotechnical characteristics are taken – the wear intensity I_n and the friction coefficient μ.

Friction and wear tests were carried out under conditions that are as close as possible to the actual operating conditions of aircraft parts made of 30HGSA steel: lubricant – CIATIM-201, specific load – 2.5...25 MPa; sliding speed – 0.4...1.3 m/s. The samples were subjected to heat treatment (quenching from 1143 K in oil, tempering at 823 K), as well as IN (reactive gas composition: 95% N_2+5% C_3H_8; saturation temperature t = 873 K; reactive gas pressure P = 100 Pa; diffusion saturation time τ = 2.5 hours).

Standard tests were carried out according to the scheme: disc – block. The disc-counterbody is made of the same steel, hardened at 1143...1163 K in oil, tempered at 783...543 K, hardness – 37...38 HRC. The surface roughness of the block, depending on the processing modes, corresponded to R_a = 0.29...0.41 μm, and the disc-counterbody – R_a = 0.53 μm.

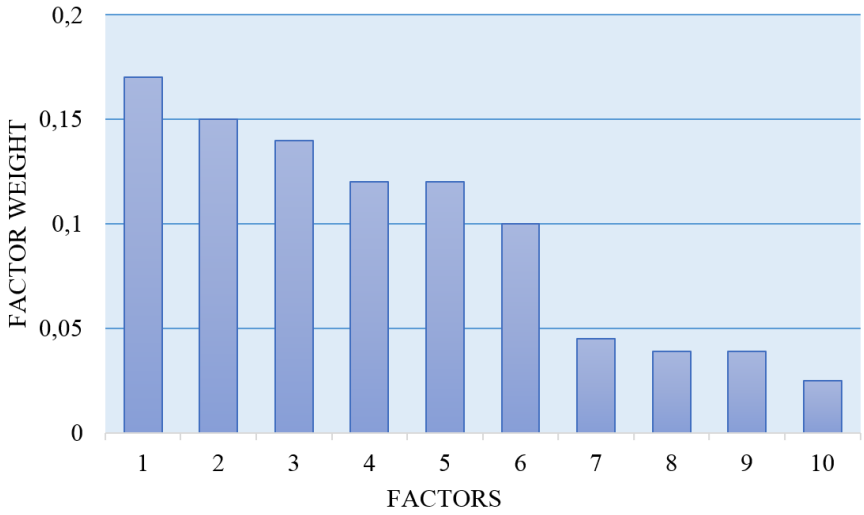

Fig. 1. A ranked row of structural, technological and operational factors: 1 – saturation temperature; 2 – reactive gas pressure; 3 – composition of reactive gas; 4 – ion treatment time; 5 – operational load; 6 – sliding speed; 7 – coating thickness; 8 – part material; 9 – operating current of the saturation process; 10 – operating voltage of the saturation process

Results

As a result of carrying out experiments on friction and wear, the tribotechnical characteristics of coatings were obtained depending on structural, technological and operational factors (Fig. 2, a-f).

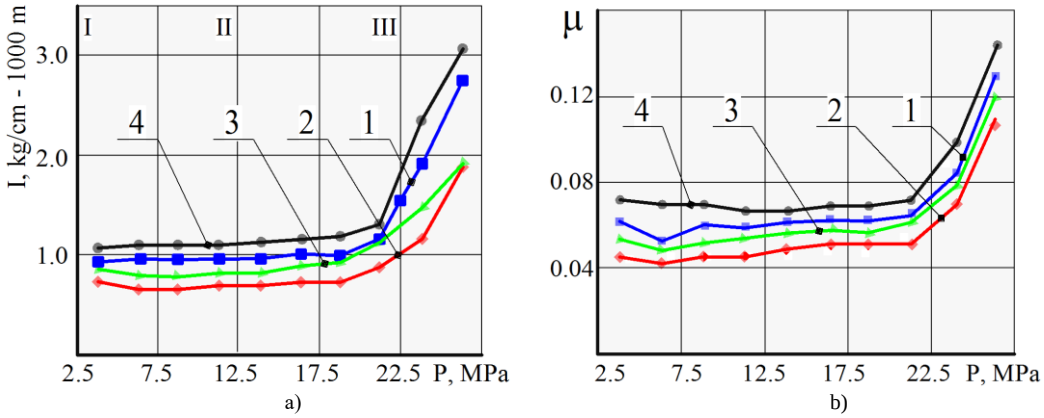

Fig. 2. Dependence of wear intensity *I* (a) and friction coefficient *μ* (b) of HT+IN treatment on specific load *P* at sliding speed *V*: *1* – *V* = 0.4 m/s; *2* – *V* = 0.7 m/s; *3* – *V* = 1.0 m/s; *4* – *V* = 1.3 m/s
I – running-in zone; II – zone of uniform wear; III – zone of accelerated wear

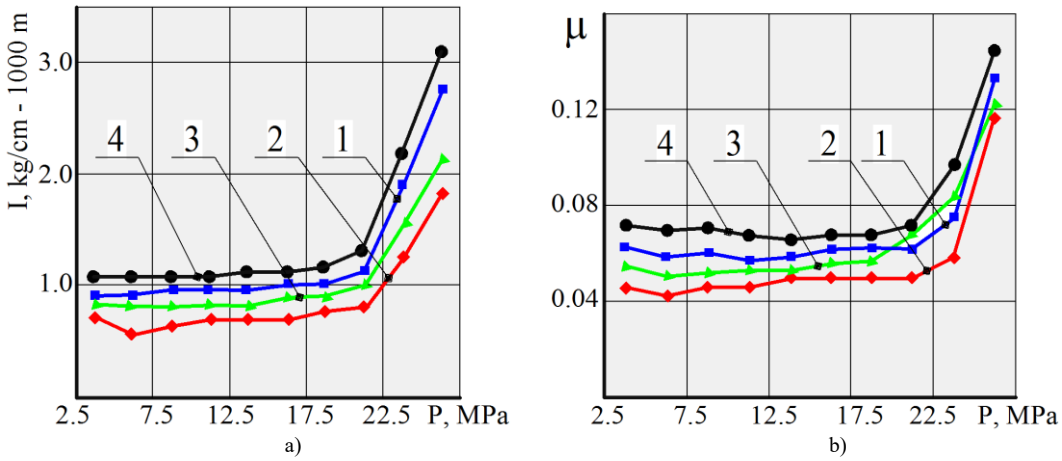

Fig. 3. Dependence of wear intensity *I* (a) and friction coefficient *μ* (b) of IN treatment on specific load *P* at sliding speed *V*:
***1* – *V* = 0,4 m/s; *2* – *V* = 0,7 m/s; *3* – *V* = 1,0 m/s; *4* – *V* = 1,3 m/s**

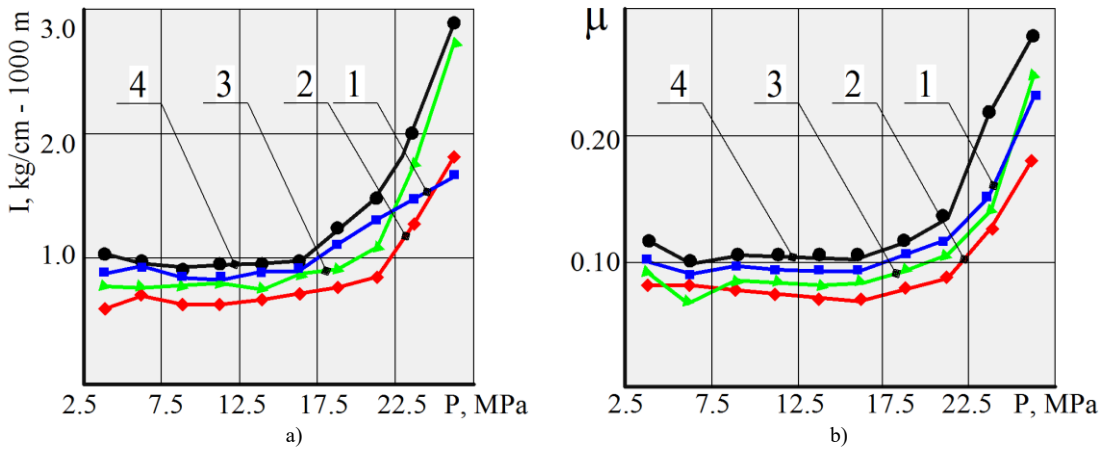

Fig. 4. Dependence of wear intensity *I* (a) and friction coefficient *μ* (b) of HT treatment on specific load *P* at sliding speed *V*: *1* – *V* = 0,4 m/s; *2* – *V* = 0,7 m/s; *3* – *V* = 1,0 m/s; *4* – *V* = 1,3 m/s

The study of the obtained dependences (Fig. 2-4) showed the leading role of preliminary heat treatment (HT) of samples according to the mode – quenching from 1143...1163 K in oil – tempering at 783...843 K.

The analysis of the obtained results (Fig. 2-4) revealed the presence of three clearly defined zones, in the dependences of *I* and *μ* on the specific load at different sliding speeds and technological parameters of the IN: running-in zones, uniform and catastrophic wear. The nature of the dependences of hardened by IN samples (with and without preliminary HT) and heat-treated samples (without IN hardening) is similar. This type of dependencies coincides with the modern, generally accepted views on the laws of friction and wear processes.

However, the dependences of *I* and *μ* on the specific load *P* for heat-treated and hardened by IN samples have significant differences (Fig. 5). Increased wear is observed in heat-treated samples starting at *P* values of 13...14 MPa order, while hardened by IN begin to wear out intensively – at 18...19 MPa.

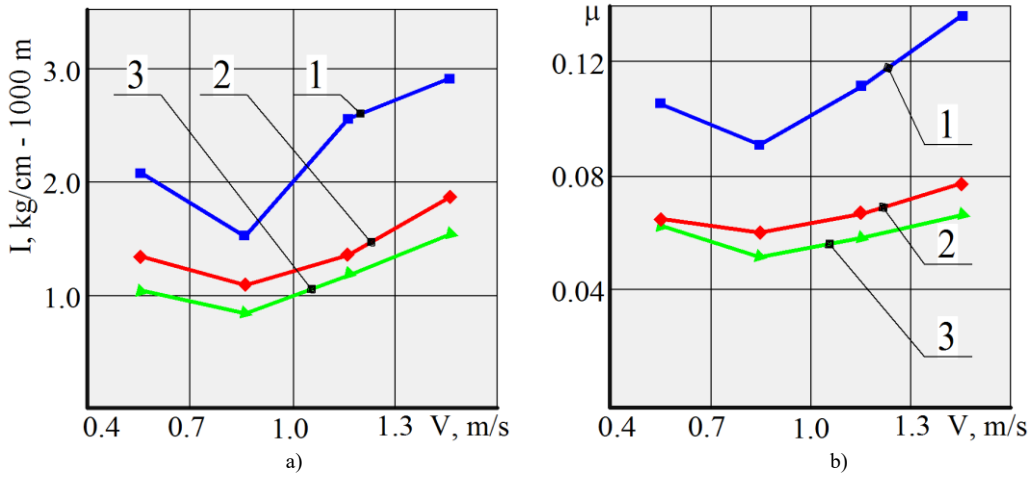

Fig. 5. Dependence of wear intensity *I* (a) and friction coefficient *μ* (b) on sliding speed *V* at specific load *P* = 20 MPa and following treatment: 1 – HT; 2 – IN; 3 – HT+IN

Thus, there is an increase in the zone of uniform wear, which, of course, provides an extension of parts normal operation range at increased specific loads. With the same values of specific loads *P* and sliding speeds, the wear intensity *I* of hardened by IN samples is 1.7...2.1 in absolute values, and the friction coefficient *μ* is 1.9 times less than heat-treated samples. This implies the effectiveness of IN in comparison with traditional heat treatment.

Studies of the dependences of *I* and *μ* on the sliding speed *V* established (Fig. 3) that with an increase in *V* from 0.4 m/s, they gradually decrease, reaching a minimum at 0.7 m/s. With a further increase in *V*, these characteristics increase. Thus, the optimal sliding speed for the studied steel in this triboconjugation is *V* = 0.7 m/s.

Conclusions

The conducted studies allowed us to draw the following conclusions:

1. The proposed approach to optimizing the IN technology made it possible to improve the tribotechnical characteristics of the material, namely:

- reduce wear by 1.7...2.1 times, reduce friction coefficient by 1.9 times at a load increased by 1.4...1.5 times and the recommended sliding speed of 0.7 m/s for steel substrates hardened by ion nitriding, compared to surfaces that are heat treated in a classical way;

- expand the range of parts normal operation by increasing the zone of uniform wear.

2. The following optimized parameters of coating formation are recommended for use: process duration t = 140…190 min; reactive gas pressure p = 100…115 MPa; composition of the reaction mixture N_2 = 80…90% + Ar = 5…15%; saturation temperature T = 843…873 K.

3. The effectiveness of IN application in comparison with traditional heat treatment has been proven.

References

1. Lyashenko B.A., Solovyih E.K., Mirnenko V.I. i dr. (2010). Optimizatsiya tehnologii naneseniya pokryitiy po kriteriyam prochnosti i iznosostoykosti. Kiev, NAN Ukrainyi, IPP im. G.S. Pisarenko, 193 s.

2. Chernovol M.I., Shepelenko I.V. (2012). Sposobyi formirovaniya antifriktsionnyih pokryitiy na metallicheskie poverhnosti treniya [Zbirnik naukovih prats Kirovogradskogo natsionalnogo tehnichnogo universitetu. Vip.25 (1)] – S.3–8.

3. Solovyih E.K. (2012). Tendentsii razvitiya tehnologiy poverhnostnogo uprochneniya v mashinostroenii. Kirovograd, KOD, 92 s.

4. Novikov N.V., Bidnyiy A.A., Lyashenko B.A. i dr. (1989). Metodyi uprochneniya poverhnostey mashinostroitelnyih detaley. Kiev, ISM AN USSR, 112 s.

5. Kaplun V.G. (1991). Nauchnyie osnovyi tehnologii uprochneniya detaley mashin i instrumenta ionnyim azotirovaniem v bezvodorodnyih sredah [avtoreferat dissertatsii doktora tehnicheksih nauk] 38 s.

6. Lyashenko B.A., Novikov N.V., Klimenko S.A. (2017). Diskretnoe modifitsirovanie poverhnostnogo sloya detaley mashin i instrumentov. Kiev, ISM im. V.N.Bakulya, 264 s.

7. Sushko O.V., Posvyatenko E.K., Kyurchev S.V. i dr. (2019). Prikladne materialoznavstvo. Melitopol, TOV «Forward press», 352 s.

Солових Е.К., Шепеленко І.В., Солових А.Е., Катеринич С.Е. Особливості багатокритеріальної оптимізації технології іонного азотування

В роботі виконано оптимізацію технології іонного азотування сталі 30ХГСА за триботехнічними характеристиками – інтенсивністю зношування та коефіцієнтом тертя. При виборі керованих факторів враховано вплив усіх існуючих груп, які можуть впливати на процес іонного азотування. Випробування на тертя та знос проведені в умовах, які максимально наближені до реальних експлуатаційних режимів деталей авіаційної техніки. В результаті проведення експериментів на тертя та знос отримані триботехнічні характеристики покриттів залежно від конструкційних, технологічних та експлуатаційних факторів відповідно до матриці. Проведені дослідження показало наявність трьох, чітко виражених зон у залежностях інтенсивності зношування та коефіцієнта тертя від питомого навантаження при різних швидкостях ковзання та технологічних параметрах іонного азотування: зони припрацювання, рівномірного та катастрофічного зношування. Характер залежностей зразків зміцнених іонним азотуванням та термооброблених зразків подібний та збігається із сучасними поглядами на закономірності процесів тертя та зношування. Аналіз триботехнічних характеристик показало ефективність технології іонного азотування порівняно із традиційною термообробкою. Встановлено оптимальні режими обробки для досліджуваних сталі та трибосполучення.

Ключові слова: іонне азотування, оптимізація, інтенсивність зношування, коефіцієнт тертя, режими обробки, експлуатаційні фактори.

***Problems of Tribology**, V. 27, No 4/106-2022,19-26*

Problems of Tribology
Website: http://tribology.khnu.km.ua/index.php/ProbTrib
E-mail: tribosenator@gmail.com

DOI: https://doi.org/10.31891/2079-1372-2022-106-4-19-26

Influence of emulsols type on energy-power consumption and surface contamination at DC01 steel cold rolling on the continuous four-stand mill

V. Kukhar[1*], Kh. Malii[1], O. Spichak[1,2]

[1] Technical University "Metinvest Polytechnic", LLC, Ukraine
[2] PJSC "Zaporizhstal", Ukraine
**E-mail: kvv.mariupol@gmail.com*

Received: 31 September 2022: Revised: 01 October 2022: Accept: 25 October 2022

Abstract

The article presents the results of experimental and industrial tests of physical and chemical parameters of the experimental emulsol "Quakerol". According to the physicochemical parameters the experimental emulsol "Quakerol" differs from the used emulsol "Universal-1TS" by higher lubricating properties. Operating modes of stand and coiler electric motors of tandem mill at rolling of melts from experimental emulsol "Quakerol" lubricated with emulsol "Quakerol" and serial emulsol "Universal-1TC" lubricated with conservation oil "OK-2" at LPTs were analyzed. The results of analysis of loads at rolling of strips with 0.68×1000 mm cross-section from pre-rolled sheet with thickness of 3.0 mm showed that the values of average total loads on stand motors and coiler of four-stand mill 1680 were higher when using experimental emulsol "Quakerol". The comparative analysis of experimentally obtained data on influence of technological conditions of cold-rolled coils production at four-stand continuous tandem mill 1680 with using emulsols "Quakerol" and "Universal-1TS" on rolling power parameters, power consumption and contamination of DC01 flat carbon steel surface is presented. Multiple regression equations were obtained to describe power consumption during rolling using different emulsions, the values of cross-sectional area were taken as a varying factor. Specific power consumption and average total load on stands and coiler motors during rolling with the use of emulsion prepared from experimental emulsion "Quakerol" and emulsion prepared from standard emulsion "Universal-1TS" were estimated. The reasons of higher specific power consumption during LCL operation with the experimental emulsion were analyzed. A quantitative assessment of contamination of the surface of steel samples using the experimental emulsion "Quakerol", oil "OK-2" and standard emulsion "Universal-1TS" is given. The necessity of further tests to determine the optimal concentration of emulsion from "Quakerol" to ensure the reduction of energy costs per ton of cold rolled steel has been substantiated.

The practical significance of the work lies in the development of methods for analysis of lubricants with regard to the prospects of using "Quakerol" emulsion instead of "Universal-1TS" emulsion in order to improve the quality and increase the productivity of the cold-rolling shop.

Key words: cold rolling, 1680 continuous mill, emulsol, energy consumption, specific consumption of electricity, surface contamination

Introduction

Today, four-high mills are the most common rolling equipment for the production of cold rolled flat (& coiled) steel. Such equipment is quite powerful and energy-consuming. Four-high mills are used for production of cold-rolled sheets and strips 0.6-2.5 mm thick and 1300-1800 mm wide as finished products from 3-8 mm thick hot-rolled steel in coils weighing 25-50 tons. High energy consumption in such mills is due to the presence of a barrel 1500-2000 mm with a diameter of working rolls 500-550 mm and reserve 1300-1500 mm for the transfer of torque [1]. Rolling speed - at least 5-12 m/s, productivity - from 0.6-0.8 million tons per year [2]. The wide use of mills with 4-high stands of the tandem type in the composition of four and five stands for the production of strips, and five and six stands for the production of tinplate [3, 4] should be noted from the modern foreign experience in the field of cold rolling mills. The use of modern emulsions leads to improved quality indicators and increased production of the cold rolling shop (CRS) [5, 6]. The application of the "Quakerol" as a new emulsol instead of "Universal-1TS" requires establishing the effect of this lubricating and cooling liquid (LCL) on not only the indicators of quality and

manufacturability, but also on the rolling power parameters. Thus, of scientific interest is the study of the effect of technological conditions for the production of cold rolled coils on a four-stand continuous tandem mill 1680 with the use of emulsions "Quakerol" and "Universal-1TS" on the power parameters of rolling, energy consumption and surface contamination at the cold rolled coils manufacturing in the CRS. On the metal strip after cold rolling there is always some amount of contamination particles, which are the wear products of rolls and strips and products of thermal transformation of technological lubricants. Therefore, when rolling cold-rolled sheets and strips, the issue of ensuring the quality of the surface arises. Determinations of contamination indicators of the metal surface contribute to the prevention of defects such as "sooty deposits", "emulsion spots, oil spots" and "spots of contamination".

Literature review

In this paper [7], considerable attention is paid to increasing the energy efficiency of rolling on tandem mills 1700 (in relation to the conditions of PJSC "Iron and Steel Works of Mariupol"). Through industrial rolling mills, it has been shown that the use of lubricants has an effect on the synchronization of the stands and on the power modes of rolling mills, which reduces the consumption of electricity during mill rolling by 1–6%. In tandem rolling mills, the modes of operation of electric motors of the stands must be synchronized [7] taking into account deformation phenomena (different hoods on the stands, heating-cooling during rolling, etc.), which affects quality indicators and electricity consumption. The conditions of the power load on the electric motor of the 1680 reversible mill of cold rolling are considered in this paper [8]. The importance of ensuring the reliability and stability of the operating modes of electrical equipment and automation in order to achieve high quality and the absence of defects in the rolling of thin cold-rolled coils has been revealed. Moreover, the necessity of carrying out rolling with emulsions of the type "Universal-1TS" and "Cold Roller" in order to achieve softening of the conditions of operation of electric motors of the rolling mill is especially emphasized. Studies [6, 9] are devoted to identifying the influence of the characteristics and physical and chemical properties of various emulsions, which has an effect on the friction coefficient, on the energy consumption of continuous cold rolling mills. They determined that the use of emulsol with a higher kinematic viscosity allows in some cases to reduce the specific consumption of electricity. Friction and lubrication conditions, as a rule, significantly affect the energy-force modes of deformation [10]. The coefficient of deformation friction is determined in various ways, among which the most common is the compression of samples with different conditions at the tool-workpiece contact [11]. In this paper [12] it was noted that for reversible one- and two-stand cold rolling mills, both by changing the contact conditions and by varying the tension, it is possible to set up energy-saving rolling modes of a coil with a thickness of 0.15-0.8 mm. The authors [13] established the regularities of the effect of lubricant composition on the wear of work rolls and energy consumption of cold rolling mills, and it is recommended to introduce Ti into the lubricating liquid. The paper [14] presents the test results of three rolling emulsions: "Gerolub 3022", "Gerolub CTS 87-1" and "Gerolub 6528". It was determined that the use of these rolling emulsols allows to increase the rolling speed while maintaining the quality of the product surface and reducing the energy parameters of rolling compared to the parameters previously obtained when using "Quakerol 683" and "Quakerol NLM 4.0" lubricants. At the same time, researchers [15] note that during their one-time evaluations, a more effective emulsol than "Quakerol 671" was not found for the conditions of 1700 CRS of OJSC "AMT". Electricity consumption during rolling depends not only on the type of emulsion used, but also on many factors: on the setting of inter-stand tension [1, 16], the realized stress-strain state of the material [16, 17], rheological properties of steels [18], efficiency of intermediate recrystallization annealing [19] and other methods of processing rolled steel [20], structural features of the rolling stock and its working and conductive elements [21], technological state and obsolescence of electrical equipment designs [22]. Indicators of power quality [23], which depends on the efficiency and stability of workshop converters and transformers [24], have a significant influence on the stability of the electrical equipment of heavy-loaded machines, and, as a rule, the controllability of rolling mills. However, when research is carried out on one piece of equipment under equal influence of all these conditions, it becomes obvious that the effect on electricity consumption depends only on the factor that changes, that is, the emulsol used.

Purpose of the work

The purpose of the study was to evaluate the loading of electric motors, power consumption and the value of contamination of the metal surface in conditions of continuous cold rolling, taking into account the prospects of using emulsion "Quakerol" instead of emulsion "Universal-1TS".

Research methodology, materials and equipment

For experimental and industrial tests 11 m^3 (~9900 kg) of experimental emulsol "Quakerol" was delivered. Emulsol samples were taken to determine the actual physical and chemical parameters. Physicochemical parameters of the experimental emulsol "Quakerol" in comparison with "Universal-1TS" emulsol currently used for cold rolling of carbon steel in the CRS-1 (PJSC "Zaporizhstal") delivered with an actual saponification value of 38.57 mgKOH/g, as well as previously tested by "Quakerol" emulsol are presented in Table 1.

Table 1

Results of laboratory tests for "Quakerol" emulsol in comparison with "Quakerol ZAP 3.0" emulsols manufactured by Quaker, and Universal-1TS manufactured by LLC "METINVEST - Mariupol Repair and Mechanical Plant"

№	Physical and chemical indicators	"Quakerol"		"Quakerol ZAP 3.0"	"Universal-1TS"	
		Actual batch	*Quality certificate*	*Actual sample*	*Actual batch*	*Technical conditions*
1	Appearance	homogeneous brown liquid	clear dark amber liquid	clear dark amber liquid	responds	homogeneous oily liquid
2	Scent	responds	characteristic weak smell	specific not annoying	responds	specific not annoying
3	Density at 20 ºC, kg/m^3	927	929	930	934	920-960
4	Kinematic viscosity at 50 ºC, mm^2/s	40.58	not standardized	42.92	34.07	≤35.0
5	Kinematic viscosity	60.97	60.60	61.90	–	–
6	Acid value, mg KOH/g	11.60	11.70	11.90	11.23	> 12.5
7	Saponification value, mgKOH/g	164.44	163.0	174.31	38.57	≥13.5
8	Water content, %	0.09	not standardized	0.06	0.28	≤0.5
9	Stability during storage	withstands	not normal	withstands	withstands	withstands
10	Ash content, %	0.06	Not stand-ardized	0.031	–	≤0.04
11	The freezing point, ºC	minus 5 (at 0ºC – lost mobility)	0	minus 3	–	–
12	Flash point, °C	170	>150	–	–	–
3% emulsion						
13	Stability of the emulsion prepared on hard water 4.6 mg-eq/dm^3 during 6 hours, % of oil	withstands, 1.5% drain	not normal	withstands, 3.0% drain	withstands 0%	withstands (the allocation of traces of "draining" and oily secretions is allowed)
14	Corrosive attack on gray cast iron by water emulsion	can't stand	not standardized	can't stand	stands	stands
15	Hydrogen index pH of 3% aqueous emulsion (on hard water 4.6 mEq/dm^3)	3.8	not standardized	4.0	9.18	8.2-9.2
16	Tendency to foaming at (20±5) °C, см^3	0 points	not normal	2 points	–	> 40

Taking into account the fact that hot-rolled pickled rolls can be in an open space for no more than 48 hours before rolling, and the test campaign of the experimental emulsion "Quakerol" lasted about a month, the distribution of the experimental melt for the comparative rolling of part of the rolls on the serial emulsol "Universal-1TS" did not perform. For comparison, we used the data obtained earlier on the rolls rolled on emulsion from the "Universal-1TS" emulsol of earlier deliveries. The incoming control of compliance of the characteristics of the emulsol with the requirements of the technical conditions of the enterprise was carried out. It was established that the tested sample of experimental emulsol "Quakerol" meets the requirements of the quality passport. According to its physicochemical parameters, the experimental emulsol "Quakerol" differs from the used emulsol "Universal-1TS" in that it has higher lubricating properties (the saponification value is 164.44 mgKOH/g, against 38.57 mgKOH/g in the emulsol "Universal-1TS").

The continuous four-standmill 1680 (see Fig. 1) is the main rolling mill of the CRS-1 (PJSC

"Zaporizhstal"). It consists of 4 consecutively arranged quarto stands, which include two supporting and two working rolls, as well as auxiliary equipment (under-receiving device, rotary bed, unwinder, drum-type winder, etc.). The characteristics of the roller drive are given in Table 2. The drive of the working rolls from electric motors is carried out through intermediate shafts with a toothed clutch, gear stands and spindle connections. The rolls' characteristics are given in Table 3.

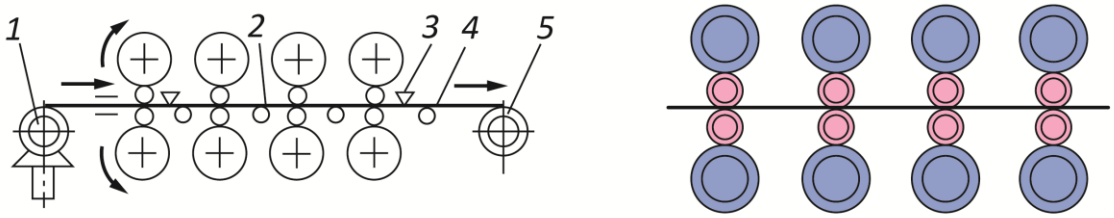

Fig. 1. Schemes of rolling on a four-stand continuous tandem mill 1680:
1 – unwinder, 2 – tensiometr, 3 – gauge of thickness, 4 – strip, 5 – winder

Table 2

Characteristics of the rolls' drives

Stand No.	Engine power, kW	Armature rotation number, rpm	Rolling speed, m/s
1	3300	110/200	2.75 – 5.0
2	3300	160/280	4.0 – 7.0
3	3300/2800	220/280	5.8 – 9.5
4	2 x 1650	200/450	2.6 – 10

Table 3

Characteristics of the continuous mill rolls

Kind of rolls	Roll diameter, mm	Roll length, mm	Roll mass, t	Bearing's type
Working	510	1680	3.12	roller
Support	1300	1680	23.6	liquid friction

Notched working rolls are used to improve the grip of the first stand. In the fourth stand, working rolls with a notched surface are also used to make it impossible to weld the turns of the rolls during subsequent heat treatment. For each grade of steel, as well as the final section of cold-rolled strips, crimping modes have been developed. The mill is equipped with a technological lubricant supply system (emulsion with an emulsol concentration of 2–4%), anti-bending systems of work rolls, control and measuring equipment, which was used to control the energy parameters of rolling and energy consumption. No comments (fluctuations in loads, tension instability) were noted by the technological personnel of the continuous four-standmill 1680 during the testing period.

Analysis of rolling energy parameters

The modes of operation of the electric motors of the stand and the winder of tandem mill were analyzed during the rolling of melts on the LCL from the experimental emulsol "Quakerol", lubricated with the emulsol "Quakerol" and the serial emulsol "Universal-1TS", lubricated with preservation oil "OK-2". The results of the loads analysis when rolling strips with the 0.68×1000 mm cross-section from a 3.0 mm thick pre-roll plate are summarized in the Table 4.

Table 4

Average total loads on engines during rolling

Steel grade	Size	Average total load on the electric motors of the stand and the winder when rolling one coil of experimental melt, kVA	
		Rolling on emulsion from experimental emulsol "Quakerol"	*Rolling on emulsion from emulsol "Universal-1TS"*
DC01	3.0/1.0x1265 mm	10.965	10.505

As it can be seen from the table 4, the average total load on the stand motors and the winder of the four-

standmill 1680 in the established rolling mode when using the emulsion from the experimental emulsol "Quakerol" on the metal oiled with the emulsol "Quakerol" is 4.19% higher than during rolling of the same assortment, oiled in continuous pickling unit (CPU-4) with "OK-2" oil and rolled on emulsion with "Universal-1TS".

Consumed electricity analysis

The electricity consumption during rolling of the same assortment of DC01 carbon steels during rolling of melts on LCL from experimental emulsion "Quakerol" lubricated with emulsion "Quakerol" and serial emulsion "Universal-1TS" lubricated with preservation oil "OK-2" was analyzed. Data on consumed electricity are presented in the Table 5.

Table 5

Power consumption during rolling on tandem mill

Strip cross-section, mm	Number of coils, pcs	Emulsion concentration during rolling, %	Electricity consumption, KWh	Coils mass, t	Specific electricity consumption, KWh/t	Total electricity consumption during rolling, KWh/t
X1	X2	X3	-	X4	Y	-
"Quakerol"						
0.5×1000	10	1.5	9063.9	98	92.49	504
1.5×1250	4	1.8	1746.9	53.06	32.92	
0.5×1000	13	1.9	12852	143.16	89.77	
1.5×1250	9	1.8	4236.3	117.23	36.14	
0.5×1000	6	1.7	5595.3	68.13	82.13	
1.5×1250	9	2	3919.5	113.76	34.45	
0.5×1000	5	2.4	5344.2	56.89	93.94	
1.5×1250	10	2	4609.8	109.75	42.00	
Average value of the emulsion concentration		1.9				
"Universal-1TS"						
0.5×1000	4	3.1	3800.7	44.21	85.97	490
1.5×1250	4	2.6	1693.8	54.74	30.94	
0.5×1000	7	3.8	6930.9	78.58	88.20	
1.5×1250	8	3	3631.5	93.95	38.65	
0.5×1000	9	2.7	8404.2	101.23	83.02	
1.5×1250	11	3.3	4701.6	147.54	31.87	
0.5×1000	9	2.2	9208.8	96.94	94.99	
1.5×1250	6	3	2781.9	76.58	36.33	
Average value of the emulsion concentration		3.0				

As a result of data processing from Table 5 obtained multiple regression equations, taking into account that instead of multiplying the linear dimensions of 0.5×1000 mm and 1.5×1250 mm, the cross-sectional area values of 500 mm^2 and 1875 mm^2 were used as the X1 factor. The measurement units of factors X2...X4 correspond to those indicated in the Table 4. Dependencies of specific electricity consumption (Y) on factors X1...X4 (see Table 5) for experimental emulsols:

- "Quakerol" (R^2=0.994):

$$Y = 81.096 - 0.035X1 + 4.946X2 + 11.146X3 - 0.403X4; \quad (1)$$

- "Universal-1TS" (R^2=0.995):

$$Y = 96.275 - 0.034X1 + 7.373X2 + 0.483X3 - 0.577X4. \quad (2)$$

As it can be seen from the Table 5, the total specific consumption of electricity during rolling on an emulsion prepared from the experimental emulsol "Quakerol" is slightly higher (by 2.7%) than the consumption during rolling on an emulsion prepared from the serial emulsol "Universal-1TS". At the same time, the average concentration of emulsion when rolling on "Quakerol" emulsol was 1.9% against 3.0% on rolls rolled on LCL prepared from "Universal-1TS" serial emulsol. A higher specific consumption of electricity during the operation of the LCL from the experimental emulsol, which has a higher saponification number, may be the reason for an incorrectly selected and underestimated concentration of the emulsion in order to reduce the consumption of emulsol for rolling.

Contamination of rolled steel after rolling

In addition, the indicators of contamination after rolling were investigated. The results of the determination are given in Table 6.

Table 6

Surface contamination of the test metal after cold rolling

Steel grade, size	Coil	Contamination, mg/m^2		Average value, mg/m^2		Average total contamination mg/m^2
		Fat	Mechanical	Fat	Mechanical	
Experimental coils rolled on emulsion of emulsol "Quakerol" oiled by "Quakerol"						
DC01, 2.3/0.65x1000 mm	1	585	500	470	522	992
		458	579			
		367	486			
	2	400	560	360	649	1009
		470	520			
		210	867			
Average contamination of the rolled surface on the LCL with emulsol "Quakerol" oiled by "Quakerol"				415	586	1001
Coils rolled on emulsion from serial emulsol "Universal-1TS" oiled by "OK-2"*						950

* – data obtained from other studies.

As can be seen from Table 6, the average value of surface contamination of metal samples oiled and rolled with the use of experimental emulsion "Quakerol" is 51 mg/m^2 or 5% higher than that of samples oiled with emulsion "OK-2" and rolled on serial emulsion "Universal-1TS" and is 1001 mg/m^2 against 950 mg/m^2.

Conclusions

1. The method with the use of emulsions has been developed and tested to estimate the energy-power parameters during cold rolling. The influence of rolling process conditions on energy-power parameters of rolling with the use of emulsol "Quakerol" is described for a four-roller mill.

2. The average total load on the stands' motors and the winder of the 1680 four-standmill in the stable rolling mode was found when using the "Quakerol" emulsion is 4.19% higher than when rolling the same assortment rolled on the emulsion from "Universal-1TS".

3. The level of energy consumption during rolling in the four-standmill using "Quakerol" and "Universal-1TS" emulsols was established. It is shown that the total specific consumption of electricity when rolling on an emulsion prepared from the experimental emulsol "Quakerol" is 2.7% more than when rolling on an emulsion prepared from the serial emulsol "Universal-1TS". The higher specific energy consumption during the operation of the LCL from the experimental emulsol, which has a higher saponification number, may be the reason for the incorrectly chosen and underestimated concentration of emulsion in order to reduce the emulsol for rolling consumption.

4. The average concentration of the emulsion on the analyzed coils rolled on LCL from the experimental emulsol "Quakerol" was 1.9% versus 3.0% on the coils rolled on LCL from emulsol "Universal-1TC".

5. The assessment of contamination of the metal surface after rolling is given. It was found that the use of the investigated emulsol "Quakerol" increases the average value of surface contamination.

References

1. Vasilev Y.D., Samokish D.N., Bondarenko O.A., Mospan N.V. (2022) Determination of particular relative reduction in cold rolling of thin and extra thin strips to implement the process with the least force. Science and Innovation, 18 (3), 49–57.

2. Buchmayr B., Degner M., Palkowski H. (2018) Future challenges in the steel industry and consequences for rolling plant technologies. Berg Huettenmaenn Monatsh, 163, 76–83.

3. Pittner J., Simaan M.A. (2008) Optimal control of continuous tandem cold metal rolling. American Control Conference. Seattle, Washington, USA, 2834–2839.

4. Asghar M.T., Jungers M., Morarescu I.-C., Khelassi A., Francken J. (2016) Tandem cold rolling mill modeling for multi-variable control synthesis. 17th IFAC Symposium on Control, Optimization and Automation in Mining, Mineral and Metal Processing, Vienna, Austria, hal-01393445.

5. Tahir M., Ståhlberg U. (2002) Environmental improvement by using a water-based synthetic lubricant in steel-strip rolling. Iron and Steel Society/AIME, 44th Mechanical Working and Steel, Orlando, USA, 40, 291–302.

6. Mazur V.L., Timoshenko V.I., Prikhod'ko I.Y. (2019) Stability loss and defects in coils of cold-rolled strip. Steel in Translation, 49, (1), 58-65.

7. Kurpe O., Kukhar V., Puzyr R., Balalayeva E., Klimov E. (2020) Electric motors power modes at synchronization of roughing rolling stands of hot strip mill. 25th IEEE Int. Conf. on Problems of Automated Electric Drive. Theory and Practice (PAEP' 2020), Kremenchuk, 510–513.

8. Kukhar V., Korenko M., St'opin V., Karmazina I., Elchaninov A., Hurkovska S., Prysiazhnyi A., Zubrytskyi V. (2019) Operation modes of electric motors of reversing cold rolling mill 1680 while rolling with emulsions. 2019 IEEE Int. Conf. on Modern Electrical and Energy Systems (MEES), Kremenchuk, 46–49.

9. Vasilev Y.D., Dementienko A.V. (2002) Model of friction stresses during thin sheet rolling. Izvestiya Ferrous Metallurgy, 1, 29–33.

10. Kukhar V., Artiukh V., Aleksandrovskiy M., Dykha A. (2020) Contact-deformation mechanism of boundary friction. E3S Web of Conferences, 164, 14004.

11. Kukhar V., Balalayeva E., Nesterov O. (2017) Calculation method and simulation of work of the ring elastic compensator for sheet-forming. MATEC Web of Conferences, 129, 01041.

12. H. Li. (2008) A study on wear and surface roughness of work roll in cold rolling. University of Wollongong.

13. H.C. Li, Z.Y. Jiang, , A.K. Tieu, W.H. Sun, D.B. Wei (2011) Experimental study on wear and friction of work roll material with 4% Cr and added Ti in cold rolling. Wear, 271 (9–10), 2500–2511.

14. Dolmatov A.P., Morozov A.V., Usachev M.A., Shipilov V.D., Chelyadinov A.A. (2015) Testing of rolling oils made by the Henkel company on a continuous five-stand 2030 mill. Metallurgist, 58 (9–10), 788–795.

15. Naizabekov A., Samsonov D., Krivtsova O., Lezhnev S., Talmazan V., Arbuz A. (2013) Comparative evaluation of technologic lubricants". 22nd Int. Conf. on Metallurgy and Materials (METAL 2013), Brno, 403–407.

16. Kukhar V. V., Vasylevskyi O. V. (2014) Experimental research of distribution of strains and stresses in work-piece at different modes of stretch-forging with rotation in combined dies. Metallurgical and Mining Industry, 3, 71–78.

17. Santos R.M., Rodrigues D.G., Santos M.L.D., Santos D.B. (2022) Martensite reversion and strain hardening of a 2304 lean duplex stainless steel subjected to cold rolling and isochronous annealing at low temperatures. Journal of Materials Research and Technology, 16, 168–186.

18. W. Li, J. Gu, Y. Deng, W. Mu, J. Li. (2022) New comprehension on the microstructure, texture and deformation behaviors of UNS S32101 duplex stainless steel fabricated by direct cold rolling process. Materials Science and Engineering: A, 845, 143150.

19. Q. Ye, G. Han, J. Xu, Z. Cao, L. Qiao, Y. Yan. (2022) Effect of a two-step annealing process on deformation-induced transformation mechanisms in cold-rolled medium manganese steel. Materials Science and Engineering: A, 831, 142244.

20. Lemarquis L., Giroux P. F., Maskrot H., Barkia B., Hercher O., Castany P. (2021) Cold-rolling effects on the microstructure properties of 316L stainless steel parts produced by Laser Powder Bed Fusion (LPBF). Journal of Materials Research and Technology, 15, 4725–4736.

21. Haikova T., Puzyr R., Savelov D., Dragobetsky V., Argat R., Sivak R. (2020) The research of the morphology and mechanical characteristics of electric bimetallic contacts. 25th IEEE Int. Conf. on Problems of Automated Electric Drive. Theory and Practice (PAEP 2020), Kremenchuk, 579–582.

22. Zagirnyak M., Prus V., Somka O., Dolezel I. (2015) Models of reliability prediction of electric machine taking inTo account the state of major structural units. Advances in Electrical and Electronic Engineering, 13 (5), 447–452.

23. Zagirnyak M., Maliakova M., Kalinov A. (2015) Compensation of higher current harmonics at harmonic distortions of mains supply voltage. 16th Int. Conf. on Computational Problems of Electrical Engineering (CPEE 2015), Lviv, 245–248.

24. Reva I., Bialobrzheskyi O., Todorov O., Bezzub M., Dziuban V. (2021) Power consumption mode investigation of a transformer with asymmetric load under the condition of active parts temperature change. 20th IEEE Int. Conf. on Modern Electrical and Energy Systems, (MEES), Kremenchuk, 1–5.

Кухар В.В., Малій Х.В., Спічак О.Ю. Вплив типу емульсолів на енерговитрати та забруднення поверхні при холодній прокатці сталі DC01 на безперервному чотирьохклітьовому стані

У статті представлено результати експериментальних і промислових випробувань фізико-хімічних параметрів експериментального емульсолу "Quakerol". За фізико-хімічними показниками експериментальний емульсол "Quakerol" відрізняється від використовуваного емульсолу "Універсал-1ТС" більш високими змащувальними властивостями. Були проаналізовані режими роботи електродвигунів кліті та моталки «тандемного» стану під час прокатки на ЛПЦ розплавів з експериментального емульсолу "Quakerol", змащеного емульсолом "Quakerol", та серійного емульсолу "Універсал-1ТС", змащеного консерваційною оливою "ОК-2". Результати аналізу навантажень під час прокатки полос перерізом 0,68×1000 мм із попередньо прокатаного листа товщиною 3,0 мм показали, що значення середніх сумарних навантажень на двигуни кліті та моталки чотириклітьового стану 1680 вищі за умови використання експериментального емульсолу "Quakerol". Дано порівняльний аналіз експериментально отриманих даних щодо впливу технологічних умов виробництва холоднокатаних рулонів на чотирьохклітьовому безперервному тандемному стані 1680 з використанням емульсолів "Quakerol" і "Універсал-1ТС" на силові параметри прокатки, витрату електроенергії та забруднення поверхні плоскої вуглецевої сталі DC01. Для опису витрат електроенергії під час прокатки з використанням різних емульсій отримано рівняння множинної регресії, як варійований фактор узято значення площі поперечного перерізу. Оцінено питому витрату електроенергії та середнє сумарне навантаження на кліті й двигуни моталок під час прокатки з використанням емульсолу, приготованого з експериментальної емульсії "Quakerol", і емульсолу, приготованого зі стандартної емульсії "Універсал-1ТС". Проаналізовано причини більш високої питомої витрати електроенергії при роботі ЛКЛ з експериментальною емульсією. Дано кількісну оцінку забруднення поверхні сталевих зразків під час використання експериментальної емульсії "Quakerol", оливи"ОК-2" і стандартної емульсії "Універсал-1ТС". Обґрунтовано необхідність проведення подальших випробувань з визначення оптимальної концентрації емульсії з "Quakerol" для забезпечення зниження енерговитрат на тонну холоднокатаного прокату.

Практична значимість роботи полягає в розробці методики аналізу мастильних матеріалів з урахуванням перспектив використання емульсії "Quakerol" замість емульсії "Універсал-1ТС", з метою поліпшення якісних показників і збільшення продуктивності цеху холодної прокатки.

Ключові слова: холодна прокатка, безперервний стан 1680, емульсол, енергоспоживання, питомі витрати електроенергії, забруднення поверхні

***Problems of Tribology**, V. 27, No 4/106-2022, 27-38*

Problems of Tribology
Website: http://tribology.khnu.km.ua/index.php/ProbTrib
E-mail: tribosenator@gmail.com

DOI: https://doi.org/10.31891/2079-1372-2022-106-4-27-38

Theory and experiment of tribological test methods

O. Dykha*, A. Staryi, M. Getman, V. Fasolia

Khmelnitskyi National University, Ukraine
**E-mail: tribosenator@gmail.com*

Received: 11 September 2022: Revised: 25 October 2022: Accept: 21 November 2022

Abstract

Based on the analysis of the current state of test methods for wear of friction pairs and the need for methods with certain operating conditions, the problem of developing a theory of test methods for wear of friction pairs according to the ball-cylinder scheme was solved, which makes it possible to determine the parameters of wear models and the general characteristics of the wear resistance of materials. It is shown that the type of wear within the range of properties of the friction pair parameters ensures compliance with the basic conditions in contact: materials, lubrication, pressure, speed, temperature, type of movement, and other less significant factors. It has been established that one of the fundamental issues in the development and conduct of wear tests is to take into account the influence of the stationarity of the wear mode at a point. Test methods in steady and unsteady modes (transient mode) are different. The test method should be based on the solution of the contact problem for a friction pair sample-counter-sample. Based on the solution of wear-contact problem for the "ball-cylinder" scheme, a theory has been developed for identifying the parameters of the wear pattern. To solve the inverse problem, a method of approximating function is proposed and implemented. The power approximation of the experimental function after substitution into the resolving equation gives simple expressions for calculating the model parameters. The results obtained make it possible to predict the intensity of wear of tribocouples under given initial operating conditions: according to loads, sliding speed, characteristics of lubricants and structural materials.

Keywords: wear, friction pairs, tribological tests, contact task

1. Modern approaches to the technique of tribological tests. Experiment, theory, methods, equipment.

A review of research on modern highly cited periodicals in the field of friction and wear regarding the problems of tribological testing is proposed.

The article [1] presents the development, manufacture and testing of an experimental bench for assessing the fretting fatigue of conductor materials in power lines. The friction machine has three independent drives that allow testing under a controlled load. This makes it possible to study the influence of relevant parameters on the fretting fatigue process (such as normal, tangential and body forces, wear level and wear surface morphology).

In [2], the technological problem of testing jet engine parts under conditions close to operational ones is solved. A bench for testing blade friction is proposed to study the occurring phenomena and the behavior of rotor blades during contact interactions between the blades and the engine housing. A feature of the presented installation is the possibility of increasing the number of working elements of the chamber, which makes it possible to produce more than one contact per revolution. This article discusses the test setup and its components, the experimental procedure, and examples of results.

In [3], laser microscopy was used to quantify wear mechanisms. The results showed that for some mechanisms it is possible to obtain quantitative data for the classification of wear and tear in accordance with ASTM G98. Some suggestions for modification and improvement of the standard are offered.

In work[4]. The study of the brake pad for friction and wear is carried out on an inertial brake dynamometer at various temperatures (200°C, 250°C and 300°C). The actual field tests are carried out on four

different trucks, namely a city bus (CB), a high speed bus (HSB), a highway truck (HWT) and a dump truck (TL). This study will be useful for developing the composition of the friction material and predicting the actual life of the brake pad for various trucks.

The article [5] presents experimental setups for conducting research on real machine components and obtaining more realistic results than conventional tribological test benches. Slope pad plain bearings, as well as gears and complete gearboxes for advanced industrial applications, can be tested using the benches described in the article. A double disc machine and a closed loop gear test bench are used to investigate the various wear mechanisms that occur in gears.

The authors of the study [6] study the problem of reducing friction and wear in metal-metal systems, as well as in some mechanical components. This paper presents a computational study based on Archard's linear wear law and Finite Element Method (FEM) modeling for dry sliding wear analysis in pin-on-disk testing. The Archard wear model was implemented in a FORTRAN user routine (UMESHMOTION) to describe sliding wear. The modeling of wear particle formation mechanisms was taken into account using the overall wear factor obtained from experimental measurements. In such an implementation, a step-by-step calculation of surface wear based on nodal displacements is considered using adaptive mesh tools that rebuild local nodal positions. Numerical and experimental results were compared in terms of wear rate and friction coefficient. In addition, during numerical simulation, the distribution of the stress field and the change in the surface profile across the worn track of the disk were analyzed.

In the study[7], based on the classical theory of adhesive wear by Archard, a three-dimensional finite element model was created to simulate the process of destruction of self-lubricating spherical plain bearings under conditions of oscillatory wear. The results show that self-lubricating spherical plain bearings go through two different stages in the wear process, namely an initial wear stage and a stable wear stage. The moment of friction at the initial stage of wear is somewhat less than the moment of friction at the stage of stable wear; however, the wear rate in the initial wear stage is high. The developed finite element model can be used to analyze bearing wear mechanisms and predict bearing life.

The article [8] experimentally and theoretically investigates the effect of lubrication on stresses at high temperature. A statistical formula has been developed to predict the Striebeck curves given the interaction of asperities with lubricant on the contact surface. It has been found that increasing the temperature at the interface can significantly change the performance of the lubricant due to the influence of the lubricant additive and that the conventional assumption of a constant coefficient of friction for a rough contact is not practical. As the temperature increased, the boundary layer formed by the lubricant molecules dissolved, and a soft solid layer was formed by lubricant additives at the contact boundary. It was also found that in the boundary lubrication regime, friction depends on the sliding speed due to the formation-destruction cycle of a soft hard layer,

It is noted in [9] that the characteristics and service life of structural materials at high temperatures are largely affected by the degradation of the material during wear and corrosion. To evaluate material performance at high temperature, it is necessary to understand the processes and their interactions to select and develop new advanced materials. In the present study, an experimental setup for testing and high-temperature abrasion is presented, taking into account the oxidation process.

In [10], the change in temperature over time in a deep groove ball bearing in an oil bath lubrication system was experimentally and analytically studied. The test device is a radially loaded ball bearing equipped with instruments to measure the friction torque as well as the transition temperature of the outer ring, oil and housing. The developed mathematical model provides a comprehensive thermal analysis of a ball bearing, taking into account frictional heat release, heat transfer processes and thermal expansion of the bearing components. Experiments are carried out for various speeds and loads to test the model. It has been established that the predicted temperatures at various loads and speeds agree well with those measured experimentally.

The article [11] discusses the optimization of the tribological characteristics of lubricating oils used in the processing industry. Optimum lube oil performance is determined by multivariate optimization of viscosity, temperature and oil film thickness. Experimental test results are shown for the oil used in the real plant and the new oil obtained from the simulation.

Reference [12] presents a methodology for deriving pressure-dependent friction laws from experimental tribometric testing of rubber-to-metal contacts. Tribometric tests are simulated to analyze the contact area and obtain an approximation of the contact pressure distribution. The proposed methodology is recommended for evaluating the experimental results of tribometric tests carried out according to the "flat surface" and "cylinder surface" schemes. Planar and cylindrical materials have been fabricated with very similar surface morphology and therefore theoretically the same pressure dependence of the law of friction.

Article [13] contains a description of the test bench and the first experimental data concerning the mechanical and thermal characteristics of a rotor supported by air-lubricated bearings under external pressure. The stand allows you to load the rotor radially and axially in both static and dynamic modes, as well as measure the orbits on the supports. Rotating unbalance response at various speeds has been measured up to 60,000 rpm. The rotor is stable and has no vortex instability.

The authors of this work analyzed the methods for identifying the parameters of wear patterns for various wear models and test schemes [14-17].

The above review of the literature confirms the versatility of tribological testing methods in terms of techniques, test conditions, materials, design of benches and samples, modeling procedures and processing of experimental results.

2. Basic principles of tribological testing

2.1 Duration of tribological tests

Wear reduction is carried out mainly in three directions: 1) the creation of wear-resistant surfaces based on the laws of tribomaterials science; 2) creation of lubricants, lubricating additives and lubricating systems; 3) creation of methods for reliable prediction of wear of components based on theoretical tribology.

With regard to friction units, the stages of a rational test cycle are formulated as follows: 1) selection of combinations of materials based on a priori information; 2) identification of the boundaries of compatibility of a friction pair in terms of the determining parameter; 3) modeling on samples of the operating conditions of tribocouplings; 4) full-scale simulation on the stand, taking into account the main operational parameters of the tribocouplings; 5) full-scale modeling, taking into account the typical operating conditions of the friction unit in the machine during operation.

If wear tests of a friction pair are carried out strictly under the operating conditions of the unit, taking into account the statistical nature of wear, then the duration of the testing process for a statistically representative number of samples can last for months and even years. There are various methods for forcing tests in order to speed up the process. It is shown that without building reliable mathematical models of nonlinear wear processes, the use of accelerated wear testing methods can lead to errors. Based on the considered models, the following methods of accelerated forced tests are proposed: 1) extrapolation in time; 2) extrapolation by load; 3) the principle of requests; 4) interpolation on intervals; 5) extrapolation on intervals; 6) double consecutive extrapolation; 7) double parallel extrapolation, etc.

The analysis of the methods shows that the main success in the application of various accelerated methods is determined by the reliability of the mathematical model underlying the process. The friction unit of any machine, regardless of the designer, technologist or operator, goes through at least two stages during operation: the running-in stage and the stage of steady wear. When developing methods for accelerated wear testing of materials, it is necessary to take into account the presence of transient processes and running-in at the initial stages.

2.2. Test schemes and conditions in contact

The decisive role in the validity of the laboratory test method is played by the geometry of the contacting elements. Geometric schemes are systematized or simply given in many reference books and articles. In most of the frequently used test schemes, for example, ball-plane, etc., none of the publications provides formulas for calculating contact pressures, the main parameter of test conditions. This is in most cases one of the main causes of scatter and non-reproducibility of test results. On the other hand, the lack of information about the change in pressure conditions during the test devalues the results, making them estimates, as in the case of tests on a four-ball.

Can be offereda list of factors affecting the difference between the rated contact voltages and those calculated under standard conditions. Consideration of this list gives an idea of the reasons for the dispersion of wear test results according to different test schemes: 1) subsurface stress concentrators: grain boundaries, twins and other concentrators; 2) the nature of the surface: topography, texture, residual stresses; surface energy level; microstructure, pollution; 3) surface defects: inclusions and particles of the secondary phase; dents and scratches; grooves and risks; corrosion, rust; traces of etching; fretting traces; slip marks; 4) discontinuities in contact geometry: ends of line contacts; wear particles in the contact area; 5) load distribution inside the bearing: elastic deformations; distortion of parts; clearance in contact; 6) elastic-hydrodynamic lubrication; 7) tangential forces: no slip; sliding rolling.

The first three main factors that determine wear are: pressure - P, sliding speed - V and contact temperature T. Accounting for these three factors requires a three-factor experiment. The planning of such tests can be carried out according to the well-known mathematical theory of experiment planning.

The environment in which the friction unit operates has a decisive influence on the scheme and test method. When testing friction pairs in the presence of lubricants, their ball circuit is used. The criterion for the quality of the lubricant here is the bulk temperature at which the contact oil layer is destroyed, which is fixed by a sharp increase in the friction coefficient. However, this method, in terms of physical meaning, is the furthest (in comparison with other methods) from reproducing the actual pattern that occurs in contact during friction. It is proposed to give preference to a flat contact as the most specific and corresponding to real nodes.

Obviously, to a large extent, negative conclusions about the four-ball scheme are explained by the lack of methods for estimating contact pressures and neglecting wear. Improvements in the accuracy of determining the anti-wear properties on a four-ball machine can be obtained using the pre-print method.

It is experimentally shown on a four-ball machine that the volumetric wear of a spherical sample is a single-valued linear function of the work of the friction forces. A linear dependence of wear on pressure was also obtained. Obviously, the results obtained are of a particular nature and are valid for specific test conditions.

BThe large discrepancy in determining the results of wear tests by various methods in the absence of lubrication and abrasive effects, according to studies performed in the USA, is due to factors:

1) heterogeneity and instability of surface morphology and wear marks;
2) the presence of particles on the sliding surface as a third body;
3) dynamic rigidity of the installation, as a factor leading to load fluctuations;
4) the shape of the sample or test design leads to different coefficients of variation of the results.

2.3. Wear measurements, testing machines

The wear measurement method is an integral part of the wear test method. The literature describes in detail the methods of artificial bases: the method of imprints, the method of punched imprints, the method of cut holes, and the concept of the method of radioactive isotopes is given. All methods are divided into periodic or discrete and continuous without stopping the machine. Among discrete methods, methods are distinguished: 1) micrometric measurements; 2) weighing; 3) profiling; 4) artificial bases. Continuous methods: 1) according to the content of wear products in used oil; 2) radioactive isotopes; 3) pneumatic micrometering; 4) according to the flow rate of the working medium through the slots between the rubbing surfaces; 5) lever devices and indicators; 6) mesdoses; 7) inductive sensors: 8) strain gauge micrometering.

Any testing machine can be considered as a system consisting of two main parts: 1) testing unit: sample, counter-sample and their fastening; 2) everything else: drive, gears, electrical part, loading, etc.

The study of the parameters of wear particles provides such information about the nature and intensity that it is difficult to overestimate. Obviously, this branch of tribology is still waiting for its intensive development. Photographs of the surfaces of wear particles show that their structure and geometry practically repeat the surface layers of the bodies. By the type of particles, one can judge the stage of wear. Information about particle morphology can be obtained using a bichromatic microscope. The shape of the wear products themselves corresponds to the implemented friction mechanisms. For normal wear, the particles are lamellar; for abrasive - the form of microchips; Fatigue fracture mechanisms correspond to particles of rounded geometry or even spherical ones.

At present, wear particle analysis is widely used to monitor the condition and predict the failure of lubricated components in machines. The parameters of the wear particles reflect both the nature and degree of wear of the rubbing surfaces. Methods and devices for diagnosing the state of machines based on wear particles distinguish between external and built-in. An analysis of patents and publications points to the intensive development of built-in ferrodiagnostics devices. In this case, a variety of principles are used: spectral analysis, ferrography, light scattering, in-line ultramicroscopy, activation methods.

2.4. Wear contact tasks

Contact pressures are one of the first three main factors (pressures σ ,temperature T , sliding speed V), determining the intensity of surface wear for given materials and lubricants.

The role of pressure here is close to the role of the stress state in the problem of ensuring strength. In problems of contact strength, contact pressures are also defined as the first stage in solving a strength problem. At the second stage, the stress state is determined, at the third stage, using the criteria of strength, ductility or fatigue, the question is decided whether the structure will fail or not. The logic of assessing the state of the friction unit in terms of wear is somewhat different. At the first stage, for a given pair of friction and lubrication, the dependence of wear is studied u_w or wear rate du_w/dS from the main factor - pressures and friction paths, the parameters of this dependence are determined.

At the second stage, the contact problem is solved taking into account the wear for the considered friction unit, for example, for a plain bearing, and the dependence of the wear of this unit on the load dimensions and the found model parameters is determined.

At the third stage, this dependence, taking into account the parameters of the model, calculates the wear of the assembly and compares it with the allowable wear. This stage can be performed in a deterministic setting based on average values or in a probabilistic setting with an estimate of the reliability of the node.

In the general case, the statement of the contact problem for two bodies, taking into account wear, consists of the following equations and conditions. The first basic basic relation is the condition of continuity in contact in algebraic form:

$$u_e(x, y, s) + u_w(x, y, s) = u(x, y),$$

where $u(x, y, S)$ -full elastic normal contact displacements of both bodies; x, y -coordinates, s -friction path.

The second basic equation in the formulation of the problem is the equation of equilibrium of contacting bodies:

$$Q = \int_F \sigma(x, y, S) dF ,$$

where Q -the total load acting on the bodies (the projection of the load on the vertical axis); $\sigma(x, y, S)$ - projection of contact pressures on the same axis; F -contact surface area.

The third basic relation of the contact problem with wear is the equation of the wear model in differential form:

$$\frac{du_w}{ds} = F(\sigma, s)$$

or in integral form:

$$u_w(s) = \int_0^S F(\sigma, s) ds .$$

The complexity of the final equation and the success of solving the problem as a whole largely depend on the degree of complexity of the wear model.

The development of methods for solving contact problems with wear taken into account has gone from the simplest problems to the refinement of models and the complexity of solutions. The wear model is a differential (or integral) relationship between wear and the main factors. In this paper, of these factors, only the influence of pressure is studied.

The test method should be based on the solution of the contact problem for a friction pair sample-counter-sample. Rigorous solutions of this problem with allowance for compliance are complex. It is promising to use a calculation scheme in which the contacting bodies are rigid. With sufficiently large wear, neglect of elasticity is permissible.

Based on the analysis of the current state of test methods for wear of friction pairs and the need for methods with uniquely defined operating conditions for contact pressures, the following task was set and solved in this work: development of a theory of a test method for wear of friction pairs according to the ball-cylinder scheme, which makes it possible to uniquely determine the parameters wear patterns and general characteristics of the wear resistance of materials.

2.4. Wear models

Models (law) of wear processes are dependences of the intensity of wear (or wear) on the determining factors of the process, which are used in the design of friction nodes, forecasting their wear and to optimize structural, technological and other parameters. The pattern of wear can be applied in practice, if the algorithm for determining the parameters of this pattern is known. It is the quantitative parameters that make it possible to assess the influence of determining factors (pressure, temperature speed). The parameters can be set only based on the results of experimental tests, which makes the model close to the real operating conditions of the friction unit.

The theory of determining the parameters of wear models is developed on the basis of the solution of inverse wear-contact problems (that is, when the dependences for the calculation of parameters are determined according to the accepted mathematical form of the law of wear, geometric ratios (conditions of continuity in contact), equilibrium conditions.

The more determining factors in the model, the more difficult the solution. So already two parameters (for example, pressure and speed) significantly complicate the task and require certain assumptions.

In this work, a conceptual methodology is considered, one of the main tasks of which is the development of the theory of test methods for the identification of wear parameters.

It is proposed as the most appropriate test schemes to use schemes when during the tests the contact pressure changes due to a change in the contact area, which makes it possible to have results for the pressure range based on the results of the tests of one sample. Such test schemes include: four-ball scheme, sphere - ring, cone - ring cross cylinders, cylinder - plane, sphere - plane and others.

For the tests, the scheme is adopted, which, according to geometric and technological features, most closely corresponds to the real tribo-coupling. Thus, the wear models obtained by the four-ball scheme should be used to evaluate the wear resistance of connections in which contact is made along a line or at points (gears, cam mechanisms) with small contact area sizes. For connections in which the dimensions of the contact area are commensurate with the dimensions of the contacting bodies (sliding bearings, ball bearings), other test schemes should be used: "cone-ring", "sphere-ring", which more adequately correspond to real contact.

At the initial stages of solving this problem, the theoretical foundations of test methods were considered only for the contact pressure factor. In this work, methods of the theory of tests for a larger number of determining factors for the above-mentioned test schemes with a variable contact area are developed. This made it possible to evaluate the influence of speed and temperature factors on the wear process.

Having a developed theoretical apparatus, tests of the friction unit are carried out in conditions close to real ones (in terms of materials, lubrication, temperature, etc.) and the parameters of the wear model are quantitatively calculated.

Based on the obtained wear model, you can:

- calculate (predict) the wear of the unit under different conditions based on contact pressure and sliding speed, for example, at the stage of the design calculation of the friction unit;
- to optimize the structural and technological parameters of the friction unit according to the wear criterion.

The proposed calculation-experimental approach does not give one hundred percent compliance with the real flow of the process, but it is a necessary way to create calculation engineering methods for predicting the wear resistance of friction nodes of technical tribostems.

3. Implementation of the method of tribological testing of structural and lubricant materials according to the "ball-cylinder" scheme

To simulate the wear of a spherical indenter along a cylinder, a wear regularity (model) is proposed in the form of a dimensionless complex of determining factors (contact pressure and sliding speed):

$$\frac{du_W}{dS} = fC_W \left(\frac{\sigma}{HB} \right)^n \left(\frac{VR^*}{\nu} \right)^p , \tag{1}$$

where u_W is the ball wear;
S is the friction path;
f is the coefficient of friction in the ball-cylinder pair;
σ is the normal contact pressure;
HB is the hardness of the ball material;
V is the sliding speed;
R^* is the reduced radius of the sphere and cylinder;
ν is the kinematic viscosity of the oil;
C_W, n, p are the wear resistance parameters.

Let us take the form of the worn surface of the ball in the form of a circular sector with a profile radius a (Fig. 1).

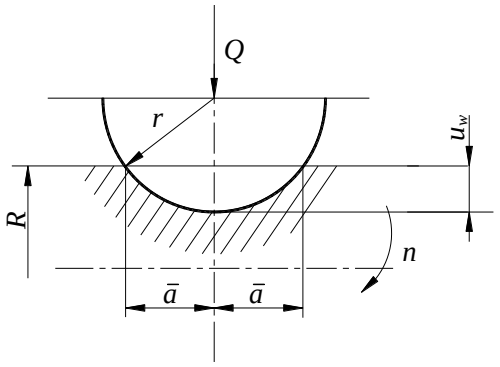

Fig. 1. Scheme of contact "cylinder-ball": Q is load; n is the speed of rotation; $\bar{a}$ is the half-width of the contact; R, r are the radius of the cylinder and balls

We also assume that the contact pressure under the wearing ball on the non-wearing surface of the cone is uniformly distributed:

$$\sigma = \frac{Q}{\pi a^2} . \tag{2}$$

In the case of ball-plane contact, the maximum wear of the ball is determined by the expression:

$$u_W = \frac{a^2}{2r}, \tag{3}$$

where r is the radius of the ball.

In the case of ball friction not along a plane, but along a cylindrical rotating surface, the dependence of wear on the contact radius will to some extent differ from that accepted for a plane. Let us estimate the magnitude of this deviation.

For friction on the cylinder, the contact area on the ball is curved and is performed along the radius of the cylinder R. In this case, with the same (with a plane) contact area, the wear value (3) is added to the wear value:

$$u_{W_1} = \frac{a^2}{2R}, \tag{4}$$

where R is the radius of the cylinder.

The relative error in determining wear from not taking into account the curvature of the cylinder, taking into account (3) and (4), is determined by the ratio:

$$\frac{u_W}{u_{W_1}} = \frac{r}{R}. \tag{5}$$

It follows that an error of 1% is provided for a ratio of radii of 1/100. Yes, at $r = 6.35$ mm the radius of the cylinder should be $R = 635$ mm, which does not seem correct for the design of the test facility.

It follows from the obtained estimate that the use of the formula for calculations when testing a ball-cylinder pair can lead to errors. Therefore, it is necessary to take into account in the calculations of the parameters of wear models the total wear over the entire contact area:

$$u_W^* = \frac{a^2}{2r_1} + \frac{a^2}{2R} = a^2 \frac{r+R}{2Rr} = \frac{a^2}{R^*}.$$

where

$$R^* = \frac{Rr}{R+r}. \tag{6}$$

Thus, when testing for wear according to the ball-cylinder scheme, the dependencies for the ball-plane scheme can be used, if the ball radius is replaced by the reduced radius according to formula (6).

Let us represent the experimental dependence of the radius of a truncated sphere as a power approximating function:

$$a(S) = cS^{\beta}, \tag{7}$$

where c and β – approximation parameters, which are determined by the results of wear tests.

Integrating the wear pattern (1), we obtain the integral form of the ball wear model:

$$u_W(S) = fC_W \int_0^S \left(\frac{\sigma(S)}{HB}\right)^n \left(\frac{VR^*}{\nu}\right)^p dS. \tag{8}$$

Substituting the expression for wear into the left side of the obtained dependence $u_W = \frac{a^2}{2R^*}$, and to the right - the expression for the contact pressure (2), we get:

$$\frac{a^2(S)}{2R^*} = fC_W \int_0^S \left[\left(\frac{Q}{\pi \bar{a}^2(S)}\right)\frac{1}{HB}\right]^n \left(\frac{VR^*}{\nu}\right)^p dS, \tag{9}$$

or, taking into account (7), after integrating along the friction path, we obtain:

$$\frac{c^2 S^{2\beta}}{2R^*} = fC_W \left(\frac{Q_1}{c^2 \pi HB}\right)^n \left(\frac{VR^*}{\nu}\right)^p \frac{S^{1-2\beta n}}{1-2\beta n}. \tag{10}$$

From the condition of satisfiability of equation (10) for all values of S it follows:

$$2\beta = 1 - 2\beta n, \tag{11}$$

where:

$$n = \frac{1-2\beta}{2\beta}. \tag{12}$$

To define a parameter p tests are carried out at two values of the sliding speed V1 and V2, from which we obtain two groups of experimental data with approximating functions:

$$\begin{aligned} a_1 &= c_1 S^{\beta}; \\ a_2 &= c_2 S^{\beta}. \end{aligned} \tag{13}$$

Here we consider the problem of determining wear parameters based on the results of testing specimens with a changing contact area during wear. A change in the wear area causes a change in the values of the contact pressures. Exponent n expression (1) characterizes the rate of change of contact pressures during wear and is related to the index β experimental dependence (7), which characterizes the rate of change of the contact area during wear. Connection n and β in the accepted wear pattern (1) is uniquely described by relation (12). Since in the relations under consideration the sliding speed V does not depend on friction path S, then it does not affect the parameters n and β in the process of testing. In this case, changing the sliding speed V only affects the scale factor C_w in expression (1). The above reasoning is confirmed by the test results.

Substituting expressions (13) into (10) we obtain the system of equations:

$$\left.\begin{aligned} \frac{c_1^2 \beta}{R^*} &= fC_W \left(\frac{Q}{c_1^2 \pi HB}\right)^n \left(\frac{V_1 R^*}{\nu}\right)^p; \\ \frac{c_2^2 \beta}{R^*} &= fC_W \left(\frac{Q}{c_2^2 \pi HB}\right)^n \left(\frac{V_2 R^*}{\nu}\right)^p. \end{aligned}\right\} \tag{14}$$

Dividing the first equation by the second, after transformations we get:

$$(c_1 / c_2)^{2n+2} = (V_1 / V_2)^p. \tag{15}$$

Where:

$$p = (2n+2)\frac{\lg(c_1 / c_2)}{\lg(V_1 / V_2)}. \tag{16}$$

To determine the coefficient K_w we use one of the equations (14):

$$C_W = \frac{\beta c_1^{2n+2}}{fR^*} \left(\frac{\pi HB}{Q}\right)^n \left(\frac{\nu}{V_1 R^*}\right)^p. \tag{17}$$

Thus, formulas (12), (16) and (17) make it possible to determine the parameters of the wear pattern in the accepted form (1).

Methodology of experimental studies.

The tests of the bronze-steel pair were carried out according to the scheme of a spherical sample - a cylindrical counter-sample. A spherical surface with a radius of R = 6.35 mm was made at the end of a cylindrical specimen made of bronze with a diameter of 10 mm. The counterbody disk 96 mm in diameter and 12 mm thick was made of 40X steel, hardened and polished. The setup diagram is shown in fig. 2. The spherical sample 9, fixed in the body 8, is pressed against the counter-sample - disk 10 with the help of weights 7. The disk is lubricated by dipping in an oil bath 13. The disk is fixed on the shaft 4, which rotates in bearings 6 with the help of an electric motor 1 through a pulley 2 and a belt transmission 3.

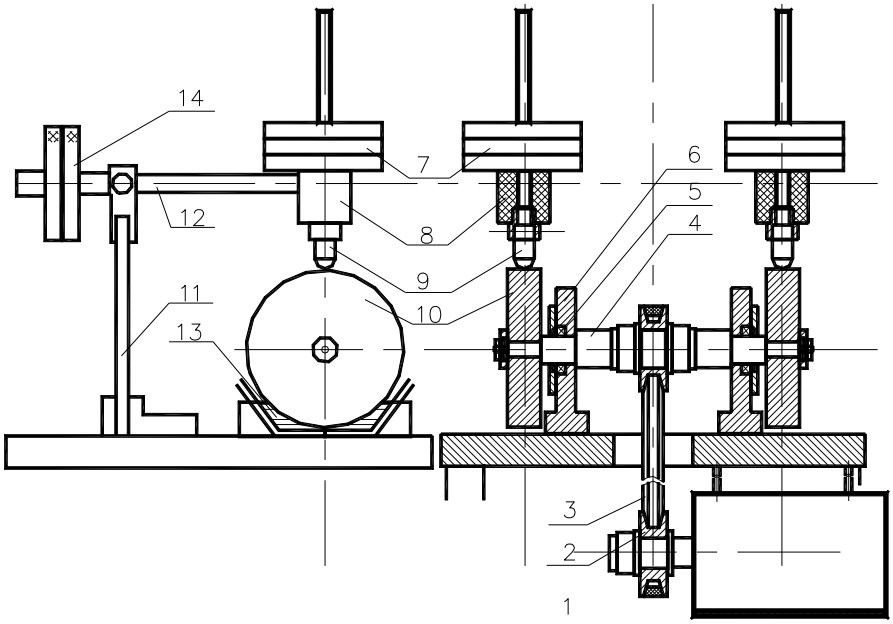

Fig. 2. Scheme of the ball-cylinder test setup: (1-motor, 2-pulley, 3-belt transmission, 4-shaft, 5-case, 6-bearing, 7-weights, 8-sample holder, 9-spherical sample , 10-counterbody (disk), 11-tension beam, 12-lever, 13-oil bath, 14-balance weight

The motor speed is adjustable from 0 to 1500 rpm. The load can be set up to 1 kg=10 N per sample. The installation provides for measuring the friction force using a strain gauge beam and lever 12.

The tests were carried out with the following initial data: the radius of the ball (sphere) of bronze - $r = 6,35$ mm; radius of counterbody, rotating disk $R = 48$ mm; sample load: $Q = 1$ H; the material of the ball is bronze, the disk is hardened steel; lubrication by dipping a rotating disk in a liquid lubricant; disk rotation speed 200 rpm, basic friction path of the ball surface 12 km = $12 \cdot 10^6$ mm. Lubrication was carried out with Magnum 15W–40 oil (TNK, Ukraine) with a viscosity of ν=40 mm2/s; friction coefficient f=0.08. Bronze hardness BrOF10-1 HB=90 MPa.

Reduced radius according to formula (6):

$$R^* = \frac{Rr}{R+r} = \frac{48 \cdot 6.35}{48+6.35} = 5.6 \text{ mm.}$$

When tested after a certain number of cycles, using a microscope, the diameter of the ball contact area is measured with an accuracy of microns. The test results are presented in table 1.

Table 1

Test results of a bronze sample during friction against a steel counterbody

No.	S, km	$a(V = 0.2m/s)$, mm	$a(V = 0.4m/s)$, mm
1	0.2	0.115	0.135
2	0.4	0.135	0.16
3	1.0	0.175	0.2
4	2.0	0.21	0.235
5	6.0	0.29	0.32
6	12.0	0.335	0.38

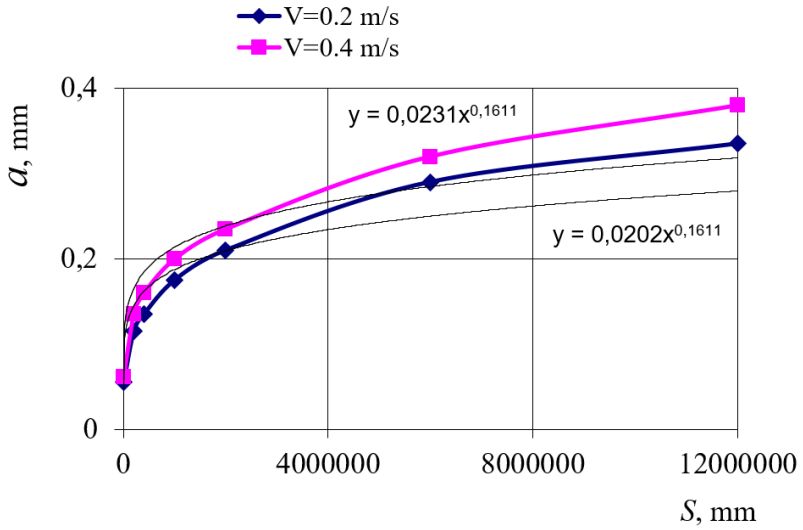

Fig. 2. Graphical interpretation of the test results and power-law approximation of the dependences of wear on the friction path a(S)/

On fig. 2, based on the test results, the dependence curves of the wear area dimensions on the friction path for two values of the sliding speed are plotted. The Excel program allows you to carry out a power-law approximation of the test results in the form (13) with a numerical determination of the parameters of this approximation, shown on the graphs in the form of equations of the trend line (9 approximating curves). The results of determining the parameters of these dependencies are shown in Table 2.

Table 2.

The results of the determination of the approximation parameters (13)

Options	V=0.2m/s	V=0.4m/s
c	0.0202	0.0231
β	0.1611	0.1611

In accordance with the procedure shown above, the parameter n can then be determined from formula (12):

$$n = \frac{1-2\beta}{2\beta} = \frac{1-2\cdot 0.1611}{2\cdot 0.1611} = 2.1.$$

According to formula (16), the parameter p is calculated:

$$p = (2n+2)\frac{\lg(c_1/c_2)}{\lg(V_1/V_2)} = (2\cdot 2.1+2)\frac{\lg(0.0202/0.0231)}{\lg(0.2/0.4)} = 1.19.$$

To calculate the coefficient C_w we use formula (17):

$$C_W = \frac{\beta c_1^{2n+2}}{fR^*}\left(\frac{\pi HB}{Q}\right)^n\left(\frac{\nu}{V_1R^*}\right)^p = \frac{0.1611\cdot 0.0202^{2\cdot 2.1+2}}{0.08\cdot 5.6}\left(\frac{3.14\cdot 90}{1}\right)^{2.1}\left(\frac{40}{0.2\cdot 5.6}\right)^{1.19} = 0.001402$$

.

Thus, we have the following calculated values of the parameters in the wear pattern (1): $n = 2.1$; $p = 1.19$; $C_W = 0.001402$, which identify this dependence and make it possible to predict the wear intensity of tribocouples under given initial operating conditions: by loads, sliding speed, characteristics of lubricants and structural materials.

Conclusions

1. Based on the analysis of the current state of test methods for wear of friction pairs and the need for methods with certain operating conditions, the problem of developing a theory of test methods for wear of

friction pairs according to the ball-cylinder scheme was solved, which makes it possible to determine the parameters of wear models and the general characteristics of the wear resistance of materials.

2. Models (law) of wear processes are dependences of the intensity of wear (or wear) on the determining factors of the process, which are used in the design of friction nodes, forecasting their wear and to optimize structural, technological and other parameters.

3. Based on the solution of wear-contact problem for the "ball-cylinder" scheme, a theory has been developed for identifying the parameters of the wear pattern. To solve the inverse problem, a method of approximating function is proposed and implemented.

4. The theory of determining the parameters of wear models is developed on the basis of the solution of inverse wear-contact problems (that is, when the dependences for the calculation of parameters are determined according to the accepted mathematical form of the law of wear, geometric ratios (conditions of continuity in contact), equilibrium conditions.

5. Having a developed theoretical apparatus, tests of the friction unit are carried out in conditions close to real ones (in terms of materials, lubrication, temperature, etc.) and the parameters of the wear model are quantitatively calculated.

References

1. Miguel A. Garcia, Luís Augusto Mendes Veloso, Fabio Comes de Castro, José Alexander Araújo, Jorge L.A. Ferreira, Cosme Roberto Moreira da Silva. Experimental device for fretting fatigue tests in 6201 aluminum alloy wires from overhead conductors, Wear,Volumes 460–461,2020, https://doi.org/10.1016/j.wear.2020.203448

2. S. Nitschke, T. Wollmann, C. Ebert, T. Behnisch, A. Langkamp, T. Lang, E. Johann, M. Gude. An advanced experimental method and test rig concept for investigating the dynamic blade-tip/casing interactions under engine-like mechanical conditions, Wear, Volumes 422–423,2019, Pages 161-166, https://doi.org/10.1016/j.wear.2018.12.072

3. J.A. Siefert, S.S. Babu. Experimental observations of wear in specimens tested to ASTM G98, Wear, Volume 320, 2014, Pages 111-119, https://doi.org/10.1016/j.wear.2014.08.017.

4. Surya Rajan, B., Sai Balaji, M.A. & Velmurugan, C. Correlation of field and experimental test data of wear in heavy commercial vehicle brake liners. *Friction* **5**, 56–65 (2017). https://doi.org/10.1007/s40544-017-0138-x

5.Ciulli, E. Experimental rigs for testing components of advanced industrial applications. *Friction* **7**, 59–73 (2019). https://doi.org/10.1007/s40544-017-0197-z

6.E.M. Bortoleto, A.C. Rovani, V. Seriacopi, F.J. Profito, D.C. Zachariadis, I.F. Machado, A. Sinatora, R.M. Souza. Experimental and numerical analysis of dry contact in the pin on disc test, Wear, Volume 301, Issues 1–2, 2013, Pages 19-26, https://doi.org/10.1016/j.wear.2012.12.005.

7. Xue, Y., Chen, J., Guo, S. *et al.* Finite element simulation and experimental test of the wear behavior for self-lubricating spherical plain bearings. *Friction* **6**, 297–306 (2018). https://doi.org/10.1007/s40544-018-0206-x

8. Chuhan Wu, Peilei Qu, Liangchi Zhang, Shanqing Li, Zhenglian Jiang. A numerical and experimental study on the interface friction of ball-on-disc test under high temperature, Wear, Volumes 376–377, Part A, 2017, Pages 433-442, https://doi.org/10.1016/j.wear.2016.11.035.

9. Maksim Antonov, Irina Hussainova. Experimental setup for testing and mapping of high temperature abrasion and oxidation synergy. Wear, Volume 267, Issue 11, 2009, Pages 1798-1803, https://doi.org/10.1016/j.wear.2009.01.008

10. Jafar Takabi, M.M. Khonsari. Experimental testing and thermal analysis of ball bearings, Tribology International, Volume 60, 2013, Pages 93-103, https://doi.org/10.1016/j.triboint.2012.10.009

11. Steven Chatterton, Paolo Pennacchi, Andrea Vania, Andrea De Luca, Phuoc Vinh Dang. Tribo-design of lubricants for power loss reduction in the oil-film bearings of a process industry machine: Modelling and experimental tests, Tribology International, Volume 130, 2019, Pages 133-145, https://doi.org/10.1016/j.triboint.2018.09.014.

12. J.M. Bielsa, M. Canales, F.J. Martínez, M.A. Jiménez. Application of finite element simulations for data reduction of experimental friction tests on rubber–metal contacts, Tribology International, Volume 43, Issue 4, 2010, Pages 785-795, https://doi.org/10.1016/j.triboint.2009.11.005

13. Guido Belforte, Terenziano Raparelli, Vladimir Viktorov, Andrea Trivella, Federico Colombo. An experimental study of high-speed rotor supported by air bearings: test RIG and first experimental results, Tribology International, Volume 39, Issue 8, 2006, Pages 839-845, https://doi.org/10.1016/j.triboint.2005.07.013.

14. Dykha A. Prediction the wear of sliding bearings / A. Dykha , D. Marchenko // International Journal of Engineering & Technology.–2018.– Vol. 7 No.2.23.– P. 4–8. DOI: 10.14419/ijet.v7i2.23.11872.

15. Dykha, A.V., Marchenko, D.D. & Dytynyuk, V.A. Determination of the Parameters of the Wear Law Based on the Results of Laboratory Tests. *J. Frict. Wear* **41,** 153–159 (2020). https://doi.org/10.3103/S1068366620020038

16. Dykha, A., Artiukh, V., Sorokatyi, R., Kukhar, V., & Kulakov, K. (2021). Modeling of wear processes in a cylindrical plain bearing. In *Advances in Intelligent Systems and Computing* (Vol. 1259 AISC, pp. 542–552). Springer. https://doi.org/10.1007/978-3-030-57453-6_52

17. Dykha A., Padgurskas J., Musial J., Matiukh S.. Wear models and diagnostics of cylindrical sliding tribosystem. Monograph. Bydgoszcz: Foundation of Mechatronics Development, 2020, 196p. ISBN 978-83-938655-5-0. http://znm.khnu.km.ua/wp-content/uploads/sites/23/2020/12/Wear_Models_and_Diagnostics.pdf

Диха О.В., Старий А.Л., Гетьман М.М., Фасоля В.О. Теорія та експеримент методів трибологічних випробувань

На основі аналізу сучасного стану методів випробувань на знос пар тертя та потреби в методах з певними умовами роботи вирішувалося завдання розробки теорії методів випробувань на знос пар тертя за схемою шар-циліндр, що дозволяють визначати параметри моделей зношування та загальну характеристику зносостійкості матеріалів. Показано, що вид зношування в межах розкиду властивостей параметрів пари тертя забезпечує дотримання основних умов контакту: матеріали, мастило, тиск, швидкість, температура, вид руху та інші менш істотні фактори. Встановлено, що одним із важливих питань при розробці та проведенні випробувань на знос є облік впливу стаціонарності режиму зношування у точці. Методики випробувань в режимах (режим перехідних процесів), що встановився і невстановлений, різні. В основі методу випробувань має лежати вирішення контактного завдання для пари тертя зразок-контрзразок. На основі рішення зворотної зносоконтактної задачі для схеми «куля-циліндр» розроблена теорія ідентефікації парметрів закономірності зношування. Для вирішення зворотного завдання запропоновано та реалізовано спосіб апроксимуючої функції. Ступенева апроксимація експериментальної функції після підстановки в вирішальне рівняння дає прості вирази для розрахунку параметрів моделі. Отримані результати дають можливість прогнозування інтенсивності зношування трибосполучень за заданих вихідних умов експлуатації: за навантаженнями, швидкістю ковзання, характеристиками мастильних і конструкційних матеріалів.

Ключьові слова: знос, пари тертя**,** трибологічні випробування, контактна задача

Problems of Tribology, V. 27, No 4/106-2022, 39-44

Problems of Tribology
Website: http://tribology.khnu.km.ua/index.php/ProbTrib
E-mail: tribosenator@gmail.com

DOI: https://doi.org/10.31891/2079-1372-2022-106-4-39-44

Effect of discrete basalt fiber on operational properties of polytetrafluoroethylene

O. Yeromenko[1*], A.-M. Tomina[1], I. Rula[2]

[1]*Dniprovsk State Technical University, Ukraine*
[2] *Dnipro State Agrarian and Economic University, Ukraine*
E-mail: eromenko81@gmail.com

Received: 15 September 2022: Revised: 30 October 2022: Accept: 29 November 2022

Abstract

The article examines the effect of discrete basalt fibers on the tribotechnical characteristics of DF-101 polytetrafluoroethylene according to the "disk-pad" scheme under conditions of friction without lubrication. It was established that the introduction of filler leads to decrease in the intensity of wear and the coefficient of friction of the base polymer 1,7 and 360 times, respectively. The improvement of these properties occurs because "anti-friction layer" that is more stable compared to unfilled polytetrafluoroethylene is formed in the process of friction of basalt plastics. As a result, friction occurs according to the "polymer-polymer" scheme. This is confirmed by a profound change in the morphology of the friction surface. For example, deep ploughing furrows and traces of adhesion with the counterbody are observed for polytetrafluoroethylene, while basalt plastics are more resistant to deformations, which, in turn, leads to a reduction of ploughing furrows. A sharp decrease in wear resistance 1,35-3,3 times is observed for basalt plastics containing 30-40 mass.% of fiber. It is probably a consequence of the growth of defects in the volume of the material due to the uneven location of the fiber in the polymer matrix. The confirmation of the presence of defects in the volume of basalt plastics is confirmed by a comparison of the calculated and experimental (hydrostatic) density. It was found that polytetrafluoroethylene loses 10% of its mass at a temperature of 823K, while the temperature of losing 10% of mass increases by 10 degrees for basalt plastic. It was determined that the effective content of the filler in the polymer matrix is 20 mass.%. The obtained basalt plastic (20 mass.% fiber) is recommended in manufacturing rolling and sliding bearings (as anti-friction protection) for tribological units of modern technology operating under the influence of high temperatures, aggressive environments and friction conditions without lubrication.

Key words: polytetrafluoroethylene, basalt fiber, wear intensity, coefficient of friction, friction unit

Introduction

Reliable and failsafe operation of friction units of systems and aggregates of mining, metallurgical and agricultural [1] machinery directly depends on their wear. It is known [2] that in operation process, the working bodies of friction units made of traditional metals undergo catastrophic wear manifested in the destruction of their surfaces, violation of the initial geometric shapes and weight. All the above leads to the loss of efficiency of the friction units, resulting in increased operating costs and a decrease in their efficiency.

Using fluoropolymer composite materials (FPCM) allows us to solve this problem and obtain a number of advantages. Thus, sliding [3] and rolling bearings (like anti-friction protection) [4], as well as piston and seal rings [5] made of FPCM, made it possible to increase the service life of the friction units of KINZE-7600 seeding-machine and sintering pallet cars, piston compressors of SO-7B and 4GM 2,5 U–3,4/2,8–251 2,5 times on average. The effectiveness of using these FPCM consists in the complete rejection of lubricants, increased wear resistance, reduced coefficients of friction and linear expansion, the number of planned preventive maintenances and equipment downtime.

Literature review

Effective fillers for creating wear-resistant FPCM are fibers of various natures such as carbon, organic, glass, etc. However, these composites are characterized by insufficient heat resistance and alkali resistance [5, 6], high hygroscopicity (this indicator is 10-20% for glass fibers).

As the analysis of literary sources [7] showed, basalt fibers (BF) are one of the promising fillers for creating wear-resistant polymer composites. The unique multi-component composition of basalt (except for oxides, it contains almost all the elements of Mendeleev's table) provides the fiber with a successful combination of high technical characteristics [8] which are not inferior to organic, carbon and glass fibers. Thus, basalt plastics (BP) 3 times surpass steel in strength. High damping properties, resistance to aging, corrosion and many natural factors characterize them. Environmental and economic aspects are not the last argument in favor of using BF. BF is a more ecological product compared to glass, carbon, and organic fibers, since the raw material from which it is made is igneous rock (basalt). In addition, the technological process of manufacturing BF has an energy-efficient production technology. Only basalt crushed stone only is used for fiber production, without using acids, dyes and solvents. Given the above, looking for a new BP based on a fluoropolymer matrix with high functional characteristics is an urgent task.

Technique for researching the properties of composites

DF-101 polytetrafluoroethylene (PTFE) (manufactured by Shandong Dongyue Polymer Material Co., Ltd, China) was chosen as the polymer matrix for creating basalt plastics. This polymer is characterized by a unique complex of functional properties (see Table 1) in combination with increased resistance to thermal degradation, erosion, as well as the effect of organic and aqueous environments.

Table 1

Main properties of DF-101 polytetrafluoroethylene

Indicator	Value
Density, g/cm^3	2,13-2,16
Tensile strength, MPa	27,0
Elongation at rupture, g/L	500 ± 100
Moisture content, %	0,04
Operating temperature, K	4-533

The disadvantages of PTFE are a high coefficient of thermal expansion, the ability to undergo irreversible deformation under the influence of mechanical loads at room temperature, a tendency to residual deformation and low resistance to abrasion, which is why it is recommended to use fillers.

Discrete BF (Research Institute of Fiberglass and Fibers PJSC (NDISV in Ukrainian), Ukraine) was chosen as filler for PTFE. BF was produced using compression moulding according to the method given in the paper [3].

The tribotechnical characteristics of polytetrafluoroethylene and basalt plastics based on it were studied using the “disk-pad” scheme on SMC-2 friction machine, under conditions of friction without lubrication, at a load of 1,0 MPa, and a sliding speed of 1,0 m/s. Steel 45 (45-48 HRC, R_a=0,32 μm) was used as a counterbody. The density of PTFE and BP based on it was determined using hydrostatic weighing method.

The study of the friction surfaces of the unfilled polymer and BP based on it was carried out using a BIOLAM-M optical microscope.

The thermal stability of polytetrafluoroethylene and BF based on it was carried out using the method of thermogravimetric analysis using MOM Q-1500D derivatograph of the Paulik-Paulik-Erdey system (Hungary). The temperature range of the research was 273-900 K, the rate of temperature rising was 10 K/min, the weight of the test sample was 100 mg.

Results

According to the results of tribotechnical characteristics research (Table 2), it was established that the introduction of BF leads to a decrease in the coefficient of friction and the intensity of linear wear of PTFE 1,7 and 360 times, respectively, reaching the minimum values of the latter at a fiber content of 20 mass.%. The improvement of these properties occurs because finely dispersed products of frictional transfer of BP fill in the microdepressions of the steel counterbody and form a more stable, compared to pure PTFE, an “anti-friction layer” [9]; as a result, friction occurs not according to the “metal–polymer” scheme, but according to the “polymer-polymer” scheme [10].

Table 2

Tribotechnical characteristics of basalt plastics based on polytetrafluoroethylene

Indicator	Basalt fiber content, C, mass.%				
	0	10	20	30	40
Coefficient of friction, f	0,35	0,33	0,32	0,20	0,20
Intensity of linear wear, $I_h \times 10^{-9}$	1120	5,31	3,12	4,30	10,40

The study of friction surfaces of PTFE and BP showed a deep change in the surface morphology. It can be seen from the microstructure of the friction surface of PTFE that there are traces of adhesion and deep furrows of ploughing of the surface layer on its surface (Fig. 1, a). The introduction of BF leads to the reduction of ploughing furrows (Fig. 1 b and c); it can be explained by the fact that the fibers give stiffness to the soft polymer, and as a result, BP resists deformations.

A sharp decrease in wear resistance 1,35-3,3 times is observed for basalt plastics containing 30-40 mass.% of the filler, which is probably a consequence of the growth of defects in the volume of the material (the formation of microcracks and pores) due to the uneven location of the fiber in the polymer matrixes. Pronounced friction tracks, which are formed due to the dominance of the process of mechanical destruction of the surface, and those formed as a result of the transfer of spent particles to the friction area are observed on the friction surface of basalt plastic containing 40 mass.% of the fiber (see Fig. 1, d).

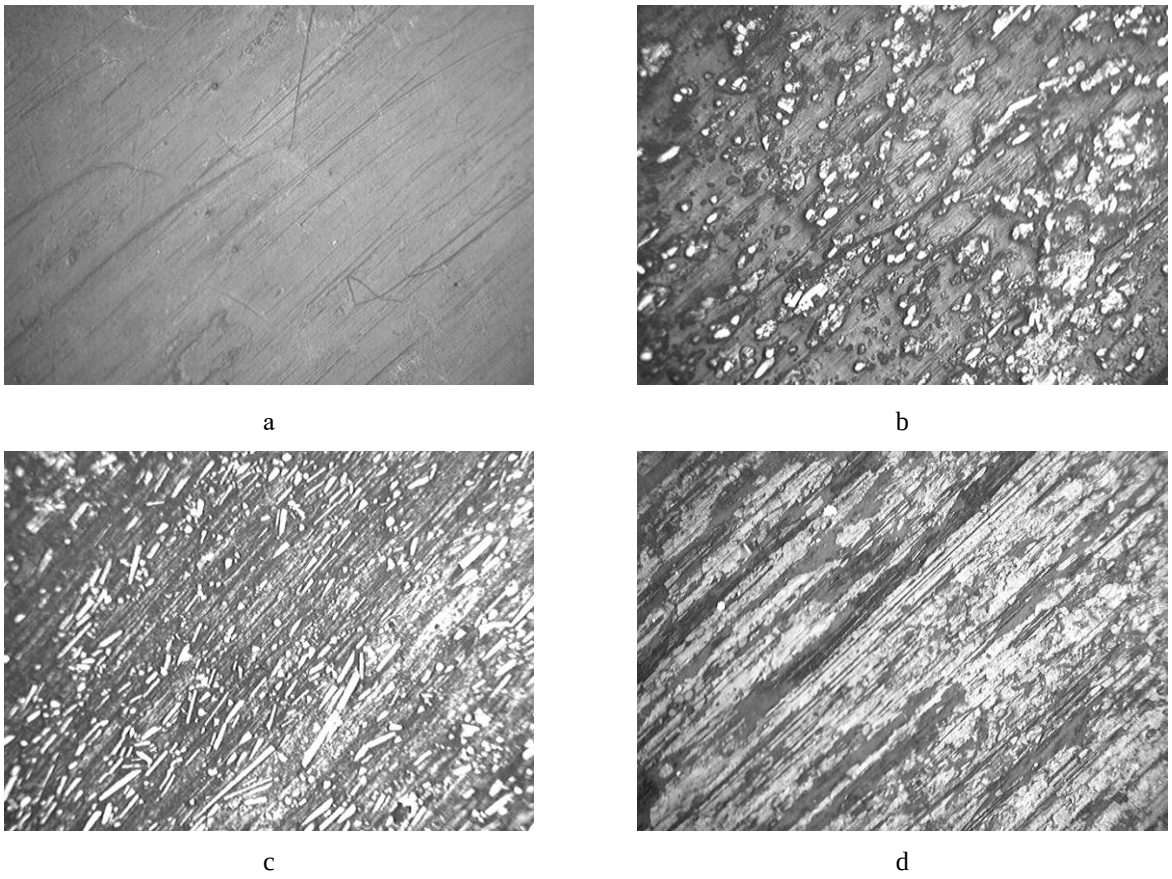

a b c d

Fig. 1. Microstructures (×150) of friction surfaces of polytetrafluoroethylene (a) and basalt plastics based on it, containing: 10 (b); 20 (c), 40 (d) mass.% of basalt fiber

The confirmation of the presence of defects in the volume of BP is confirmed by the comparison of the calculated and experimental density. It can be seen from fig. 2 that experimental BF density is higher than the calculated one at a BF content of 10-20 mass.%. According to this, we conclude that the supramolecular structure of the obtained materials is more ordered due to strong intercomponent interaction at the "polymer-fiber" interface. With a further increase in BF content, the opposite dependence is observed, which can be explained by the fact that it becomes more challenging to achieve a uniform distribution of polytetrafluoroethylene on its surface; as a result, during the formation of the surface layer, the packing of macromolecules in it becomes looser, therefore, the material contains pores.

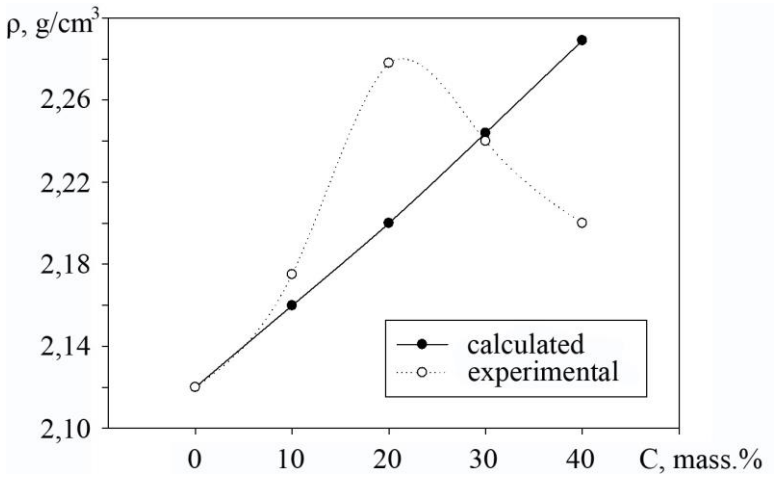

Fig. 2. Dependence of calculated and experimental density (ρ, g/cm^3) of polytetrafluoroethylene on basalt fiber content (C, mass.%)

Another important property that ensures the stable operation of friction units is the thermal stability of the composite. It was established that the introduction of BF (Fig. 3) leads to an increase in the thermal stability of PTFE.

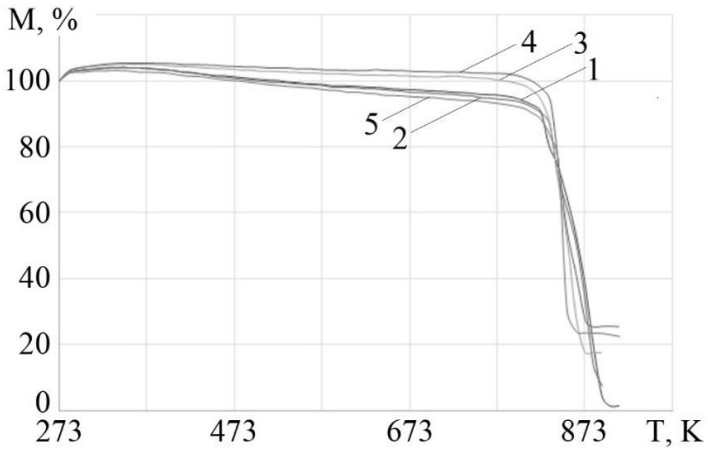

Fig. 3. Dependence of mass loss (M, %) on temperature (T, K) of polytetrafluoroethylene (1) and basalt plastics based on it containing: 10 (2); 20 (3), 30 (4), 40 (5) mass.% of basalt fiber

There is no mass loss observed up to 423 K on the thermogravimetric curves of PTFE and basalt plastics based on it; that is, the materials are hydrophobic [7]. It is interesting to note that PTFE loses 10% of its mass (T_{10}) at a temperature of 823 K, while for BP the temperature of losing 10% of mass increases by 10 degrees, which is due to a decrease in the mobility of molecular chains of PTFE when reinforcing its BF. It, in turn, leads to an increase in its thermal oxidation resistance. There is a significant mass loss after 823 K due to intensive thermal destruction of both PTFE and BP based on it.

Fig. 4. Sintering cars of Zaporizhstal PJSC

The positive results of laboratory studies allowed us to proceed to production ones. Basalt plastic with an effective (20 mass.%) filler content was used as an anti-friction protection for sliding bearings (No. 315) of sintering cars of Zaporizhstal PJSC (Fig. 4).The friction units of the cars work in dusty conditions and under high temperatures (about 573 K). The bearings with the developed BP worked without failure for 11 months, which made it possible to recommend bringing them into serial production

Conclusions

According to the results of tribological studies using the "disk-pad" scheme, it was established that the introduction of discrete basalt fiber leads to a decrease in the coefficient of friction and the intensity of linear wear of DF-101 polytetrafluoroethylene 1,7 and 360 times, respectively. At the same time, the thermal stability of basalt plastics increases. Based of the obtained results, BP with an effective fiber content (20 mass.%) is recommended for manufacturing friction units of machines and mechanisms of modern technology that operate under the influence of high temperatures and friction conditions without lubrication.

References

1. M.L. Shulyak Influence of friction forces between connected parts of a car engine on the wear process. "Motor transport in the agricultural sector: planning, design and technological operation": materials of the All-Ukrainian scientific and practical conference (May 16-17, 2019, Kharkiv). Kharkiv: KhNTUSG, 2019. P. 123.

2. O.V. Melnyk Causes of wear of aircraft parts of friction units and methods for their availability supporting. Problems of Friction and Wear. 2020. No. 1. P. 87–92.

3. O.I. Burya, S.V. Kalinichenko, I.I. Nachovniy The impact of organic tanlon fiber on performance indicators of polychlorotrifluoroethylene. Journal Problems of Tribology. 2019. No. 2. P. 61–66.

4. O.I. Burya, S.V. Kalinichenko, Yu.S. Proydak Polymer composition: pat. 111584 Ukraine. IPC: C08L 81/10, C08L 27/18. No. U 2016 06147; statement 06.06.2016; published 10.11.2016, Bull. No. 21. 4 p.

5. K.V. Berladir, V.A. Sviderskiy Designing and examining polytetrafluoroethylene composites for tribotechnical purposes with activated ingredients. Eastern-European Journal of Enterprise Technologies. 2016. No. 6. P. 14–21.

6. Yu.Ye. Zubko Optimization of production and use processes fibers, microfibers and microsphere obtained by the method superheated melts of basalt: diss. for the degree of Cand. tech. Sciences: 05.02.01. Kyiv. 2021. 209 p.

7. S.I. Starchenko, N.I. Domantsevych, Y.E. Zubko Prospective basalt composite. Bulletin of the Lviv Commercial Academy. Commodity science series. 2015. No. 15. P. 28–32.

8. Ashokkumar R. Tavadi, Yuvaraja Naik, K. Kumaresa, N.I. Jamadar, C. Rajaravi Basalt fiber and its composite manufacturing and applications: An overview International Journal of Engineering, Science and Technology. 2021. No. 4. P. 50–56.

9. O.S. Kabat, O.D. Derkach, N.V. Pavlushkina, I.I. Pikula Polymeric composites of tribotechnical purpose based on fluoropolymers. Problems of Tribology. 2019. No. 2. P. 75–81.

10. A.V. Buketov, M.V. Brailo, O.S. Kobelnyk, O.V. Akimov Tribological properties of epoxi composite materials filled with dispersed particles and thermoplastic materials. Materials Science. 2016. No. 1. P. 28–35.

Єрьоменко О.В., Томіна А.-М.В., Рула І.В. Вплив дискретного базальтового волокна на експлуатаційні властивості політетрафторетилену

У статті розглянуто вплив дискретного базальтового волокна на триботехнічні характеристики політетрафторетилену марки DF-101 за схемою «диск-колодка» в умовах тертя без змащення. Встановлено, що введення наповнювача призводить до зменшення інтенсивності зношування та коефіцієнту тертя базового полімеру у 1,7 та 360 разів відповідно. Покращення даних властивостей обумовлено тим, що в процесі тертя базальтопластиків утворюється більш стабільний, порівняно з ненаповненим політетрафторетиленом, «антифрикційний шар», внаслідок чого тертя відбувається за схемою «полімер–полімер». Підтвердженням цього служить глибока зміна морфології поверхні тертя. Так, для політетрафторетилену спостерігаються глибокі борозни проорювання й сліди схоплювання з контртілом, в той час як базальтопластики чинять більший опір до деформацій, що в свою чергу призводить до зменшення борозн проорювання. Для базальтопластиків, що містять 30-40 мас.% волокна спостерігається різке зменшення зносостійкості у 1,35-3,3 рази, що імовірно, є наслідком зростання дефектів в об’ємі матеріалу через нерівномірне розташування волокна в полімерній матриці. Підтвердження наявності дефектів в об’ємі базальтопластиків підтверджує порівняння розрахункової та експериментальної (гідростатичної) густини. Встановлено, що політетрафторетилен втрачає 10% маси при температурі 823 K, в той час як для базальтопластику температура втрати 10% маси збільшується на 10 градусів. Визначено, що ефективний вміст наповнювача в полімерній матриці складає 20 мас.%. Отриманий базальтопластик (20 мас.% волокна), рекомендовано при виготовленні підшипників кочення та ковзання (як антифрикційний захист) для трибологічних з’єднань сучасної техніки, що працюють під впливом високих температур, агресивних середовищ та умовах тертя без змащення.

Ключові слова: політетрафторетилен, базальтове волокно, інтенсивність зношування, коефіцієнт тертя, вузол тертя

Problems of Tribology, V. 27, No 4/106-2022, 45-50

Problems of Tribology
Website: http://tribology.khnu.km.ua/index.php/ProbTrib
E-mail: tribosenator@gmail.com

DOI: https://doi.org/10.31891/2079-1372-2022-106-4-45-50

Effect of fullerene-like nanoparticles on the tribological properties of industrial lubricants for steel rolling

I.M. Kartun[1], O.A. Remez[2], O.O. Haidai[1], O.A. Spaska[3], O.B. Yanchenko[4], V.S. Pyliavsky[1], Ye.V. Polunkin[1]

[1]*Institute of Bioorganic Chemistry and Petrochemistry named V.P. Kukhar of the National Academy of Sciences of Ukraine*
[2] *Ukrainian State University of Science and Technology, Dnipro, Ukraine*
[3]*University of Silesia in Katowice, Katowice, Poland*
[4]*Vinnitsa National Technical University, Vinnytsia, Ukraine*
E-mail: ik.chemic@gmail.com

Received: 20 September 2022: Revised: 05 November 2022: Accept: 05 December 2022

Abstract

The paper shows the results of studying the possibility of using fullerene-like nanoparticles as a lubricating additive in the composition of technological lubricant MT-216 M. The lubricity properties were evaluated on a laboratory rolling mill DUO-180 during cold rolling of strips of steel 08kp. The rolling force, the coefficient of friction in the deformation zone were measured, the values of the elongation coefficient and the parameter reflecting the costs of the rolling force per unit deformation of the metal were calculated.

Keywords: technological lubrication, cold rolling of steel, lubricating properties, fullerene-like nanoparticles

Introduction

Lubricating-cooling technological agents (LUTA), used in the processing of metals by pressure, are called technological lubricants (TL). The right choice of process lubricant helps to increase the productivity of rolling equipment, improve the quality of products. The technology of using the TL is also of great importance - i.e. a method of supplying lubricant to rolls and metal, determining the optimal lubricant consumption and improving lubrication systems.

Technological lubricants must meet a number of technical, economic and sanitary-hygienic requirements. Depending on the production conditions, the type of metalworking, the nature of the metal being processed, the parameters of the technological process, the list of requirements for lubrication may vary [1].

However, based on the fact that the performance properties of lubricants depend on many factors, taking into account the effect of lubricants on the quality of rolled products, as well as the variety of rolled products and the characteristics of rolling mills, it is possible to determine the main requirements for the TL for cold thin sheet steel rolling on modern high-speed mills:

- the ability to provide the lowest friction coefficient acceptable for this type of metalworking;
- ability to provide high adhesion to a metal surface;
- high cohesion in the film and its resistance to high pressure and shear resistance;
- ability to form polymolecular layers and provide a strong film;
- maximum resistance to temperature, improved adhesion and increased strength of the lubricating layers with increasing temperature;
- high viscosity index;
- stability of composition and properties;
- high lubricating properties;
- do not stick to the metal, do not degrade the quality of the surface;
- convenience of giving on rolls and metal;
- no harmful effects on metal and equipment (corrosion, contamination, etc.);
- non-toxicity, absence of an unpleasant smell.

Compliance of the TL with the above listed requirements is ensured by the component composition of the TL. The most important for the TL are lubricating properties. The technological environment used in the cold rolling of steel plays an important role in reducing the energy and power parameters of rolling, affects the productivity of the process, the consumption of rolls and bearings, the geometry and surface quality of the rolled strips [2].

Literature review

Studies show that the lubricating properties of TL are due to the complex effect of their component composition on the formation of boundary layers - surface protective films. Depending on the nature of the TL components, the chemical composition, structure, and properties of boundary surface layers can change significantly.

Currently, new carbon-based spatial nanostructures are considered as promising antiwear additives for lubricants. According to the recommendation of the International Union of Pure and Applied Chemistry (IUPAC), single- and multilayer closed spherical polyhedra consisting of carbon pentagonal and hexagonal faces (resembling a soccer ball in structure) are classified as fullerenes (or fullerene-like nanoparticles (FLN) [3].

The mechanism of action of FLN on the tribological characteristics of lubricants is explained by the deposition of fullerenes from the liquid phase on the contact surfaces during friction. It is assumed that a layer of ball-like fullerene nanoparticles formed on the friction surfaces transforms sliding friction into rolling friction with a decrease in the friction coefficient and minimization of wear [4, 5].

In accordance with such ideas, it should be expected that the positive effect of these additives on the tribological characteristics should increase as the contact surfaces are filled with fullerene particles. In turn, the precipitation of fullerenes accelerates with an increase in their concentration in the solution.

In V.P. Kukhar Institute of Bioorganic Chemistry and Pertochemistry of the National Academy of Sciences of Ukraine were developed methods for obtaining fullerene-like carbon nanoparticles (CNOs) by the plasma-chemical method and alkaline pyrolysis of vegetable carbohydrates (lignin, wood waste cellulose). The methods of atomic force and transmission electron microscopy, infrared and Raman spectroscopy were used to study the structural and dimensional features of the synthesized carbon nanoparticles.

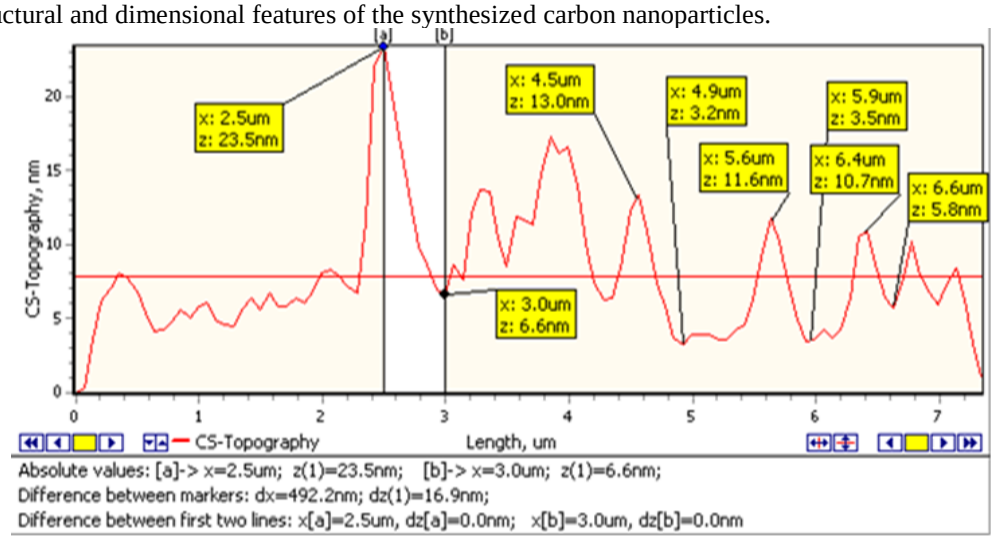

Fig. 1. Evaluation by atomic force microscopy of the size of fullerene-like nanoparticles obtained by carbonization of wood waste

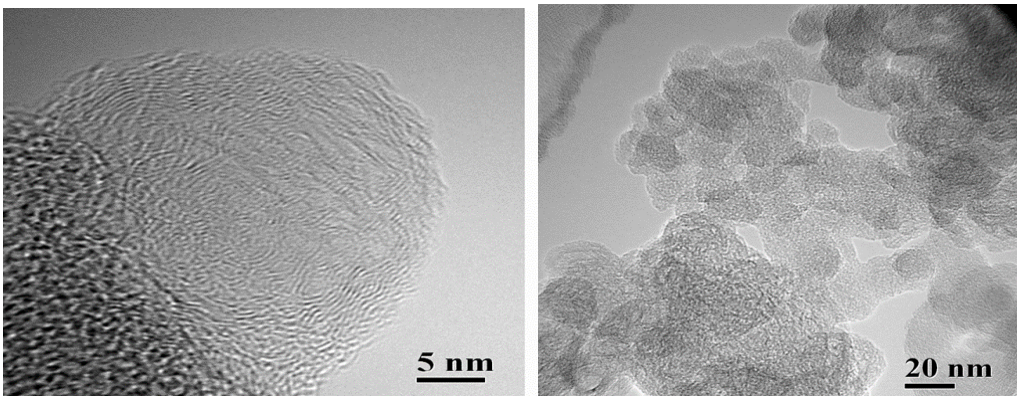

Fig. 2. Transmission electron microscopy image of fullerene-like nanoparticles obtained by carbonization of wood waste

Figure 1 shows images of the synthesized FLN obtained by atomic force, and in Figure 2 - transmission electron microscopy. The average size of individual synthesized nanoparticles is in the range of 15–25 nm.

Purpose

The authors studied the possibility of using spherical carbon nanoparticles obtained by carbonization of bio-raw materials as a lubricant additive in the composition of TL. The object of the study was a Ukrainian-made technological lubricant MT - 216 M produced by "Chemical Investment Company LTD".

Results

Technological lubricant MT-216 M is a balanced composition of synthetic esters of fatty acids and polyhydric alcohols, vegetable oils, emulsifiers, corrosion inhibitors and other multifunctional additives that give it a set of necessary performance properties. TL MT-216 M is designed for use in high-speed cold rolling of carbon and alloy steels, pipe rolling and drawing, wire drawing, stamping and cutting of carbon and alloy steels. Physical and chemical requirements for technological lubricant MT-216 M are given in Table 1.

Table 1

Physical and chemical requirements for TL MT-216M

№	The name of indicators	Norm according to Specifications 20.5-32734997-003:2016	Test Methods
A. Concentrate			
1	Appearance and color	Homogeneous oily liquid from yellow-red to brown	GOST 6243
2	Density at 20°C, kg/m^3 within	920-1000	ASTM D 1298
3	Kinematic viscosity at 50°C, mm^2/s (cSt), within	30-70	ASTM D 2196
4	Flash point in an open crucible, °C, min	180	ASTM D 92
5	Pour point, °C, max	minus 5	ASTM D 97
6	Acid number, mg KOH/g, max	20	ASTM D 664
7	Saponification number, mg KOH/g, min	210	GOST 17362 or GOST 21749
8	Mass fraction of water, %, max	0,5	ASTM D 6304
9	Storage stability	Withstands	GOST 6243
10	Ash content, %, max	0,05	GOST 1461
11	Mass fraction of mechanical impurities, %, max	0,03	ASTM D 189 or ASTM D 524
12	Corrosive effect on metals: steel 10	Withstands	ASTM D 130
13	pH value, within	6,0 -8,0	GOST 6243
14	Emulsion stability: oil release is allowed within 1 hour,%, max	2,0	GOST 6243
B. 5% emulsion prepared according to GOST 6243			
16	pH value, within	6,0 -8,0	GOST 6243
17	Emulsion stability: oil release is allowed within 1 hour,%, max	2,0	GOST 6243
18	Corrosive effect on metals: steel 10	Withstands	GOST 6243

Experimental study of the effectiveness of the lubricating properties of fullerene-like nanoparticles in the composition of technological lubricants during cold strip rolling

An alcoholic solution of fullerene-like nanoparticles was prepared by extracting a dry CNOs-Br powder with absolute ethanol with a content of nanoparticles of 0.4862 g/l of the solution.

Fullerene-like nanoparticles were introduced into the TL MT-216 M in the form of an alcohol solution in an amount of 0.01% wt; 0.10% wt; 1.00% wt. Experimental studies were carried out on the basis of the A.P. Chekmarev Department of Metal Forming of the Ukrainian State University of Science and Technology (National Metallurgical Academy of Ukraine) (DMF USUST (NMetAU).

Studies of antifriction efficiency were carried out during cold rolling of thin strips 0.5 mm thick (l/h_{av} > 3–5), which, according to A.P. Grudev [6], is the most favorable condition for such experiments. The samples were a strip in a roll of 08kp steel in the annealed state ($\sigma_{t.init.}$=260 N/mm^2) with a width b=200.5 mm and an initial thickness h_0=0.5 mm. The study was carried out for 15 samples with a length of l_0=540 mm, based on 3 pcs. for each sample of the investigated lubricant, and 3 pcs. for rolling without lubrication.

TL studies were carried out on a laboratory two-roll mill "duo"-180 of the Department of DMF USUST (NMetAU). The mill is equipped with rolls with a diameter of 180 mm, the rotation speed of which is 0.264 m/s. A general view of the rolling stand is shown in fig. 3.

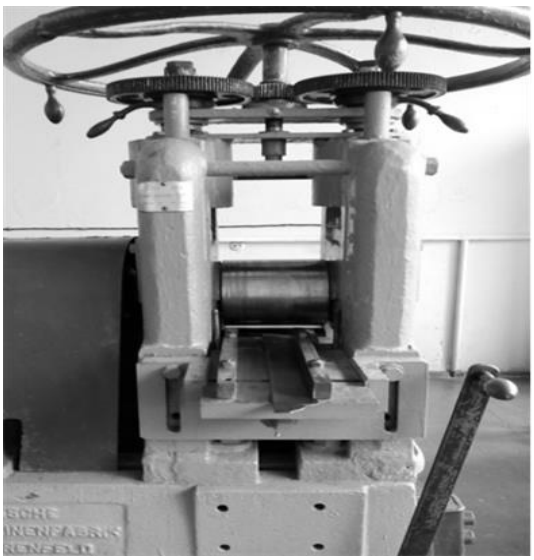

Fig. 3. General view of the stand of the laboratory mill 180-"duo" of the Department of DMF USUST (NMetAU)

Before rolling, the prepared strips were cleaned and degreased with “Kalosha” gasoline-solvent (Nefras S2-80/120). Also, the rolls and the receiving table of the mill stand were subjected to cleaning and degreasing.

The degree of compression of steel samples was preliminarily chosen, the value of which is equal to 12% of the initial height of the sample. At the first stage of experimental studies, 3 samples were rolled without lubrication, which will later serve as a standard for comparing the power parameters of rolling samples with lubrication. Lubricants were generously applied with a brush to the surface of each strip along the entire length. Before rolling each strip, the rolls and the receiving table of the mill stands were degreased with the solvent indicated above. Fig. 4 shows a sample of the indicated length with lubrication applied.

Fig. 4. Initial sample with applied lubricant (top view)

After rolling, changes in their geometric parameters were measured on the test samples: thickness h_1 (10 measurements were made along the length of the strip on each strip, the average value is indicated in the table), width and length of the samples b_1, l_1. The elongation ratio, which is an indirect method for determining the lubricity properties of TL during rolling, was calculated from the ratio of the sample cross section before and after rolling.

$$\lambda = \frac{F_0}{F_1} = \frac{h_0 b_0}{h_1 b_1}, \tag{1}$$

were

F_0 is the sample cross section before rolling,
F_1 is the cross section of the sample after rolling,
h_0 is the sample thickness before rolling,
h_1 is the sample thickness after rolling,
b_0 is the sample width before rolling,
b_1 is the width of the sample after rolling.

During the rolling of the specimens, the rolling force was measured using pressure gauges installed under the pressure screws. Mesdoses were previously calibrated. The value of the rolling force (the previously used expression "pressure of the metal on the rolls") was taken from the molds, and with the help of an ADC device (analogue-to-digital converter) was transmitted to a computer. The research data on the effect of TL on the rolling force are presented in Table 2. The obtained data on the rolling force of steel specimens indicate the effect of technological lubricants on the rolling force. The most effective lubricant in this case is MT-216M +

1.00% fullerene-like nanoparticles (FLN), the other lubricant samples showed approximately the same result of force measurements.

Table 2

Comparison of rolling force

Lubricant	**Force at the initial capture of the strip ($P_з$), кN**	**Average force at steady state (P_c), кN**	**Minimum rolling force (P_{min}), кN**
Without lubrication	26,8	25,5	24,0
MT-216 M	27,4	24,5	22,6
MT-216M + 0,01 % FLN	24,5	24,5	22,6
MT-216M + 0,10 % FLN	26,8	24,5	19,6
MT-216 M+1,00 % FLN	29,4	22,6	20,6

The second criterion for evaluating the lubricating properties of lubricants is the determination of the average coefficient of friction in the deformation zone (f). The calculated dependence for determining the coefficient of friction during cold strip rolling, proposed by A.P. Grudev [7]:

$$f = k_l \frac{1}{1+0.25\sqrt{\nu_{50}}-0.005\nu_{50}}[1 + (0.4 + \varepsilon)R_z] \cdot \left[0{,}07 - \frac{0.1V_r^2}{2(1+V_r)+3V_r^2}\right] \quad (2)$$

where k_l is a coefficient that takes into account the nature of the lubricant; ν_{50} is the kinematic viscosity of the lubricant at a temperature of 50 °C, mm^2/s; ε is the partial relative reduction of the strip during cold rolling, fractions of a unit; R_z is the height of microroughnesses on the surface of work rolls, μm; V_r is the circumferential speed of the work rolls during rolling, m/s.

According to A.P. Grudev coefficient k_l is equal to: for vegetable oils – 1.0, for mineral oils – 1.4. When rolling with emulsions from emulsols based on mineral oils, the viscosity of the corresponding mineral oils is taken as the calculated value of ν_{50} [7].

The geometric dimensions of the samples after rolling, the values of the elongation coefficient, as well as the calculated values of the friction coefficient are shown in Table 3. Also, as mentioned above, to indirectly determine the lubricating properties of the TL during rolling, the values of the elongation coefficient and the parameter K (kN/%), reflecting the cost of rolling force per unit of metal deformation were calculated.

Table 3

Geometric dimensions of specimens, elongation coefficient and coefficient of friction during rolling of steel specimens on a laboratory mill 180 "duo"

Lubricant	Final strip thickness h_1, mm	Relative compression, ε, %	Strip width after rolling b_1, mm	Relative drawing, λ	Roll speed m/s	Medium contact stress p_m, N/mm^2	Friction coefficient, f	K, кN/%
Without lubrication	0,46	8	20,15	1,079	0,264	473	0,229	3,187
MT-216	0,44	12	20,1	1,131	0,264	372	0,097	2,043
MT-216 M + 0,01 % FLN	0,44	12	20,1	1,131	0,264	372	0,077	1,879
MT-216 M + 0,10 % FLN	0,44	12	20,1	1,131	0,264	372	0,062	2,043
MT-216 M+1,00 % FLN	0,44	12	20,1	1,131	0,264	342	0,058	2,043

Analysis of the data given in Table 3 showed that when rolling without lubrication, large values of the friction coefficient are observed and the cost of force per unit of deformation of the metal K increases. The lowest values of the friction coefficient f were obtained when rolling strips using TS MT-216 M + 1.00% wt. FLN.

Conclusions

An analysis of the obtained data shows that the addition of fullerene-like nanoparticles to the composition of the technological lubricant MT-216M improves the lubricating properties. The lubricating effect is manifested at a concentration of 1.00% FLN in the composition of the lubricant, which is mainly due to the deposition of fullerene nanoparticles on the surface and, to a lesser extent, to the effect on the structure of the liquid phase.

In the future, to study the lubrication efficiency, it is possible to conduct experiments to determine the advance during rolling as an indirect parameter of the TL efficiency, as well as to study the thickness of the lubricating layer by the drop method.

References

1. Roberts V. Cold rolling of steel. Per. from English; under. ed. Polukhina P.I., Polukhina V.P. - M .: Metallurgy, I982 - 542 p. (Roberts V. Kholodnaya prokatka stali. Per. s angl.; pod. red. Polukhina P.I., Polukhina V.P. – M.: Metallurgiya, I982 – 542 s.)

2. Grudev A.P., Zilberg Yu.V., Tilik V.T. Friction and lubrication in the processing of metals by pressure. Reference edition. - M.: Metallurgy, 1982. - 312 p. (Grudev A.P., Zil'berg YU.V., Tilik V.T. Treniye i smazki pri obrabotke metallov davleniyem. Spravochnoye izdaniye. – M.: Metallurgiya, 1982. – 312 s.)

3. Lyubchuk T.V. Fullerenes and other aromatic surfaces (structure, stability, ways of formation). K.: Publishing House-Printing Center "Kyiv University". 2005. 322 p. (Lyubchuk T.V. Fulereny ta inshi aromatychni poverkhni (struktura, stabilnist′, shlyakhy utvorennya). K.: Vydavnytstvo-polihrafichnyy tsentr «Kyyivs′kyy universytet». 2005. 322 s.)

4. Jiang G., Guan W., Zheng Q. Wear. 2005. V. 258. P. 1625 – 1695.

5. Tuktarov A.R., Khuzyn A.A., Dzhemilev U.M. Fullerene-containing lubricants: achievements and perspectives (review). Petrochemistry. 2020. Vol. 60, No. 1. P. 125 – 147. (Tuktarov A.R., Khuzin A.A., Dzhemilev U.M. Fullerenosoderzhashchiye smazochnyye materialy: dostizheniya i perspektivy (obzor). Neftekhimiya. 2020. T. 60, № 1. S. 125 – 147.)

6. Grudev A.P. External friction during rolling: Metallurgy, 1973. - 288 p. (Grudev A.P. Vneshneye treniye pri prokatke - Moskva: Metallurgiya, 1973. - 288 s.)

7. Grudev A.P., Mashkin L.F., Khanin M.I. Technology of rolling production: Metallurgy, 1994 - 656 p. (7. Grudev A.P., Mashkin L.F., Khanin M.I. Tekhnologiya prokatnogo proizvodstva: Metallurgiya, 1994 – 656 s.)

І.М. Картун, О.А. Ремез, О.О. Гайдай, О.А Спаська, О.Б. Янченко, В.С. Пилявський, Є.В. Полункін. Вплив фулереноподібних наночастинок на трибологічні властивості технологічних мастил для прокачування сталі

В роботі показані результати дослідження можливості застосування фуллереноподібних наночастинок як змащувальна присадка у складі технологічного мастила МТ-216 М. Оцінка змащувальних властивостей проводилася на лабораторному прокатному стані ДУО-180 при холодній прокатці смуг зі сталі 08кп. Були виміряні сила прокатки, коефіцієнт тертя в осередку деформації, розраховано значення коефіцієнта витяжки і параметра, що відображає витрати сили прокатки на одиницю деформації металу.

Ключові слова: технологічне змащення, холодна прокатка сталі, змащувальні властивості, фуллереноподібні наночастки

Problems of Tribology, V. 27, No 4/106-2022, 51-57

Problems of Tribology
Website: http://tribology.khnu.km.ua/index.php/ProbTrib
E-mail: tribosenator@gmail.com

DOI: https://doi.org/10.31891/2079-1372-2022-106-4-51-57

The influence of alloying with manganese and chromium of steel hardened and tempered auger on its relative wear resistance during dehydration in a municipal solid waste truck

O.V. Bereziuk[1], V.I. Savulyak[1], V.O. Kharzhevskyi[2]

[1]Vinnitsa National Technical University, Ukraine
[2]Khmelnytskyi National University, Ukraine
E-mail: berezyukoleg@i.ua

Received: 22 September 2022: Revised:105 November 2022: Accept: 05 December 2022

Abstract

The article is dedicated to the study of the influence of alloying with manganese and chromium followed by hardening and tempering of the auger on its wear resistance during the dehydration of municipal solid waste truck. The use of a mathematical apparatus and appropriate regression analysis programs made it possible to determine the dependence of the wear resistance of the auger on the content of manganese and chromium in the steel of the auger for the case of its quenching and tempering. Constructed graphical dependences of relative wear resistance with the indicated alloying and heat treatment of the screw revealed a significant influence of the concentration of manganese and chromium in steel, sufficient convergence of the obtained patterns was confirmed. It was established that after operation and wear on the path s = 56850 m during the dehydration of solid waste in a garbage truck, an increase in the manganese content in the steel of the heat-treated screw from 0.32% to 1.8% leads to a decrease in energy intensity by 10 kWh/tons, and an increase chromium content in screw steel after similar heat treatment from 0% to 6% leads to a decrease in energy consumption by 11.5 kWh/tons and to a reduction in the cost of the solid waste dehydration process in the garbage truck. It was determined that tempering the chromium-manganese screw steel after its hardening allows reducing energy consumption by 1.26...2.56 kWh/tons, depending on the chromium content. The expediency of conducting further research on determining the rational composition and structural state of the auger material and ways to increase its wear resistance has been revealed

Key words: wear, wear resistance, manganese content, chromium content, tempering, auger press, garbage truck, dehydration, municipal solid waste, regression analysis.

Introduction

Increasing the wear resistance and reliability of operative links of machines occupies a prominent place among the important tasks of municipal machinebuilding [1, 2]. A promising technology for the primary processing of municipal solid waste (MSW), aimed at reducing both the costs of transporting solid waste and the negative impact on the environment, is their dehydration during the process of loading into a garbage truck, which is done by accompanying processes of preliminary compaction and partial grinding.

Dehydration of MSW in the garbage truck is carried out with the help of a conical auger, the surfaces of which are intensively worn. This is due to the presence in the waste of small metal products, glass, ceramics, stones, bones, polymer materials that have abrasive properties. In addition, the moisture occuring in MSW in the range of 39...92% by mass forms an aggressive corrosive environment. As a rule, alloyed iron alloys are used for the production of screws. The use of steels and cast iron alloyed with chromium and manganese is justified [3]. Such alloys are well amenable to heat treatment and have high resistance against corrosive and abrasive wear. Therefore, the study of the influence of the content of manganese and chromium in the steel of the auger, the manufacturing technology of which includes quenching and tempering operations, on its relative wear resistance during the dehydration of s municipal solid waste in a garbage truck is an urgent task.

Analysis of recent research and publications

The analysis of the influence of the main alloying and modifying elements on the properties of wear-resistant steels is carried out in the article [3]. It has been established that manganese in steel after tempering at 760 °C with an increase in its content to 1.8% contributes to an increase in the degree of dispersion of pearlite, while the amount of pre-eutectic ferrite or, accordingly, post-eutectic carbides decreases. A further increase in the manganese content is undesirable due to a decrease in the plasticity of the steel, but the strength increases. It is noted that chromium is the most common element that is introduced into manganese steel in order to increase wear resistance. It stabilizes austenite and is also an active carbide former. When 1% Cr is introduced into steel, the relative wear resistance increases significantly (from 1.0 to 1.32). But even with the addition of 3% Cr, the impact toughness decreases. Therefore, steel with approximately 2% Cr has the most satisfactory set of properties.

In the paper [1], a study of the influence of structure, phase composition, and properties on the abrasive wear resistance of chromium-manganese cast irons in the cast state was carried out. It is shown that the abrasive wear resistance of chromium-manganese cast irons is determined by the microhardness of the matrix and the austenite-carbide eutectic based on Me7C3 carbide, is determined by the degree of alloying and the shape parameter of the eutectic carbide, and also depends on the deformation-phase transformations that occur during abrasive wear tests.

The materials of the article [4] show the prospects of obtaining an economically alloyed manganese and chromium-manganese surfacing metal, which can be deposited by surfacing on low-carbon steel without preheating, which is important for the use of developed surfacing materials in industry. It was also established that the highest wear resistance for various types of wear is provided by the superimposed metal with martensitic-austenitic and austenitic structures, while the presence of ferrite in the structure of the superimposed metal reduces the wear resistance.

A mathematical model for calculating the rate of wear of triboelements in the tribosystem under conditions of corrosive-abrasive wear was proposed by the author of the work [5]. The input factors were: active acidity, abrasiveness, roughness, load and sliding speed. The degree of influence of the above factors on the rate of wear has been theoretically determined: abrasiveness is the most important factor, followed by the level of active acidity and load in descending order of influence

A new design of an auger with a sectional elastic surface to reduce the degree of damage to grain material during its transportation is presented in the article [6]. A dynamic model was developed to determine the influence of the structural, kinematic and technological parameters of the elastic screw on the time and path of free movement of particles of loose material during their movement between sections, as well as to exclude the possibility of interaction of grain material with the non-working surface of the screw working body to reduce its damage. A theoretical calculation of the interaction of the grain with the elastic section of the screw was carried out.

The authors of the work [7] note that wear-resistant steels should have high strength, fracture toughness, thermal conductivity, and the ability to form strong films of secondary structures during friction. In the presence of aggressive environments, elevated temperatures, and the action of other physical and chemical factors that reduce surface strength, wear resistance depends on the corrosion resistance of the material, its heat resistance, and other properties

The influence of geometric parameters on the performance and design of a briquetting machine using a pressure model based on the theory of piston flow is studied in the article [8]. An analytical model using a pressure model was also developed based on Archard's wear law to investigate the wear of biomass briquetting machine screws. The developed model satisfactorily predicted the wear of the screw and showed that the speed of rotation and the choice of material have the greatest influence on it. The amount of wear increases exponentially towards the end of the screw, where the pressure is highest. Changing the auger design to select the optimal geometry and speed with appropriate material selection can increase auger life and biomass briquetting machine performance.

In the paper [9], it was established that the greatest strengthening after high-temperature thermomechanical treatment with a simultaneous significant increase in its strength limit is observed in steels with a troostite structure, since the factor of reducing the size of austenite grains contributes to a significant increase in the strength of steels. The strengthening of steel in this structural state reaches its maximum value after doping with 1...2% chromium. When the chromium content is further increased to 5%, the strengthening effect remains unchanged.

Combined treatment, consisting of a combination of methods of alloying 1...5% chromium and high-temperature thermomechanical treatment, can be recommended for practical use as an effective means of increasing the strength of steels, but it is not recommended to be used as a means of increasing wear resistance in conditions of sliding friction on a monolith.

In the materials of the article [10], the wear of a double-auger extruder of rigid PVC resins was investigated. The pressures around the cylinder during the extrusion of two rigid PVC resins in a laboratory extruder with a diameter of 55 mm were measured and the forces acting on the screw core were determined. Numerical modeling of the flow was carried out using power-law functions of resin viscosity.

The main features of the process of pressing wood shavings in screw machines are studied in [11]. The processes that take place in different sections of the screw are established, formulas are defined, the use of which allows you to calculate the loads acting on the turns of the screw, as well as determine the pressing power. Specific energy consumption and the degree of heating of raw materials during pressing are established.

The results of experimental studies of the solid waste dehydration process, obtained on the basis of planning the experiment using the Box-Wilson method, are given in [12]. By means of rotatable central composite planning, quadratic regression equations with 1st-order interaction effects were obtained for the objective functions: moisture and density of pre-compacted and dehydrated MSW, maximum drive motor power, energy consumption of MSW dehydration. This made it possible to determine the optimal parameters of the dehydration equipment (rotation frequency of the auger, the ratio of the radial gap between the auger and the body, as well as the ratio of the diameter of the auger core to the outer diameter of the auger on the last turn) for mixed and "wet" solid waste, according to the criterion of minimizing the energy intensity of the process.

In the the article [13], an improved mathematical model of the operation of the solid waste dehydration drive in the garbage truck is proposed, taking into account the wear of the auger, which made it possible to determine with the help of a numerical study of the dynamics of this drive during start-up that with increasing wear of the auger, the pressure of the working fluid at the inlet of the hydraulic motor of the drive increases, and the angular speed and rotation frequency of the screw are significantly reduced with constant supply of working fluid. Power-laws of changes in the nominal values of pressures at the hydraulic motor inlet, angular velocity and rotation frequency of the auger depending on the amount of its wear were determined, the last of which describes the deviation from the optimal rotation frequency of the auger during its wear and was used to determine the energy intensity of solid waste dehydration taking into account the wear of the auger. It was found that the wear of the auger by 1000 μm leads to an increase in the energy intensity of solid waste dehydration by 11.6%, and, therefore, to an increase in the cost of their dehydration in the garbage truck and acceleration of the wear process.

By means of regression analysis, the influence of chromium alloying of the hardened steel of the auger on its wear during the dehydration of solid waste in a garbage truck was investigated [14], and it was also established that during the operation and wear of the auger on the path s = 56850 m during the dehydration of solid household waste in the garbage truck, an increase in the content of chromium in the hardened material of the auger from 0.25% to 12% allows to reduce the rate of wear and energy consumption of dehydration of municipal solid waste from 12.2% to 3.1%, and, therefore, to reduce the cost of the process of their dehydration in the garbage truck.

Aim of the articles

Study of the effect of manganese and chromium content in the steel of the auger after tempering on its relative wear resistance during the dewatering of solid household waste in a garbage truck.

Methods

The determination of paired dependences of the relative wear resistance of the auger from the content of manganese and chromium after quenching and tempering was carried out by the method of regression analysis [15]. Regressions were determined on the basis of linearization transformations, which allow to reduce the non-linear dependence to a linear one. The coefficients of the regression equations were determined by the method of least squares using the developed computer program "RegAnaliz", which is protected by a certificate of copyright registration.

To determine the energy intensity of solid waste dehydration, taking into account the wear of the auger, the following laws were used [13]:

$$\begin{aligned} E = {} & 1504 - 15,92w_0 + 0,3214\rho_0 - 1,069n(u) - 2061(\Delta_{aug} + u)/(D_{\min} - 2u) - 1947(d_{\min} - \\ & -2u)/(D_{\min} - 2u) + 9,118 \cdot 10^{-4} w_0\rho_0 + 0,002142w_0 n(u) + 18,12w_0(\Delta_{uu} + u)/(D_{\min} - 2u) - \\ & -2,115w_0(d_{\min} - 2u)/(D_{\min} - 2u) + 4,392 \cdot 10^{-4}\rho_0 n(u) - 2,005\rho_0(\Delta_{aug} + u)/(D_{\min} - 2u) + \\ & +0,3361\rho_0(d_{\min} - 2u)/(D_{\min} - 2u) + 0,09031w_0^2 - 7,923 \cdot 10^{-4}\rho_0^2 + 0,008241n(u)^2 + \\ & +104172[(\Delta_{aug} + u)/(D_{\min} - 2u)]^2 + 1318[(d_{\min} - 2u)/(D_{\min} - 2u)]^2 \left[kW \cdot h/tons\right]; \end{aligned} \quad (1)$$

$$n = 52,43 - 1,276 \cdot 10^{-3} u^{1,5} \ [rpm], \quad (2)$$

where E is the energy intensity of solid waste dehydration, kWh/t; ρ_0 – initial solid waste density, kg/m3; w_0 – initial relative humidity of solid waste, %; n – nominal auger rotation frequency, *rpm*; u – auger wear, *m*; Δ_{aug} – radial clearance between the screw and the housing, *m*; D_{min} is the outer diameter of the screw on the last turn, *m*; d_{min} – the diameter of the screw core on the last turn, *m*.

The values of the relative wear resistance of steel after tempering for different values of the content of alloying elements: manganese and chromium are given in the Table 1 and Table 2 [3].

Table 1

Effect of manganese content on the relative wear resistance of steel after tempering [3]

Manganese content, %	0,32	0,68	1,11	1,35	1,8
Relative wear resistance	1	1,18	1,11	1,2	1,26

Table 2

The effect of chromium content on the relative wear resistance of steel after tempering [3]

Chromium content, %	0	1	2	3	6
Relative wear resistance	1	1,32	1,5	1,61	1,62

As a result of the regression analysis of the data in the Table 1 and Table 2, the dependences of the relative wear resistance of the auger depending on the content of manganese and chromium in its steel after tempering are determined:

$$\varepsilon = \frac{C_{Mn}}{0{,}08605 + 0{,}7642 C_{Mn}}; \tag{3}$$

$$\varepsilon = \frac{1}{0{,}6113 + 0{,}3897 e^{-C_{Cr}}}, \tag{4}$$

where ε is relative wear resistance; C_{Mn} – manganese content in the screw material, %; C_{Cr} – chromium content in the screw material, %.

Fig. 1 shows graphical dependences of the relative wear resistance of the screw depending on the content of manganese and chromium in its steel after tempering, constructed using dependences (3, 4), which confirm the sufficient convergence of the obtained patterns compared to the data given in Table 1.

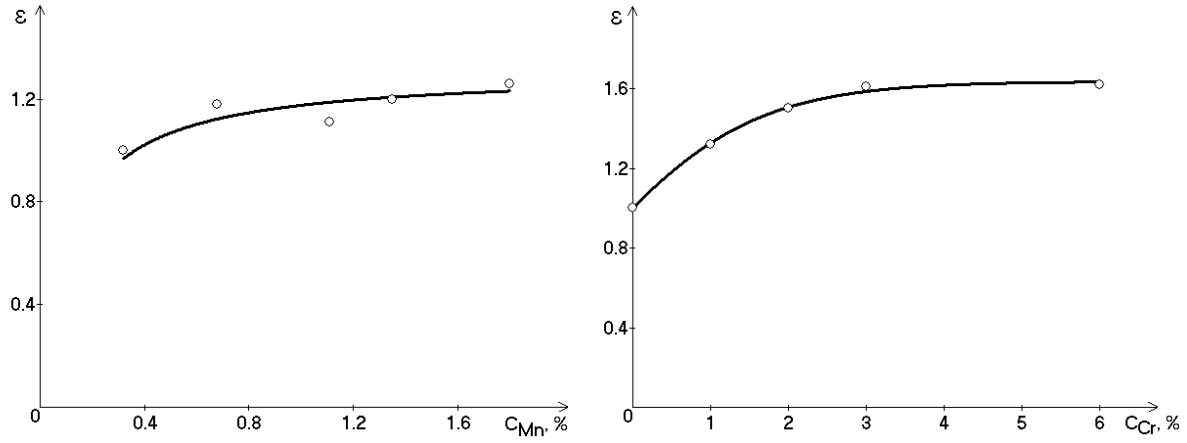

a) **b)**

Fig. 1. The relative wear resistance of the screw depending on the content of alloying elements in its steel after tempering the steel (a) – manganese, (b) – chromium: actual ○, theoretical —

The results of the regression analysis are shown in Table 3, where cells with the maximum values of the correlation coefficient *R* for each of the paired regressions are marked in gray.

It was established that the relative wear resistance of the auger after tempering increases according to a hyperbolic dependence with an increase in the manganese content and an exponential dependence with an increase in the chromium content.

In the Fig. 2 are shown the graphical dependences of the influence of the manganese and chromium content in steel after the auger of the solid household waste dehydration device has been released on the energy intensity of the process (when it wears out along the path s = 56850 *m* [14]), constructed using dependences (1-4).

Table 3

The results of the regression analysis of the dependence of the relative wear resistance of the auger depending on the content of manganese and chromium in its steel after tempering

№	Type of regression	Correlation coefficient R		№	Type of regression	Correlation coefficient R	
		$\varepsilon=f(C_{Mn})$	$\varepsilon=f(C_{Cr})$			$\varepsilon=f(C_{Mn})$	$\varepsilon=f(C_{Cr})$
1	$y = a + bx$	0.84446	0.81748	9	$y = ax^b$	0.87408	0.91249
2	$y = 1 / (a + bx)$	0.83369	0.76931	10	$y = a + b\cdot\lg x$	0.87074	0.88508
3	$y = a + b / x$	0.87157	0.88513	11	$y = a + b\cdot\ln x$	0.87074	0.88543
4	$y = x / (a + bx)$	0.99587	0.99907	12	$y = a / (b + x)$	0.83369	0.76931
5	$y = ab^x$	0.83932	0.79422	13	$y = ax / (b + x)$	0.89122	0.93566
6	$y = ae^{bx}$	0.83932	0.79422	14	$y = ae^{b / x}$	0.88186	0.91253
7	$y = a \cdot 10^{bx}$	0.83932	0.79422	15	$y = a \cdot 10^{b / x}$	0.88186	0.91253
8	$y = 1 / (a + be^{-x})$	0.86049	0.99935	16	$y = a + bx^n$	0.80388	0.62168

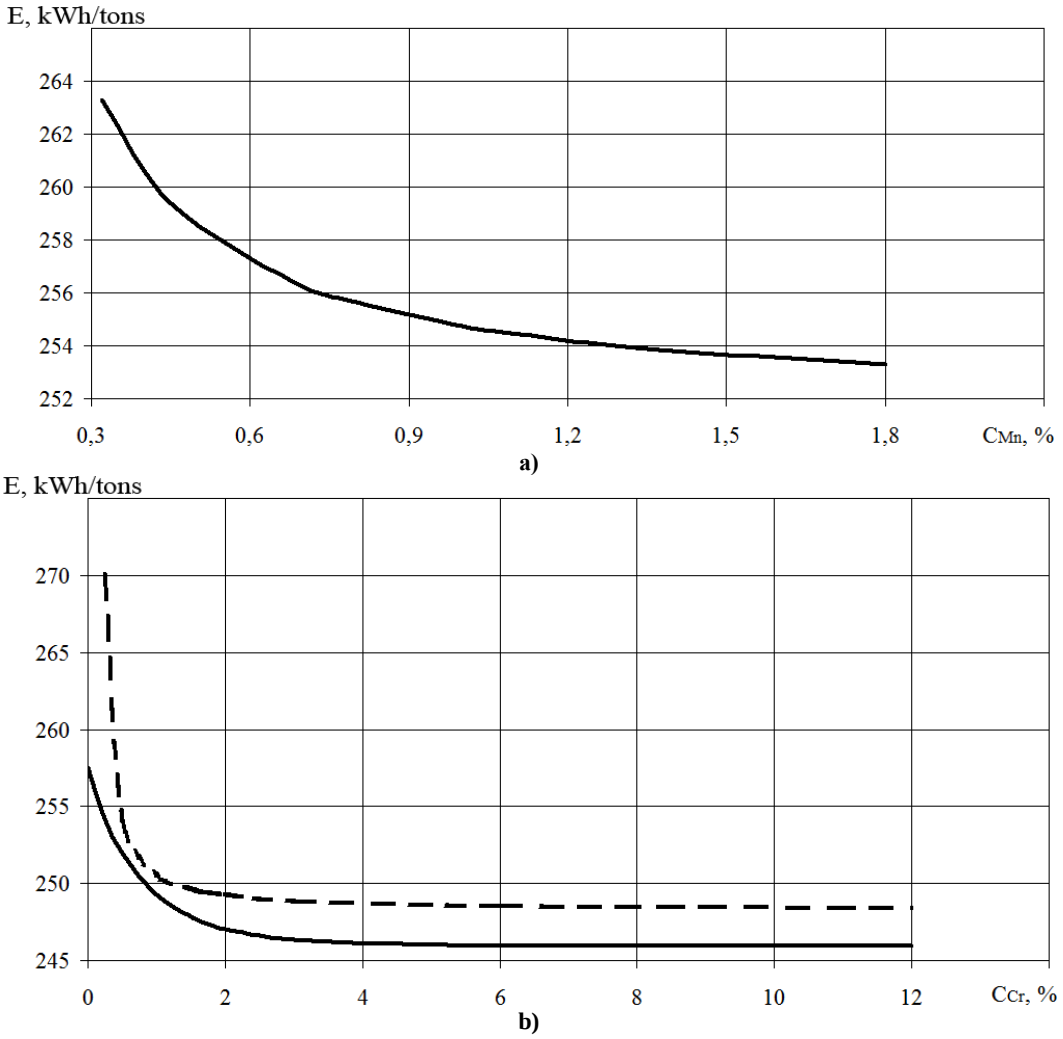

Fig. 2. The influence of an increase in the content of alloying elements in the steel of the auger after tempering on the energy intensity of the solid waste dehydration process after its operation and wear on the path s = 56850 m (a) – manganese, (b) – chromium

From the Fig. 2, it can be seen that after operation and wear on the path s = 56850 m during the dehydration of solid waste in the garbage truck, the increase in the manganese content in the auger steel after tempering from 0.32% to 1.8% leads to a decrease in energy intensity by 10 kWh/tons or 3.8%, increasing the chromium content in the auger steel after tempering from 0% to 6% leads to a decrease in energy intensity by 11.5 kWh/tons or 4.8% and to a reduction in the cost of the solid waste dehydration process in the garbage truck. In addition, the comparison in Fig. 2, *b* of the energy capacity of the screw steel after tempering (solid line) with the energy capacity of the hardened screw steel determined in [14] (dashed line) showed that the tempering of the screw steel after its hardening allows reducing the energy capacity by 1.26...2.56 kWh/tons depending on the

chromium content, which indicates the importance of determining the rational composition and structural state of the material of the friction surfaces of the screw and ways to increase its wear resistance.

Conclusions

The dependences of the relative wear resistance of the auger from the content of manganese and chromium in its steel after tempering have been determined. It was found that after operation and wear on the path s = 56850 m during the dehydration of solid waste in a garbage truck, an increase in the manganese content in the auger steel after tempering from 0.32% to 1.8% leads to a decrease in energy intensity by 10 kWh/tons or 3.8%, increasing the chromium content in the auger steel after tempering from 0% to 6% leads to a decrease in energy consumption by 11.5 kWh/tons or 4.8% and to a reduction in the cost of the solid waste dehydration process in the garbage truck. It was determined that the tempering of the auger steel after its hardening allows reducing the energy consumption by 1.26...2.56 kWh/tons depending on the chromium content. Therefore, the determination of the rational composition and structural state of the material of the friction surfaces of the auger and ways of increasing its wear resistance require further research.

References

1. Kutsova V.Z., Kindrachuk M.V., Kovzel M.A., Tisov O.V., Grebeneva A.V., Shvets P.Yu. (2016) Vplyv struktury, fazovogo skladu ta vlastyvostej na abrazyvnu znosostijkist' hromomargancevyh chavuniv u lytomu stani [The impact of the structure, phase structure and power on the abrasive wear resistance of chromium-manganese chavuns at the cast steel]. Problem of Friction and Wear, 2, 78-85.

2. Dykha O.V.(2018) Rozrahunkovo-eksperymental'ni metody keruvannja procesamy granychnogo zmashhuvannja tehnichnyh trybosystem [Computational and experimental methods of controlling processes of boundary lubrication of technical tribosystems]: monograph. Khmelnytskyi: KhNU.

3. Vlasyuk I.A., Mogylatenko V.G., Yamshinskyi M.M., Tovkach A.M. (2011). Vplyv lehuvalnykh elementiv na strukturu i vlastyvosti znosostiikykh stalei [The influence of alloying elements on the structure and properties of wear-resistant steels]. Metal and casting of Ukraine, 1, 26-28.

4. Malinov V.L. (2011) Vlijanie soderzhanija marganca i rezhimov otpuska na strukturu i iznosostojkost hromomargancevogo naplavlennogo metalla [The influence of manganese content and tempering regimes on the structure and wear resistance of chrome-manganese deposited metal]. Protection of metallurgical machines from breakdowns: coll. of scientific papers, 13, 247-254.

5. Tsymbal B.M.(2017) Pidvyshhennja znosostijkosti shnekovyh ekstruderiv dlja vyrobnyctva palyvnyh bryketiv u kyslotnyh ta luzhnyh seredovyshhah [Increasing the wear resistance of screw extruders for the production of fuel briquettes in acidic and alkaline environments]: abstract dis. … cand. tech. sciences: 05.02.04 – Friction and wear in machines, Kharkiv, 20.

6. Hevko R.B., Zalutskyi S.Z., Hladyo Y.B., Tkachenko I.G., Lyashuk O.L., Pavlova O.M., ... & Dobizha N.V. (2019). Determination of interaction parameters and grain material flow motion on screw conveyor elastic section surface. INMATEH-Agricultural Engineering, 57(1).

7. Goldshtein M.I., Grachev S.V., Veksler Y.G. (1999) Special'nye stali [Special steels]. M.: MISIS.

8. Orisaleye J.I., Ojolo S.J., Ajiboye J.S. (2019) Pressure build-up and wear analysis of tapered screw extruder biomass briquetting machines. Agricultural Engineering International: CIGR Journal, 21(1), 122-133.

9. Dvoruk V.I. (2014) Vplyv lehuvannia khromom konstruktsiinoi stali na yii abrazyvnu znosostiikist pislia vysokotemperaturnoi termomekhanichnoi obrobky [Effect of chromium alloying of structural steel on its abrasive wear resistance after high-temperature thermomechanical treatment]. Problems of Tribology, 3, 59-65.

10. Demirci A., Teke I., Polychronopoulos N. D., Vlachopoulos J. (2021) The Role of Calender Gap in Barrel and Screw Wear in Counterrotating Twin Screw Extruders. Polymers, 13(7), 990.

11. Tataryants M.S., Zavinsky S.I., Troshin A.G. (2015) Razrabotka metodiki raschjota nagruzok na shnek i jenergozatrat shnekovyh pressov [Development of a method for calculating the loads on the auger and the energy consumption of screw presses]. ScienceRise, 6(2), 80-84

12. Bereziuk O.V. (2018) Eksperymental"ne doslidzhennya procesiv znevodnennya tverdyx pobutovyx vidxodiv shnekovym presom [Experimental study of the processes of dehydration of solid household waste with a auger press]. Bulletin of the Vinnitsa Polytechnic Institute, 5, 18-24.

13. Bereziuk O.V., Savulyak V.I., Kharzhevskyi V.O. (2021) The influence of auger wear on the parameters of the dehydration process of solid waste in the garbage truck. Problems of Tribology, 26(2/100), 79-86.

14. Bereziuk O.V., Savulyak V.I., Kharzhevskyi V.O. (2022) The influence of the alloying of the auger by the chromium on its wear during dehydration process of municipal solid waste in the garbage truck. Problems of Tribology, 27(1/103), 50-57.

15. Chatterjee S., Hadi A.S. (2015) Regression analysis by example. John Wiley & Sons.

Березюк О.В., Савуляк В.І., Харжевський В.О. Вплив легування марганцем та хромом сталевого загартованого з відпуском шнека на його відносну зносостійкість під час зневоднення у сміттєвозі ТПВ.

Анотація

Стаття присвячена дослідженню впливу легування марганцем та хромом з наступним гартуванням та відпуском шнека на його зносостійкість під час зневоднення твердих побутових відходів у сміттєвозі. Використання математичного апарату та відповідних програм регресійного аналізу дозволило визначити залежність зносостійкості шнека від вмісту марганцю та хрому в сталі шнека для випадку його гартування з відпуском. Побудовані графічні залежності відносної зносостійкості із вказаним легуванням та термообробкою шнека виявили значний вплив концентрації марганцю та хрому в сталі, підтверджено достатню збіжність отриманих закономірностей. Графіки впливу легування марганцем та хромом сталевого шнека з наведеною термообробкою на енергоємність зневоднення твердих побутових відходів демонструють її доцільність. Встановлено, що після експлуатації та зношування на шляху s = 56850 м під час зневоднення ТПВ у сміттєвозі збільшення вмісту марганцю в сталі термообробленого шнека з 0,32% до 1,8% призводить до зниження енергоємності на 10 кВт·год/т, а збільшення вмісту хрому в сталі шнека після аналогічної термообробки з 0% до 6% призводить до зниження енергоємності на 11,5 кВт·год/т та до здешевлення процесу зневоднення ТПВ у сміттєвозі. Визначено, що відпуск хромо-марганцевої сталі шнека після її гартування дозволяє зменшити енергоємність на 1,26...2,56 кВт·год/т залежно від вмісту хрому. Виявлено доцільність проведення подальших досліджень з визначення раціонального складу і структурного стану матеріалу шнека та шляхів підвищення його зносостійкості.

Ключові слова: знос, зносостійкість, вміст марганцю, вміст хрому, відпуск, шнековий прес, сміттєвоз, зневоднення, тверді побутові відходи, регресійний аналіз.

***Problems of Tribology**, V. 27, No 4/106-2022, 58-68*

Problems of Tribology
Website: http://tribology.khnu.km.ua/index.php/ProbTrib
E-mail: tribosenator@gmail.com

DOI: https://doi.org/10.31891/2079-1372-2022-106-4-58-68

Thermal comfort formation of the bus interior depending on the power unit layout

K. Holenko[1*], Y. Voichyshyn[2], O. Horbai[2], M. Burian[2], V. Popovych[2], O. Makovkin[1]

[1] Khmelnytsky National University. Ukraine
[2] Lviv Polytechnic National University, Ukraine
E-mail: kgolenko@gmail.com

Received: 22 September 2022: Revised:105 November 2022: Accept: 05 December 2022

Abstract

Energy consumption and thermal comfort are among the issues that research engineers of heating, ventilation and air conditioning systems deal with when investigating the most feasible solutions for their implementation. Existing methods of thermal comfort assessment are not optimized in two important and interrelated aspects: achieving thermal comfort (a) at the lowest possible energy consumption (b). Thermal comfort is situationally achieved when occupants perceive the ambient temperature, humidity, air movement and thermal radiation as ideal and do not prefer warmer or colder air or a different humidity level. Thermal comfort is defined by ASHRAE Standard 55 as a subjective concept characterized by the sum of sensations that create physical and mental well-being in a person. That is, he/she is in a state in which he/she feels comfortable and does not need to change one or more environmental parameters. Many studies have been conducted according to the international standards for thermal comfort in vehicles. The presence of a large number of people in the bus leads to a deterioration of the air quality in its interior. The loss of quality is mainly caused by gases resulting from breathing and other organic particles. The presence of moisture, combustion products, particles can also reduce the air quality in the interior. Air quality is affected by the design features of heating, ventilation and air conditioning systems, which largely depend on the location of the power unit, which is the subject of the research. The influence of the bus engine layout is analysed in the presented work: for the rear-engine layout, the location of the engine vertically in the interior and other cases are also considered. Special fans are installed in the engine compartment to remove heat emitted by the engine.

Key words: thermal comfort, ASHRAE Standard, EN ISO 7730, HVAC, heating, ventilation and air conditioning systems, engine placement, power unit layout, driver interior, passenger compartment, PMV, PPD indices.

Introduction

People spend a lot of time in public transport every day, for example, in buses, trams, trains or subways. To make their journey comfortable, appropriate thermal conditions must be provided by HVAC (Heating, Ventilation, Air Conditioning) systems. Thermal comfort is achieved when passengers perceive the air temperature, humidity, air movement, and heat radiation of their surroundings as ideal and would not prefer warmer or colder air or a different humidity level [1].

Current methods of assessing thermal comfort are not optimized following two crucial and interrelated aspects: achieving thermal comfort (a) with the lowest possible level of energy consumption (b). Actually, the energy consumption and thermal comfort are major concerns for research engineers in heating, ventilation and air conditioning systems, which are more or less feasible to implement solutions.

The purpose of the work

The purpose of the work was to investigate air flow distribution from the engine compartment, to analyse

thermal comfort assessment in bus interior according the engine location (in case of different layouts).

Thermal comfort in transport

In fact, energy consumption and thermal comfort are major concerns for research engineers, studying solutions, which are more or less feasible to implement in heating, ventilation and air conditioning systems. For evaluating thermal comfort in the transport environment current standards which propose methods, are EN ISO 14505 and the American ASHRAE - 55. The first is divided into three parts. In ASHRAE 55 standard thermal comfort is defined by as a subjective concept characterized by a sum of sensations, which produce a person's physical and mental wellbeing, condition for which a person would not prefer a different environment. European EN ISO 7730 for assessing thermal comfort in buildings is used, based on the well-known theory of Fanger [2] and on the equivalent temperature model [3, 4]. EN ISO 7730 presents also the PMV and PPD indices proposed by Fanger over 30 years ago, Fanger conducted a study in which subjects that had "standard" clothes performing a “standard” activity.

In order to find an answer in terms of thermal comfort in vehicles many studies have been conducted following the three ways of approach the EN ISO 14505 [5] standards. Some of them take into account the subjective methods based on results collected from questionnaire surveys, others evaluate environmental quality based on experimental assessment of comfort parameters. In practice and in standards, in most cases, air temperature is the most observed and discussed of these parameters. A comfort value of the temperature is usually fixed inside the cockpit (interior) as main set point according to the outdoor air temperature.

Method to evaluate the thermal comfort as a function of air temperature is the one of the currently useds. This method uses sensors to measure local air temperature values at head and ankles level. The main purpose of this approach is to determine how quickly the temperature will increase or decrease in a warm or cold interior of the vehicle. It studies the non-homogeneity between the temperature at feet and head level and to establish if the global temperature level is situated within the limits of the accepted time. By using this method, only one of the needed parameters that concern the thermal comfort sensation is measured and any influence of air velocity and radiation (hot or cold) are neglected leading to wrong conclusions. This fact is a particularity of the thermal environment in vehicles where the air conditioning system leads to high local air velocities.

One of the principal factors of thermal discomfort both indirectly and directly is solar radiation, connected to the strong transient thermal regime. Kilic [6] recorded temperature values by 2°C higher in the case of sensors exposed to sunlight compared to those placed in the shaded zones, while a percentage between 18% - 31% of the cooling system capacity is used to reduce the load caused by the direct contribution of the solar radiation. The window colour is very important in this case. It can significantly reduce energy consumption for cooling by controlling the amount of fresh air introduced in the interior [7].

A fuzzy controller was used in study [8] in order to control two parameters - the air speed at the discharge grill and the percentage of recirculated air. By using the controller, it took less time to attain the desired interior temperature 20°C, which could be reflected on the energy consumption. Another method of reducing the fuel consumption of the vehicle is multi-zonal air distribution system. Conventional mono-zonal systems recorded an unnecessary energy consumption for cooling in the unoccupied space statistics show, if the vehicle has a low level of occupancy. Returning to the perspective of fuel consumption, authors investigated [9] the effect of the air-conditioning system. The effects obtained by reaching more efficient cooling around the occupants. The air distribution system was modified by installation discharge grills for rear passengers. The air being thus introduced through the discharge heaters from the dashboard for the front passengers, and ceiling discharge grills for the rear passengers. The PMV index was evaluated on base of computational fluid dynamics simulations correlated with empirical relations. The experimental validation of the simulations consisted in evaluating the performance of the air-conditioning system at various airflow rates and air temperatures. By the localized air-conditioning system, the energy was decreased by 20.8% and 30.2%, respectively, compared to a conventional situation [10, 11].

Another innovative air distribution system was studied [12] and concluded that in order to achieve the comfort parameters in the shortest time, the best place to install additional ventilation diffusers is behind the rear seat passengers. The authors found PMV index values between -0.3 and 0.2 during the warm season. Totally different from the values (-0.1 and 1) was obtained for situation without discharge heater behind the rear passenger’s seat. The authors noticed a non-uniformity between temperature exceeded 2°C, which measured at chest level between the front and rear parts of the vehicles.

In many cases parameters with an influence in assessing thermal comfort, actual thermal comfort indices solar radiation is not taken into consideration. This parameter does not only raise the indoor air temperature but is also a local discomfort parameter.

Implementing an anti-solar foil is a proven solution to reduce the solar radiation influence. But it has a negative influence on the driving safety during the night. Therefore, another solution is to implement local ventilation heater to reduce the energy consumption and to ensure a better uniformity for the indoor parameters of the interior.

The numerical calculation of airflow combined with heat exchange in a passenger coach was to carry out in [13]. Two cases of boundary conditions were considered with ANSYS CFX 12.1 software. The first obtained

from design calculations common for ordinary buildings and information included in standards and the second was only based on the information included in standards. After analysing of the results, similar average air velocity was 0.79 m/s and it was found for distribution of air velocity in a coach in both cases. However, the distribution of air temperature was different. For case 1 the average indoor air temperature was 25.07°C and for case 2 was 23.53°C. The method of determining the heat solar gains had an impact on the results. A further possibility of a model improvement indicated that human models will be introduced in coaches, in order to verify the conditions of their thermal comfort, and air recirculation.

Bus power unit layout variants research

Since we propose the use of an additional fan, which is installed on the engine compartment, we should consider what options there are for the location of the engine in buses (possible layouts). There are shown the examples of buses with different engine locations (layouts) on Fig. 1 [14].

Fig.1 Buses with different engine layouts: a) front with a compartment in the interior; b) front with hood layout; c) middle horizontally under the floor; d) middle vertically; e) horizontally under the rear seats; f) rear vertically with an offset to the left.

The front-engine configuration is typical for small buses and minibuses. The layout of this type can be of two kinds. The first is with the location of the engine compartment in the bus interior at the front above the front axle (Fig. 1a). The driver usually has his own separate door built in. Buses of this type can be seen on the streets of Ukrainian cities, so-called "routes". The second kind has a hood layout (Fig. 1b) (typically for some brands of buses operated in the USA or some South American countries). American school bus is the most common variant of such bus, which is still manufactured today. Front-hood buses can be found in most cities of the world in the form of minibuses or small buses built on Mercedes Sprinter, Vario, etc. chassis.

The mid-engine layout is also not very popular today, even less popular than the front-engine one, and is characteristic only for some manufacturers (Volvo, Van Hool, MAZ). There are two types of such engine layout: under the floor (Fig. 1c) and vertically in a special section (Fig. 1d). It becomes impossible to create a 100% low floor interior when placing the engine under the floor or when placing the engine vertically, which is installed in areas for standing passengers. It is impossible to ensure a 100% low floor level but with such a scheme, that's why this type of layout could be met in two- or three-section buses.

Basically, the layout with the engine in the rear part is the most popular. There can be two options, when the engine is located under the rear seats (Fig. 1e) or when the engine is placed vertically in a special locker, which is shifted to the left (Fig. 1f).

Temperature state analysis in the bus interior

Thermal balance general equation of the bus interior will have the form [15]:

$$Q = \sum Q_i = Q_1 + Q_2 + Q_3 + Q_4 + Q_5, \quad (1)$$

where: Q_1 – infiltration of solar radiation; Q_2 – heat losses at service stops during the exit and entry of passengers; Q_3 – amount of heat coming through the surfaces of the bus body; Q_4 – amount of heat entering

through the windows in the bus body; Q_5 – amount of heat emitted by passengers; Q – total amount of heat is needed to stabilize the temperature in the bus interior.

We consider heat transfer in stationary environment of constant density in the theory of thermal conductivity of materials, therefore the differential equation of thermal conductivity will have the form [16]:

$$a\left(\frac{\partial^2 t}{\partial x^2}+\frac{\partial^2 t}{\partial y^2}+\frac{\partial^2 t}{\partial z^2}\right)=\frac{\partial t}{\partial \tau}, \tag{2}$$

Based on the heat transfer equation (2), we need to find the temperature distribution over the volumetric body, taking into account the change in temperature t depending on the coordinates x, y, z in space and time τ.

The equitation (2) could be solved as a stationary one first. It is necessary to determine the initial conditions of the non-stationary problem in order to solve it (3):

$$\frac{\partial^2 t}{\partial x^2}+\frac{\partial^2 t}{\partial y^2}+\frac{\partial^2 t}{\partial z^2}=0, \tag{3}$$

We should consider our problem next as a flat heat conduction equitation, the general form of which will have such look (4):

$$\frac{\partial^2 t}{\partial x^2}+\frac{\partial^2 t}{\partial y^2}=0, \tag{4}$$

Let's reduce the final simplification of the problem (2) to the one-dimensional equitation of the thermal conductivity (5):

$$\frac{\partial^2 t}{\partial x^2}=0, \tag{5}$$

Such a equitation is further reduced to the calculation of the temperature distribution along the wall of thickness δ. The basic equation used in fluid and gas dynamics is the Reynolds-averaged Navier-Stokes. The speed in this case is divided into two components (6) [17]:

$$u_i=U_i+u_i', \tag{6}$$

where: U_i – the main component of speed; u_i' – the component of speed due to vibrations.

Instantaneous averaging over the Reynolds-averaged Navier-Stokes equation can be written as follows (7), (8) and (9):

$$\frac{\partial U_i}{\partial x_i}=0, \tag{7}$$

$$\rho\frac{\partial \mathrm{U_i}}{\partial \mathrm{t}}+\rho \mathrm{U_j}\frac{\partial \mathrm{U_i}}{\partial \mathrm{x_j}}=-\frac{\partial \mathrm{P}}{\partial \mathrm{x_i}}+\frac{\partial}{\partial \mathrm{x_j}}\left[\mu\left(\frac{\partial \mathrm{u_i}}{\partial \mathrm{x_j}}-\mathrm{u_i u_j}\right)\right], \tag{8}$$

$$\rho\frac{\partial \mathrm{T}}{\partial \mathrm{t}}+\rho \mathrm{U_j}\frac{\partial \mathrm{T}}{\partial \mathrm{x_j}}=-\frac{\partial}{\mathrm{c_p}\,\partial \mathrm{x_j}}\left(\mathrm{k}\frac{\partial \mathrm{T}}{\partial \mathrm{x_j}}\right)-\frac{\partial \mathrm{u_i T}}{\partial \mathrm{x_j}}, \tag{9}$$

where: ρ - flux density; μ - dynamic viscosity of the substance; u – flow rate; P - pressure in liquid or gas; T - temperature of liquid or gas; t – flow time; x_i – position tensor in x, y, z coordinates; c_p – specific heat capacity of substance; k – thermal conductivity; $u_i\,u_j$ is the Reynolds stress tensor.

Since we are evaluating the heating elements efficiency, we should analyse the efficiency of the bus heating system. Let's evaluate the efficiency of the heating system using the exergetic efficiency (eq.10) with some correction factors taken into account:

$$\eta_{ex}=K_1K_2K_3\left(\frac{Ex_{sa}+Ex_{ea}}{Ex_{oa}+Ex_{ra}}\right), \tag{10}$$

where: K_1 - coefficient that depends on the location of the engine; K_2 - coefficient that depends on the season; K_3 is a coefficient that depends on the mode of operation of the bus on the route; Ex_{sa} – exergy of incoming air flow; Ex_{oa} – exergy of the external air flow; Ex_{ra} – exergy of air flow in the room; Ex_{ea} - exergy of the ejected air flow.

The next step of our work will be dedicated to study of the heat flow dissipation in the bus interior with different 5 variants of bus engine placement:

A - front;
B - middle vertically;
C - middle horizontally with an opposite engine;
D - rear vertically shifted to the left;
E - rear horizontally with an opposed engine.

Basically, the temperature values on the walls that separate the engine from the passenger compartment are approximately 30-50 ^{0}C. Knowing this, we can now set the initial parameters (Table 1) to calculate and simulate the temperature distribution in the Ansys Fluent Flow software environment [18, 19] for those five different bus layouts.

Table 1

Boundary conditions for air flow modelling in the bus interior

#	Parameter	Unit	Meaning
1	Gravity	m/s^2	-9.81
2	Velocity magnitude (inlet area)	m/s	0,25
3	Temperature (inlet area)	K	318
4	Temperature of internal volume and walls	K	293
5	Convection for static air	W⁄m^{2}K	25

We will additionally use special fans, which are installed on the engine compartment regardless of its location, and serve to transfer the heat released by the engine during its operation and disperse this heat throughout the bus interior.

The calculation method should be explained first. We have designed 3D models of bus interior spaces with air intake and exhaust locations to achieve our goals. Having the necessary models, FEA mesh was generated for the appropriate models for applying of the boundary conditions. The next step was to set up the solution and run the simulation to obtain the results of the calculations.

The vast majority of real liquid or air flows will pass in a turbulent mode [20 – 22], because they carry out non-uniform movement in the required areas. We perform calculations on a simplified model of a city bus in our study - that is, we have a 3D model of the bus with only those elements that we need in the calculations, namely the elements of the internal space of the bus. Total calculation time on the equipment (2 Intel Xeon processors 24 cores, RAM 48 Gb, NVIDIA GeForce 4Gb video) was 6 hours 17 min. Later we consider the results of modelling temperature flows in bus interiors with different engine layouts.

Taking into account the fact that microclimatic parameters are standardized at three levels (floor, middle and head) in many regulatory documents, we will also further consider the distribution of temperatures in these zones as shown in fig. 2. We divided the interior of the bus into 6 zones: 3 horizontally (floor, middle and head level) and 3 vertically (driver's interior, middle storage and rear platforms).

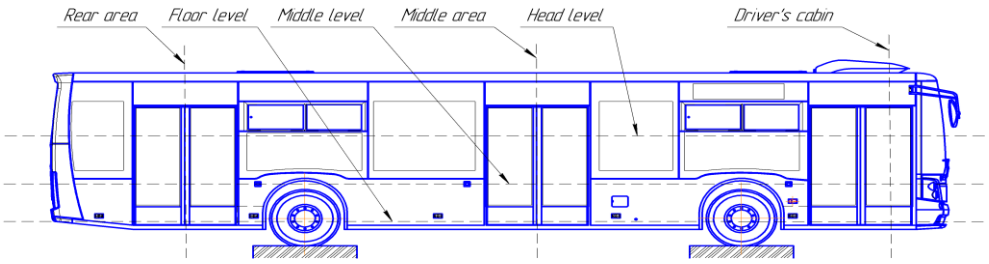

Fig. 2. Zones of the bus interior

Heat flow modelling – front layout (A)

As we can see in Fig. 3a, the air flows come out of the engine compartment from the front near the driver's workplace and then disperse throughout the bus interior. Air flows intensively at the level of the feet with temperature fluctuations in the region of 25^{0}C at the driver's workplace. Next, the air flow is dispersed throughout the interior, keeping to the floor level. The air speed at floor level is approximately 0.18-0.19 m/s. The temperature fluctuates at the level of 18-20^{0}C (Fig. 5b and 5c) in this area. As you can see, the air circulation is not very active, because the distribution of air is somewhat limited, due to the fact that a wider flow of air is hindered by the wheel arches and the fact that the air is blown lower, closer to the floor. In principle, there is no air circulation in the driver's interior. One plane is chosen at the level of the seats of the left row (Fig. 3b), and the second - in the middle of the interior (Fig. 3c). As it can be seen from Fig. 3 the hotter air is expected at floor level between the front wheel arches and the temperature in this area is approximately 20-25^{0}C. To visualize the air stream velocity we have used 300 lines modelling (Fig. 1a) – it's optimum meaning to show the situation inside of interior properly: more lines will fill the space with indistinguishable flows; less meaning will steal important information about the flow's behavior (where and how the air flows are getting and spreading inside). The highest speed of the air flow correspondents to the closer to red color and is observed near the inlet and outlet channels (both are working as funnels). The same approach with 300 lines modelling is used for all the rest calculation cases presented below.

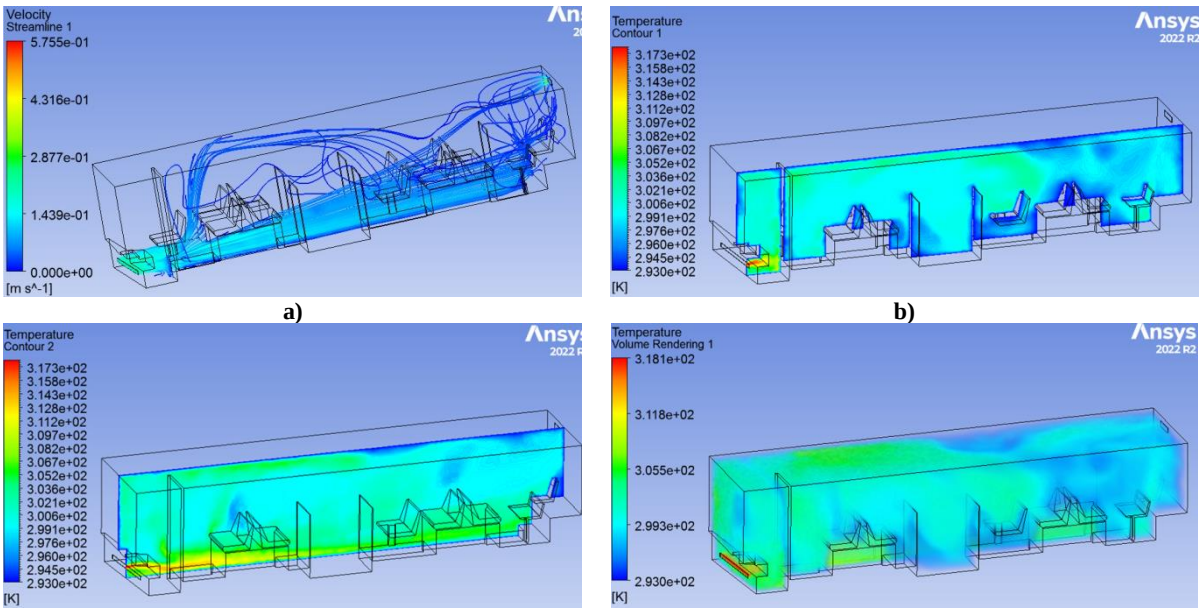

Fig. 3. Velocity and temperatures distribution in the interior with a front layout: a) velocity in the interior; b) temperature distribution along the plane at the level of the left row of seats; c) temperature distribution along the plane at the level of the middle of the interior; d) temperature maps of the interior volume

Heat flow modelling – middle vertically layout (B)

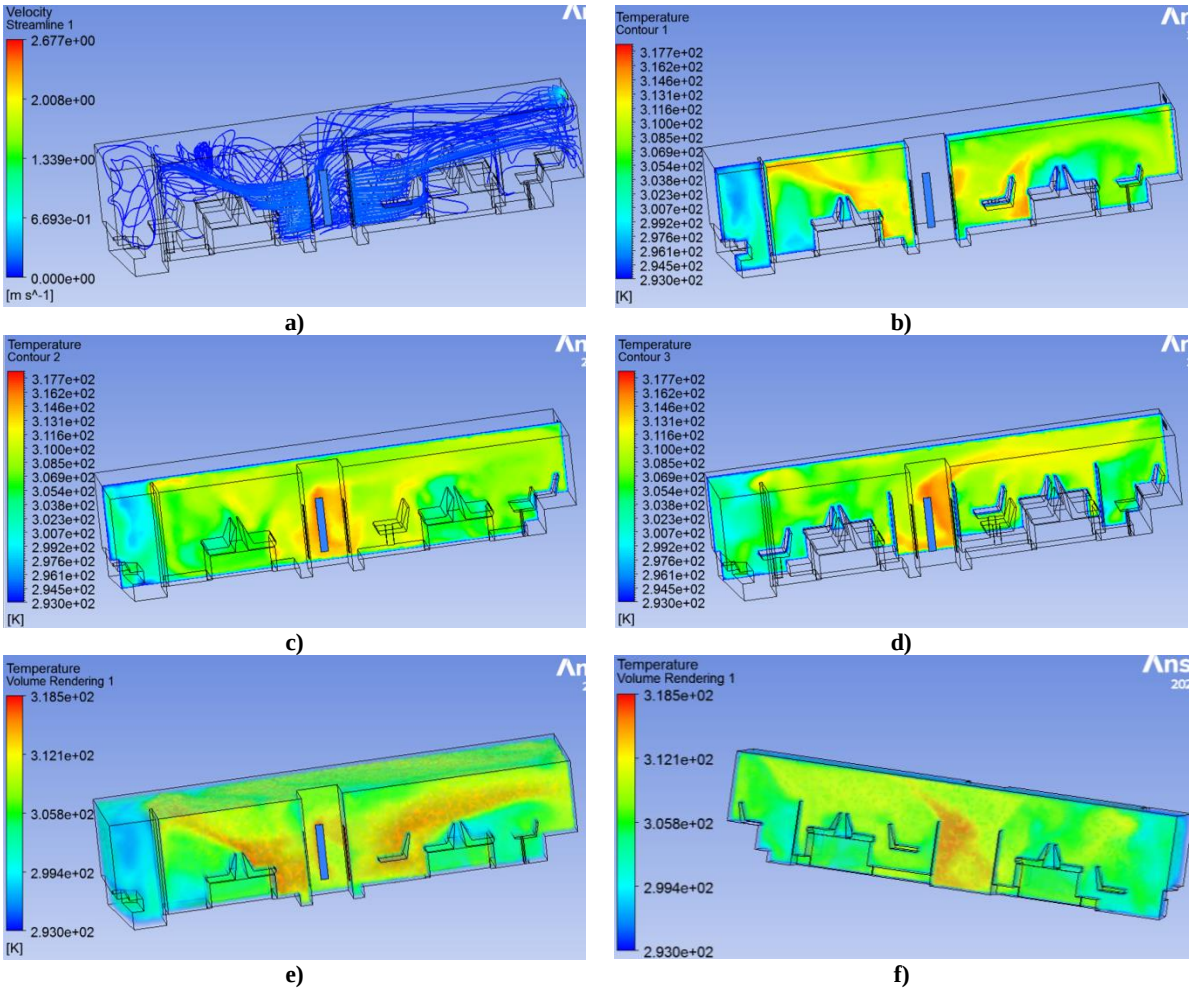

Fig. 4. Velocity and temperature distribution in the interior with a middle vertically layout: a) velocity in the interior; b) temperature distribution along the plane at the level of the left row of seats; c) temperature distribution along the plane at the level of the middle of the interior; d) temperature distribution on the plane at the level of the right row of the interior; e), f) temperature maps of the interior volume

Air flows were simulated in the middle vertically engine layout, taking into account the fact that three additional fans are installed in the middle of the engine compartment, so there are three places for blowing warm air. As we can see in Fig. 4a, the air flows from the places where warm air is blown into the engine compartment in three different directions (left to the front, right to the back, and straight towards the middle door). It can be seen that the air flows intensively disperse in places of the interior to the wheel arches at a height of approximately 1.5 m from the floor level with a speed somewhere at the level of 0.2-0.25 m/s with a temperature of approximately 25-27 ^{0}C (Fig. 4a). There are almost no air flows in the driver's interior. Air speed and temperature in the driver's interior are 0.2-0.25 m/s and 18-20 ^{0}C, respectively. This happens due to the fact that the driver's interior is separated from the interior space. Next, the air flow is dispersed throughout the interior. The highest temperature values are reached at the storage site and are 27-28 ^{0}C. As you can see, the air circulation is very active, since the air distribution comes from 3 points and is directed in different directions. The average air speed in the interior is 0.2-0.25 m/s. We choose the first plane at the level of the seats of the left row (Fig. 4b), the second in the middle of the interior (Fig. 4c) and the third - at the level of the seats of the right row (Fig. 4d). The highest temperature values are reached at the storage site and are 27-28 ^{0}C. As it can be seen from Fig. 4e and 4f, hotter air is assumed at the level of the seats near the engine compartment and, accordingly, is dispersed upwards in the space of the bus interior with a temperature of 25-27 ^{0}C. Looking at the temperature maps, it's clear that the passenger compartment is heated better than the driver's interior.

Heat flow modelling – middle horizontally with an opposite engine layout (C)

Air flows were simulated, taking into account that two additional fans are installed on the left and right walls on the floor (opposite engine compartment). It turns out that there will be two places for blowing in the middle of the bus interior.

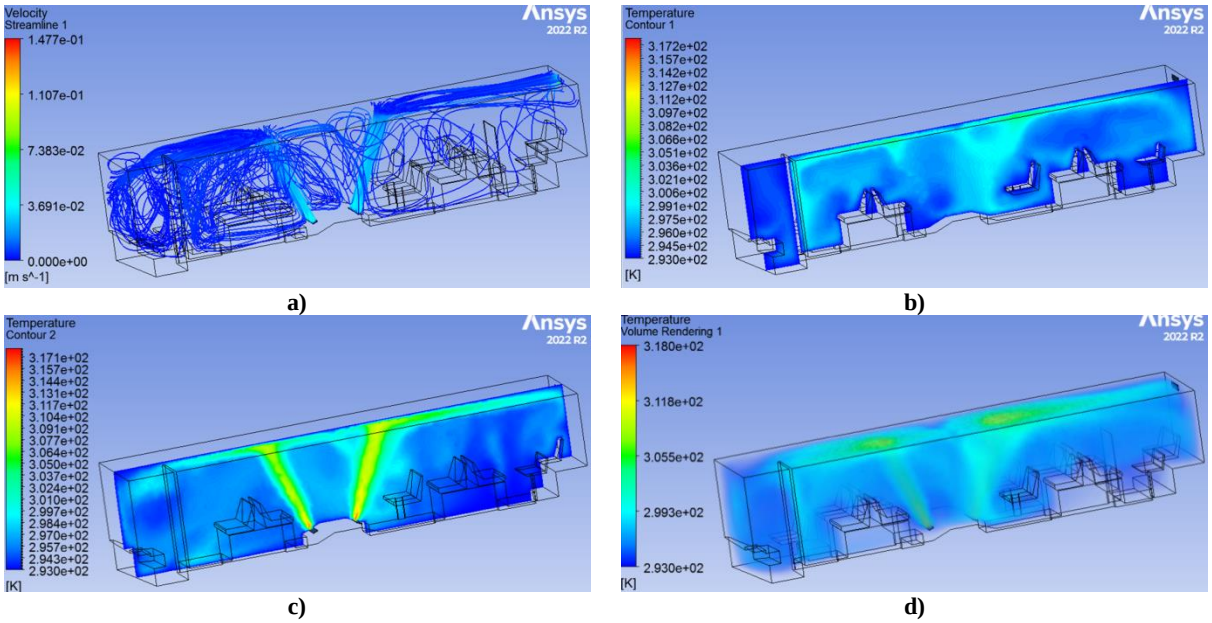

Fig. 5. Velocity and temperature distribution in the interior for middle horizontally with an opposite engine layout: a) velocity in the interior; b) temperature distribution along the plane at the level of the left row of seats; c) temperature distribution along the plane at the level of the middle of the interior; d) temperature maps of the interior volume

As we can see in Fig. 5a, the air flows from the warm air outlets on the engine compartment, which in our case is also the part of the floor, in two different directions (left up and right up) and disperse at the ceiling level. Air circulation occurs at a speed of approximately 0.2-0.25 m/s at head level. It can also be seen that the air flows are intensively dispersed in the front part of the bus and also enter the driver's interior, where the air speed is at the level of 0.2 m/s. As you can see, air circulation is very active in the driver's interior and the front part of the bus interior. In the rear part of the bus, air flows circulate in smaller quantities than in the front part.

We choose the first plane at the level of the seats of the left row (Fig. 5b) and the second - in the middle of the interior (Fig. 5c). The temperature fluctuates almost uniformly throughout the bus interior in the region of 14-16 ^{0}C, which is a fairly comfortable microclimate. Hotter air is expected in places along the flow of hot air from the fans and dissipates accordingly upwards (Fig. 5C). The temperature is around 20 ^{0}C at head level in such locations.

Heat flow modelling – rear vertically shifted to the left layout (D)

Air flows were modelled taking into account that the additional fan is located on the wall of the engine compartment above the last two seats in the left row of bus seats.

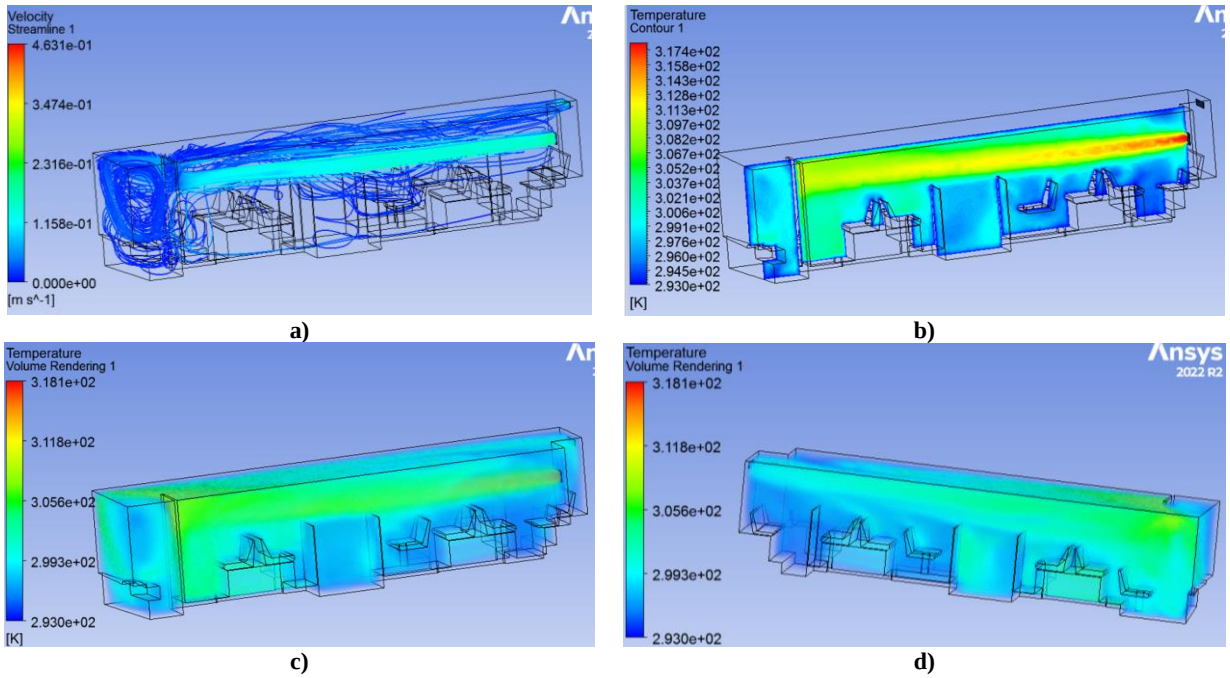

Fig. 6. Velocity and temperature distribution in the interior with rear vertically shifted to the left layout: a) velocity in the interior; b) temperature distribution along the plane at the level of the left row of seats; c), d) temperature maps of the interior volume

Air flows from the warm air outlet on the engine compartment above the seats in the rear part of the bus interior (Fig. 6a). It is clearly visible that the air flows intensively disperse above the bus interior with an air speed of Fig. 6a, approximately at the level of the standing passenger's head, and also enter the driver's place due to the fact it is not tightly separated from the interior. The speed of air flow in this area is 0.15-0.22 m/s. We choose the plane at the level of the seats of the left row (Fig. 6b). The temperature fluctuates in the area in most of the interior is around 18-20 ^{0}C, only in the rear part in the area of the thermal air outlet it reaches 22-24 ^{0}C.

Heat flow modelling – rear horizontally with an opposed engine layout (E)

An additional fan is located on the wall of the engine compartment below at the level of the feet for the presented case. Air flows come from the warm air outlet on the wall of the engine compartment under the seats in the back of the bus interior (Fig. 7a) and intensively dispersed around the interior by turbulent flows at a speed of **0.18-0.2 m/s**, and also enter the driver's interior with the low speed **0.17-0.18 m/s** due to the fact that that the driver's place is not tightly separated from the rest of the interior volume.

The plane is chosen at the level of the seats left row (Fig. 7b) and at the level of the middle of the interior (Fig. 7c). The highest temperature values are in the rare part of the bus at the level of the legs and waist are **24-28 ^{0}C**. Further, the temperature drops in the interior, it will reach **18-22 ^{0}C** in the middle of the bus and **18-20 ^{0}C** in the driver's interior.

After analysing the obtained results, we will compile data in tables with temperatures and air velocities for the researched 5 layouts different of the bus (Table 2, 3). It must be admitted that the air dispersity depends much of the convection for static air inside of the interior: either the conditioning system is activated and blows actively or the windows are opened which could be possible during the warm season of the bus exploitation. Being said the research experiments presented in the current publication were based on 25 W⁄m^{2}K (Table 1). Minimal convection of the static air could be 5 W⁄m^{2}K (typical) for the real-life buildings, etc, but the presence of a large number of people in the bus leads to a deterioration of the air quality in its interior. The loss of quality is mainly caused by gases resulting from breathing and other organic particles, so the convection should be raised however to 25 W⁄m^{2}K to achieve the necessary refreshing of the air volume. On another hand stays the fan speed, which is variable (was set 0.25 m/s in our boundary conditions) and could be increased by necessity. Should it help for the circulation and comfort? Well, it depends on the bus layout: for example, the increasing the fan speed for rear vertically shifted to the left layout (D) won't be efficient – the air stream will just pass faster near the passenger's heads, but less its portion will be renewed on the middle and especially floor level!

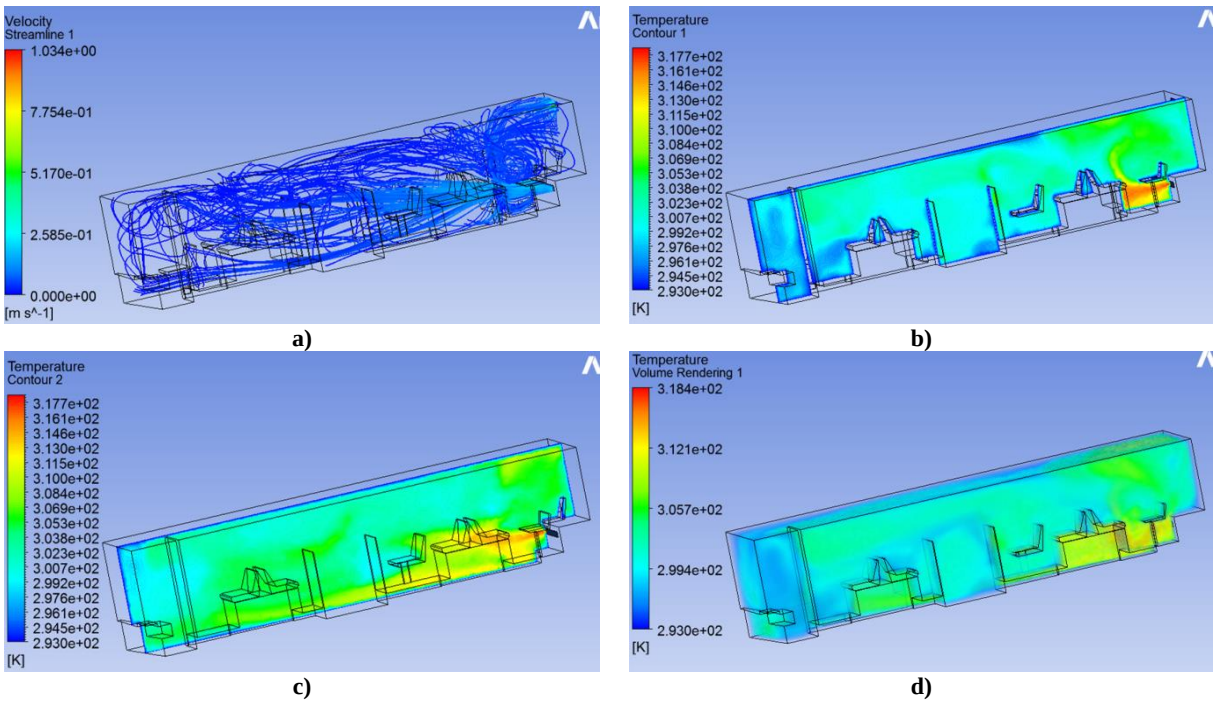

Fig. 7. Velocity and temperature distribution in the interior for rear horizontally with an opposed engine layout: a) velocity in the interior; b) temperature distribution along the plane at the level of the left row of seats; c) temperature distribution along the plane at the level of the middle; d) temperature maps of the interior volume

Table 2

Temperature parameters in the bus's interior depending on the power unit layout

#	Power unit layout	Interior level	Driver's interior, m/s	Middle area, m/s	Rear area, m/s
1.	A)	floor	25	18-20	18-20
2.		middle	19-20	18-20	14-20
3.		head	18-20	18-20	14-20
4.	B)	floor	18-20	25-27	18-20
5.		middle	18-20	27-28	18-20
6.		head	18-20	27-28	20-21
7.	C)	floor	14-16	14-16	14-16
8.		middle	14-16	14-16	14-20
9.		head	14-16	18-20	14-20
10.	D)	floor	18-19	19-20	14-16
11.		middle	18-19	19-20	16-18
12.		head	19-20	20-22	22-24
13.	E)	floor	18-20	19-22	26-28
14.		middle	18-20	19-22	24-25
15.		head	18-20	19-22	20-22

Table 3

Air velocity in the bus's interior depending on the power unit layout

#	Power unit layout	Interior level	Driver's interior, m/s	Middle area, m/s	Rear area, m/s
1.	A)	floor	0,2	0,18-0,19	0,1-0,15
2.		middle	0,05	0,18-0,19	0,1
3.		head	0,02	0,05	0,05
4.	B)	floor	0,2	0,2-0,25	0,2-0,25
5.		middle	0,2-0,25	0,2-0,25	0,2-0,25
6.		head	0,2-0,25	0,2-0,25	0,2-0,25
7.	C)	floor	0,2	0,2-0,25	0,2
8.		middle	0,2	0,2-0,25	0,2
9.		head	0,2	0,2-0,25	0,2
10.	D)	floor	0,18-0,19	0,15	0,2-0,25
11.		middle	0,18-0,19	0,15	0,2-0,25
12.		head	0,18-0,19	0,15	0,2-0,25
13.	E)	floor	0,17-0,18	0,18-0,2	0,2-0,25
14.		middle	0,17-0,18	0,18-0,2	0,2-0,25
15.		head	0,17-0,18	0,18-0,2	0,2

Conclusions

FEA computer modelling in engineering or scientific development is very important nowadays, because we can get the preliminary results of our work and its shortcomings with the help of specialized software, which will allow to eliminate problems much faster in the future without live tests. Boundary conditions and the designed calculation approach are the keys to create maximum similar to the real-life results and environment methodology, which will be accurate and efficient enough to imitate the bus interior air flow.

It was proposed to add an additional fan, which will be attached to the engine compartment, and the outlet channel on the rear wall of the bus. By using computer simulation carried out in the ANSYS Fluent Flow software environment the results of the calculation showed that the temperature with 5 different layouts of the interior remains within the normal range of approximately 296-305 K, but differs significantly by the locations. The best circulation of air flows occurs with the following layouts of the engine in the bus: middle vertically and rear horizontally with an opposite engine. Such schemes are the most efficient due to the balance of temperature vs velocity distribution and final microclimate comfort inside of interior.

References

1. Haller G. (2006). Thermal Comfort in Rail Vehicles. RTA Rail Tec Arsenal Fahrzeugversuchsanlage GmbH, Vienna.

2. P.O. Fanger, Proposed Nordic standard for ventilation and thermal comfort, in: in Proc. Int. Conf. On Building Energy Managment, 1980.

3. H. Nilsson, I. Holmér, M. Bohm, O. Norén, Equivalent temperature and thermal sensation - Comparison with subjective responses, in: Comfort in the automotive industry- Recent development and achievements, Bologna, Italy, 1997, pp. 157-162.

4. H.O. Nilsson, I. Holmér, Definitions and Measurements of Equivalent Temperature, European commission cost contract no smt4-ct95-2017.

5. ISO, Ergonomics of the thermal environment - Evaluation of thermal environments in vehicles: Principles and methods for assessment of thermal stress, in: ISO 14505-1:2007, 2007.

6. M. Kilic, S.M. Akyol, Experimental investigation of termal confrot and air qualitu in an automobile interior during cooling period, Heat MassTransfer, 48 (2012) 1375-1384.

7. B. Torregrosa-Jaime, F. Bjurling, J.M. Corberan, F.D. Sciullo, J. Paya, Transient thermal model of a vehicle's interior validated under variable ambient conditions, Applied Thermal Engineering, 75 (2015) 45-53.

8. S. Sepehr, M. Dehghandokht, A. Fartaj, Temperature control of a interior in an automobile using thermal modeling and fuzzy controller, Applied Energy, (2012) 860–868.

9. M.S. Oh, J.H. Ahn, D.W. Kim, D.S. Jang, Y. Kim, Thermal comfort and energy saving in a vehicle compartment using a localized air-conditioning system, Applied Energy, 133 (2014) 14-21.

10. P. Dancaa, A. Vartiresa, A. Dogeanu. An overview of current methods for thermal comfort assessment in vehicle interior Energy Procedia 85 (2016) 162 – 169.

11. D.W. Lee, Impact of a three-dimensional air-conditioning system on thermal comfort: An experimental study, Int.J Automot. Technol., 16 (2015) 411-416.

12. I.Sarna, A.Palmowska. Modelling of the airflow in the passenger coach. Architecture Civil Engineering Enviroment, No 4, 2019, pp.125-132

13. Şaban Ünal. An experimental study on a bus air conditioner to determine its conformity to design and comfort conditions. Journal of thermal engineering, 2017, No 1, pp. 1089-1101

14. Horbai O.Z. Mitsnist ta pasyvna bezpeka avtobusnykh kuzoviv: monohrafiia / O.Z. Horbai, K.E. Holenko, L.V. Krainyk. – Lviv: Vydavnytstvo Lvivskoi politekhniky., 2013. – 276 s.

15. O. A. Tryhub, V. V. Zahubynoha, L. A. Tarandushka. Vyznachennia produktyvnosti nahnitaiuchykh ventyliatoriv systemy avtomatychnoi ventyliatsii kuzova avtomobilia. Visnyk Vinnytskoho politekhnichnoho instytutu, 2018, №4. – S. 95-102.

16. O. Horbay, Y. Voichyshyn, E. Yakovenko. (2020). Study of the heating system of a city bus. International symposium of education and values, 4, p. 70.

17. Özgur Ekici and Gökhan Güney. (2017). Experimantal and numerical investigations of heating in a bus interior under transient state conditions. Computational methods and experimental measurements XVIII. Transactions on engineering sciences, 118, pp. 49-59.

18. Jhan Piero Rojas, Guillermo Valencia Ochoa, Jorge Duarte Forero. CFD Analysis of Swirl Effect in a Diesel Engine Using OpenFOAM. 10.15866/iremos.v13i1.18372, 2020, Vol 13 (1), pp. 8

19. Zhang, T., Yin, S. & Wang, S., An under-aisle air distribution system facilitating humidification of commercial aircraft interiors. Building and Environment, 45, pp. 907–915, 2010

20. Dolinskiy A.A., Draganov B.Kh. Optimizatsiya energeticheskikh sistem na osnove teoretiko-grafovykh postroyeniy [Optimization of energy systems based on graph-theoretic constructions]. Kiev: Akademperiodika, 2013. 67 p.

21. Zhang, T., Li, P. & Wang, S., A personal air distribution system with air terminals embedded in chair armrests on commercial airplanes. Building and Environment, 47(1), pp. 89–99, 2012.

22. Zhang, T. & Chen, Q., Novel air distribution systems for commercial aircraft interiors. Building and Environment, 42, pp. 1675–1684, 2007.

Голенко К.Е., Войчишин Ю.В., Горбай О.З., Бур'ян М.В., Попович В.В., Маковкін О.М. Формування теплового комфорту салону автобуса в залежності від компоновки силового агрегата

Енергоспоживання та тепловий комфорт належать до проблематики, якою займаються інженери-дослідники систем опалення, вентиляції та кондиціювання повітря при пошуку рішень, найбільш можливих для їх реалізації. Існуючі методи оцінки теплового комфорту не є оптимізованими за двома важливими і взаємопов'язаними аспектами: досягнення теплового комфорту при мінімально можливому рівні енергоспоживання. Тепловий комфорт ситуативно досягається тоді, коли пасажири сприймають температуру, вологість, рух повітря та теплове випромінювання навколишнього середовища як ідеальні і не надають перевагу більш теплому чи холодному повітрю або іншому рівню вологості. Тепловий комфорт визначається стандартом ASHRAE 55 як суб'єктивне поняття, що характеризується сумою відчуттів, які створюють у людини фізичне та психічне благополуччя: вона перебуває в стані, за якого почуває себе комфортно і не потребує зміни одного чи декількох параметрів навколишнього середовища. Було проведено багато досліджень за міжнародними стандартами щодо теплового комфорту в транспортних засобах. Присутність великої кількості людей в автобусі приводить до погіршення якості повітря в його салоні. Втрата якості в основному викликана газами, що утворюються в результаті дихання та виходу інших органічних частинок. Наявність вологи, продуктів згоряння, частинок також може знизити якість повітря в салоні. На якість повітря впливають і конструктивні особливості систем опалення, вентиляції та кондиціювання повітря, які в значній мірі залежать від розташування силового агрегату, що і є предметом проведених п'яти досліджень. Проаналізовано вплив розташування двигуна міського автобуса спереду, в базі та в задній частині на зміну повітрообміну в салоні. Для задньомоторної компоновки розглянуто також розташування двигуна вертикально в шафі-тумбі. Для відбору теплоти, яка виділяється двигуном у мотовідсіку встановлено спеціальні вентилятори.

Ключові слова: тепловий комфорт, ASHRAE, EN ISO 7730, HVAC, опалення, вентиляція та кондиціонування повітря, розташування двигуна, кабіна водія, пасажирський салон, PMV, PPD.

Problems of Tribology, V. 27, No 4/106-2022, 69-81

Problems of Tribology
Website: http://tribology.khnu.km.ua/index.php/ProbTrib
E-mail: tribosenator@gmail.com

DOI: https://doi.org/10.31891/2079-1372-2022-106-4-69-81

Parameters of the lubrication process during operational wear of the crankshaft bearings of automobile engines

V. Aulin[1*], S. Lysenko[1], A. Hrynkiv[1], O. Liashuk[2], A. Hupka[2], O. Livitskyi[1]

[1] *Central Ukrainian National Technical University, Ukraine*
[2]*Ternopil Ivan Puluj National Technical University, Ukraine*
**E-mail: AulinVV@gmail.com*

Received: 09 November 2022: Revised:02 December 2022: Accept:12 December 2022

Abstract

The article discusses the dynamics of the lubrication process during the operational wear of the crankshaft bearings of automobile engines. All lubrication modes and wear processes are analyzed. The main attention is paid to the steady and unsteady modes of lubrication of the crankshaft bearings. The nature of the dynamics of changing lubrication regimes is substantiated through operational tribological parameters that characterize the integral degree of existence of the lubricating layer. A model is proposed for the relationship of these parameters with a number of factors, and the nature of their changes with a change in the speed of the crankshaft of the car engine is substantiated.

The results of bench tests of diesel engines of the KamAZ series, speed and load characteristics of the engine in terms of tribological operational parameters are presented. A graphical interpretation of the tribological parameter in the field of the load-speed mode of KamAZ engines is given.

Key words: car engine, crankshaft bearings, lubrication mode, tribological parameter, speed and load characteristics

Introduction

One of the movable mates that limit the life of the engine are the crankshaft bearings. They account for about 18% of the number of failures of all elements of the power units of KamAZ vehicles, the average time between failures is 12% of the engine life before overhaul, and the share of repair costs is over 45% [1,2].

Connecting rod and main bearings of the crankshaft of automotive internal combustion engines are fluid friction bearings lubricated under pressure. The external load vector acting on the crankshaft bearings varies not only in magnitude and direction, but also rotates relative to the crankshaft axis at a certain speed. The crankshaft not only rotates, but also moves relative to the bearings, squeezing out the oil. The thickness of the oil layer changes periodically. As the load increases, it decreases. The oil pressure in the supply line practically does not affect the pressure in the oil layer, but to a large extent affects the amount of oil pumped and the thermal state of the bearing [3,4].

The nature of the duration of the existence of the lubricating layer varies depending on the condition of the plain bearing. Therefore, it is fair to assume that such an operational tribological parameter as P_g, on the one hand, is sensitive to the technical condition of the bearing, and, on the other hand, affects the intensity of its wear [5,6].

In practice, when assessing the resource of car engines with identical and different numbers of connecting rod and main bearings of the crankshaft, it is important to identify the effect of various tribological parameters on the lubrication process of mating parts during operation.

Literature review

During the operation of the engine, the conditions for the operation of bearings in the liquid lubrication mode (hydrodynamic friction) must be ensured in the entire range of operating modes for which they are

intended. Under conditions of liquid lubrication, the rubbing surfaces of the mating parts are separated by a continuous layer of lubricant material of considerable thickness, several times greater than the sum of the heights of microroughnesses of the working surfaces. The process of mechanical wear is practically absent, but the processes of fatigue wear, cavitation wear and liquid erosion take place. It is believed that the abrasive action of particles of mechanical impurities contained in engine oil for connecting rod and main bearings is weakened. Oil on its way to the bearings undergoes coarse and fine cleaning in oil filters, as well as in dirt traps located in the crankshaft cavities [7,8].

The contact interaction of friction surfaces occurs during boundary lubrication, when the thickness of the boundary lubricating layer is several molecular layers of lubricant, oriented in the direction of movement of the mating parts, and is commensurate with the sum of the heights of the microroughnesses of the contacting surfaces [9-11].

Boundary lubrication is determined by the properties of boundary lubricating layers arising from the interaction of the material of the rubbing surface and the lubricant as a result of physical adsorption or chemisorption. In this case, the bulk properties of the lubricant do not appear, and the physicochemical interactions on the surfaces determine the nature of friction and wear. With boundary lubrication, molecular-mechanical and corrosion-mechanical types of surface wear are realized. Wear intensity with boundary lubrication is 7-13 orders of magnitude higher than with liquid lubrication [12-14].

Violation of the liquid lubrication occurs when the friction surfaces approach each other so much that in the zones of the highest pressures the oil film breaks and the microroughnesses in the contact spots come into contact. In the case when the load is simultaneously perceived by the oil film and the contact surface irregularities, then this is the mixed lubrication mode.

In the case of the alternate appearance and disappearance of the oil film between the rubbing surfaces, a transient lubrication process occurs. The operation of plain bearings of the crankshaft of automobile engines under the conditions of a transient lubrication process was studied in [18-20]. The intensity of wear during the transitional lubrication process is determined by the ratio of the duration of non-contact and contact types of interactions. It is believed that if the duration of contact between the journal and the bearing is short (no more than 20% of the cycle time), then these critical positions may not be dangerous [21-23].

The transient lubrication process is a general case of interaction of surfaces in lubricated tribocouplings of machine parts. Particular cases are liquid, boundary and mixed types of lubrication, which are considered as steady. At the same time, the dynamic process of transition from one type of lubricant to another is practically not considered.

Steady-state lubrication mode – the work of tribocoupling of parts with constant indicators of the lubrication process over time: minimum thickness of the lubricating layer $h_{\min}$, average temperature of the lubricating layer T_M, friction coefficient f_{mp}, dynamic oil viscosity μ. A consistent set of steady state modes is a static characteristic of the tribocoupling of parts, usually represented as a dependence of process indicators on one of the parameters selected as an independent variable.

The main sign of an unsteady regime is a violation of the condition of constancy of the process indicators in time τ: $h_{\min} = f(\tau)$, $T_M = f(\tau)$, $f_{mp} = f(\tau)$, $\mu = f(\tau)$ etc. Unsteady modes are characterized by cycle average values of indicators that change during the period of transition from one steady state to another. The dynamic characteristic is a time-sequential set of unsteady modes, represented by the dependence of the performance indicators of tribocouplings of parts that change during the transition process [24-25].

Of the variety of transient processes, the most characteristic are the following:

– processes caused by a change in the speed of the v relative movement of the surfaces of tribocouplings of parts. The influencing parameters are the relative change $\delta_v = (v_2 - v_1)/v_H$, the period of change T_v and the nature of the change in speed $v = f(\tau)$;

– processes caused by a change in the external load N on the tribocoupling of parts. The influencing parameters are the relative change $\delta_N = (N_2 - N_1)/N_H$, the period of the change T_N and the nature of the change $N = f(\tau)$;

– processes caused by changes in the properties (eg viscosity) and supply parameters of the lubricant (eg pressure, flow, temperature). The influencing parameters in this case are the relative change of these parameters, the period and nature of the change.

– combined processes, accompanied by the simultaneous impact of changes in speed, load and properties and parameters of the lubricant supply. It is not only the main one in operational conditions, but also the most common case of transients.

The deviation of the lubrication regime from liquid lubrication has a significant effect on the intensification of wear processes. The degree and nature of the deviation are determined by the conditions under

which the transient lubrication process takes place, the degree of adaptation of the bearing to it. This indicates the need to have a unified system for comparative analysis of the lubrication process indicators in various operating conditions, the degree of their adaptation to the latter. When analyzing the quality of lubrication processes in tribo-conjugated parts, it is advisable to use relative indicators – the ratio of the indicator during the transition process to its value under steady-state lubrication modes.

An important indicator characterizing the transitional lubrication process is its duration τ_t. This value is calculated from the moment the lubrication mode is changed until the new mode is established. The last moment is determined by the achievement of stable indicators of the lubrication process, corresponding to the new steady state. In this case, the transitional lubrication process can be both incomplete and completed. The duration parameter of the lubricating layer depends on the time τ: $P_g = f(\tau)$. If the τ_t ratio has been established in the tribo-couplings of the parts over time $P_g \cong 1$, then it is considered that the transient process has ended and the non-contact interaction mode has been established, if $P_g \cong 0$ – the contact interaction mode. If the process has not been established, then it is characterized by average values $\overline{P_g}$ changing during the transition from one steady friction mode to another ($0 < P_g < 1$).

The types of interaction of the rubbing surfaces of the tribocoupling parts are described by the Gersey-Striebeck diagram (Fig. 1), which is the dependence of the friction coefficient f_{mp} on the load-speed mode (N – radial load on the bearing, v – linear velocity of the mating surfaces) and the properties of the lubricant in it (μ – dynamic viscosity).

H. Chihos [24] considers this diagram together with the dependence of the lifetime of the lubricating layer P_g and defines three characteristic areas: I – the area of continuous non-contact interactions – liquid lubrication ($P_g = 1$); II – area of alternating contact-non-contact interaction – transient lubrication process ($0 < P_g < 1$); III – area of continuous contact interactions of surfaces ($P_g = 0$).

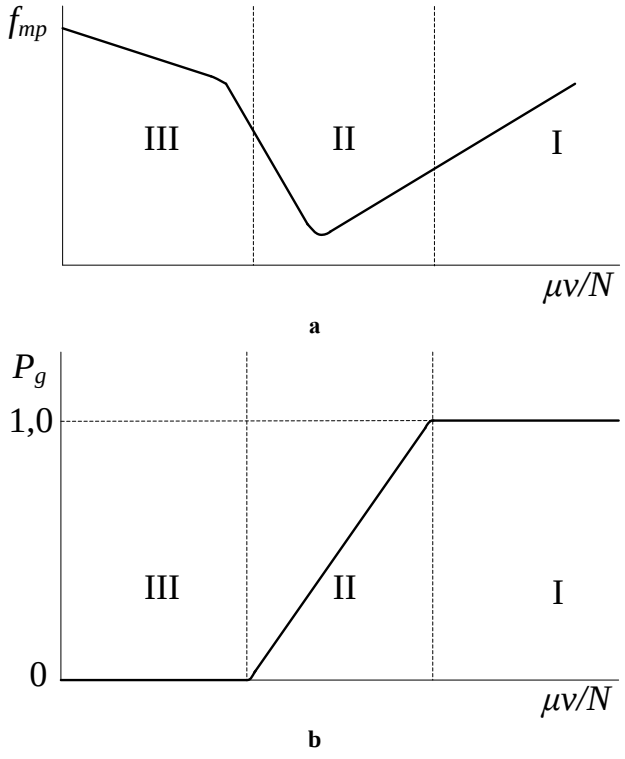

Fig. 1. Combination of the Gersey-Striebeck diagram (a) with the characteristic scheme of parameter change P_g (b).

An analysis of the lubrication process in the crankshaft bearings of automobile engines shows that:

– bearings are designed to operate in a liquid lubrication mode, which ensures minimal wear of the tribological interfaces of parts, however, in real operating conditions they can also operate in other lubrication modes – mixed, boundary, transitional lubrication process, when the wear rate of rubbing surfaces increases significantly;

– the lubrication mode is an important means of influencing the wear processes, and the violation of the liquid lubrication mode has a negative impact on the wear of the tribomechanical system, it is important to determine the conditions for establishing the liquid lubrication mode in the bearing;

– it is advisable to consider the operation of bearings from the standpoint of a transient lubrication process, which is a general case of the interaction of rubbing surfaces of mating parts.

Purpose

The purpose of the work is to substantiate the influence of tribological parameters on the lubrication process of tribocouplings of parts (rod and main bearings of the crankshaft) of the engine.

Results

For a generalized assessment of the lubrication process in the connecting rod and main bearings of the crankshaft, the method of equivalent electrical circuits [7] of automobile engines is used. (fig.2., fig.3) The equivalent electrical circuit is an electrical circuit where voltage is applied to the cylinder block and crankshaft toe, and variable electrical resistances correspond to movable mates in the crank mechanism, cylinder-piston group and gas distribution mechanism . The variability of the resistance is determined by the changing thickness of the lubricating layer with dielectric properties in the contact zone of the tribo-coupling of the parts, depending on the lubrication conditions.

For the implementation of bench tests, a scheme for connecting the electric current to parts of the CPG of diesel engines was proposed (fig. 2).

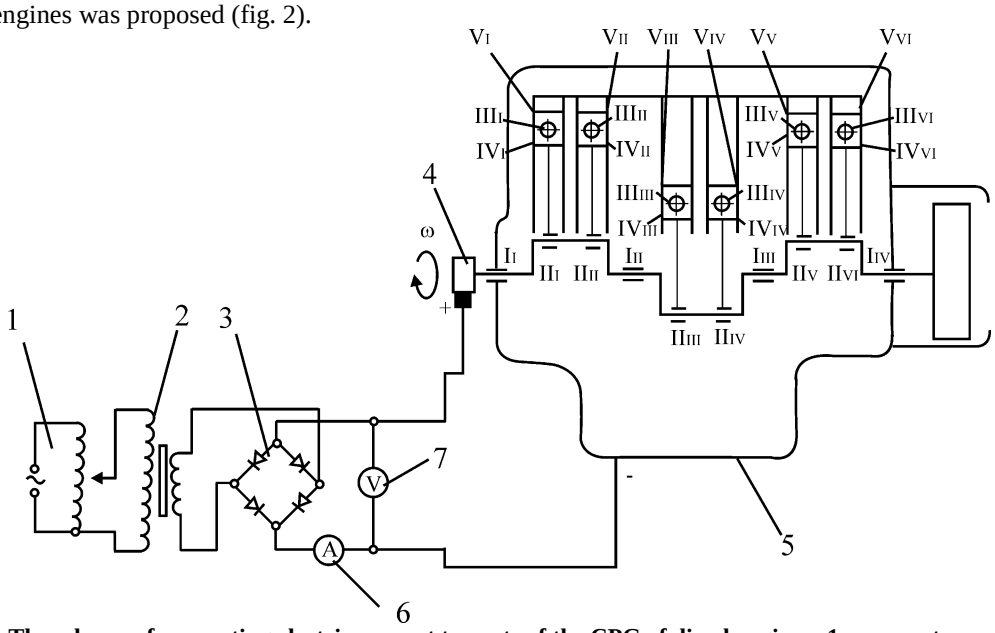

Fig. 2. The scheme of connecting electric current to parts of the CPG of diesel engines: 1 – current source; 2 – resistance for adjusting the current value; 3 – current rectifier; 4 – current collector, screwed in instead of a ratchet; 5 – engine to be run-in; 6 – ammeter; 7 – voltmeter: I – main bearings; II - connecting rod necks of the crankshaft and liners; III – piston fingers and bushings of the upper head of the connecting rods; IV – piston fingers and piston heads; V - cylinder liners, pistons and piston rings.

From the rectifier, electric current is supplied to the "plus" brush unit, and "minus" to the engine block. The brush unit is installed on the side of the oil pump drive pulley, for this it is necessary to unscrew the ratchet and screw in the copper shaft of the brush unit instead. The negative terminal is connected to the cylinder block at the place of attachment of the fuel filter.

The scheme of current distribution through the couplings of the engine (fig. 3) is a system of parallel chains, the first chain is the crankshaft, main bearings, cylinder block; the second chain – crankshaft, CPG, cylinder block. The current branches from the crankshaft to the main sliding bearings (resistance R_1), and through the connecting rods of the crankshaft to the connecting rods (resistance R_2), from the connecting rods to the piston fingers (resistance R_3), from the fingers to the piston heads (resistance R_4) and branches into two branches: from the piston to the sleeve (resistance R_7) and from the piston to the piston rings (resistance R_5) and further from the rings to the sleeve (resistance R_6).

The greatest resistance will be in the first chain (resistance R_1), because when the engine is running, the crankshaft seems to "float" in the oil medium in the main sliding bearings. The electric current will look for the path of least resistance according to Ohm's and Kirchhoff's law, then the largest part of it will pass through the second link - through the parts of the CPG.

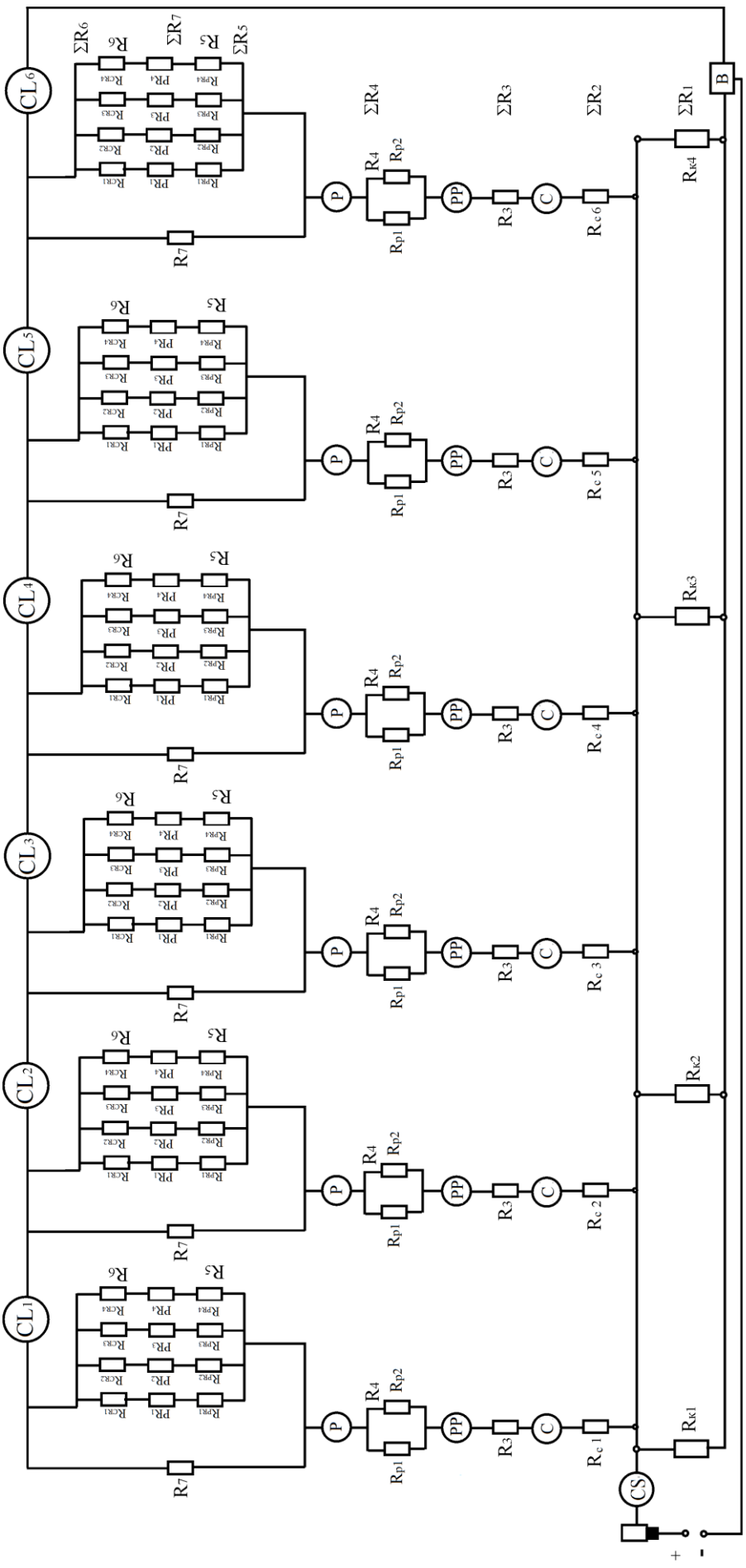

Fig. 3. Scheme of distribution of electric current on the parts of the CPG of diesel engines: CS – crankshaft; B – cylinder block (main bearings); C – connecting rod (connecting rod bushings); PP – piston pin; P – piston (piston heads); PR – piston rings; CL – cylinder liner; R_1 – total resistance between the root neck and the root liners; R_2 – total resistance between the connecting rod neck and connecting rod liners; R_3 – total resistance between the bushing of the upper head of the connecting rod and the piston fingers; R_4 – the total resistance between the piston fingers and the piston heads; R_5 – total resistance between the piston and the ring; R_6 – total resistance between the ring and the sleeve; R_7 is the total resistance between pistons and sleeves.

This is due to the fact that the oil film between the connecting rod neck and the connecting rod liner when the engine is running has a much smaller thickness than that between the main neck and the main slide bearing, that is, it has less resistance. In other elements of CPG parts, the thickness of the oil film is even smaller, since the rings perform a reciprocating movement relative to the mirror of the cylinder liner. Thus, the thickness of the oil film at TDC and TDC of the rings will be minimal to 0.1 μm. At the same time, the mode of marginal friction is observed. The maximum thickness of the oil film will be at the moment when the rings reach the maximum speed and will have a thickness within 10 microns, depending on the oil density. Therefore, the maximum part of the current will pass through the CPG parts when the piston is in the dead center position. At this moment, the current on the parts of the CPG will be distributed almost evenly in the engine, since at the same time the pistons will occupy different positions relative to the sleeve. The difference in the passage of current through the parts of the CPG for one revolution of the crankshaft will be up to 10%.

The resistance between the crankshaft and main bearings is a parallel chain of resistances and is calculated by the expression:

$$\frac{1}{R_1} = \frac{1}{R_{к1}} + \frac{1}{R_{к2}} + \frac{1}{R_{к3}} + \frac{1}{R_{к4}}.$$

Similarly, the total resistance between the crankshaft and connecting rods is calculated:

$$\frac{1}{R_2} = \frac{1}{R_{C1}} + \frac{1}{R_{C2}} + \frac{1}{R_{C3}} + \frac{1}{R_{C4}} + \frac{1}{R_{C5}} + \frac{1}{R_{C6}}.$$

Current and voltage were recorded using an ammeter and a voltmeter, and then the total resistance R was calculated according to Ohm's law $I = \frac{U}{R}$.

In modern automobile engines, there are at least 20...25 types of movable mates, and their total number depends on the design of the engine, and is 100...150 units and more. Lubrication regimes differ significantly from each other and depend on many factors: purpose, load-speed and thermal regimes, lubricant supply conditions, technical condition, etc.

An analysis of equivalent electrical circuits allows us to conclude that the probability of electric current passing between the cylinder block and the crankshaft is determined by the probability of metal contact in the movable mates of the crankshaft. The contact of the mating of bearing parts occurs when the lubricating layer is destroyed, the integral probability of the existence of a lubricating layer in the tribocoupling is equal to:

$$P_g^{\Sigma} = P_g^{tb} P_g^{gdm} P_g^{cgb} \prod_{i=1}^{i=k} P_{g.i}^{mb} \prod_{j=1}^{j=m} P_{g.j}^{ccp}, \quad (1)$$

where P_g^{tb} is the parameter P_g in the thrust main bearing; P_g^{gdm} – parameter P_g in the group of interfaces of parts of the gas distribution mechanism and its drive; P_g^{cgb} - parameter P_g in the group of interfaces of clutch and gearbox parts; $P_{g.i}^{mb}$ – parameter P_g in the *i*-th main bearing; $P_{g.j}^{ccp}$ – parameter P_g in the *j*-th group of the connecting rod bearing and the cylinder-piston group; *k* and *m* are the number of main bearings and groups of mating parts from the connecting rod bearing and the cylinder-piston group, respectively.

The analysis of formula (1) allows us to draw a conclusion about the relationship between the parameter P_g^{Σ} and the parameter values P_g in each group of mating parts. Moreover, if $P_g^{\Sigma} = 1$, then this means the conditions of non-contact interaction in all groups of triboconjugations of parts ($P_g = 1$), if $P_g^{\Sigma} = 0$, then at least one of the groups has metal contact ($P_g = 0$).

The operating conditions of the thrust bearing show that fluid friction predominates in it, and therefore the following condition can be assumed: $P_g^{tb} = 1$.

The conditions for the passage of electric current from the crankshaft to the cylinder block through the drive of the gas distribution mechanism and the gas distribution mechanism itself make it possible to assume that $P_g^{gdm} = 1$.

The parameter P_g^{ccp} can be estimated by the formula:

$$P_g^{ccp} = 1 - (1 - P_g^{cb})(1 - P_g^{ph})(1 - P_g^{pp})^2 (1 - P_g^{pc}), \quad (2)$$

where P_g^{cb}, P_g^{ph}, P_g^{pp}, P_g^{pc} is the parameter P_g in the connecting rod bearing, respectively, of the tribo-couplings of the parts "piston pin-bushing of the piston head of the connecting rod", "piston pin-piston

boss" and "piston-cylinder".

An analysis of formula (2) shows a complex dependence of the parameter P_g^{ccp} on the type of interaction in tribo-couplings of parts. If the parameter is in one of the tribological conjugations of the parts $P_g = 1$, then the values of the parameter P_g in other conjugations do not have a significant effect on the value of P_g^{ccp}.

The operating conditions of the tribocouples "piston pin-piston head sleeve", "piston pin-piston boss" and "piston-cylinder" indicate that they are dominated by boundary friction $P_g = 0$, and therefore the following relationship can be assumed:

$$(1-P_g^{cb})(1-P_g^{pp})^2(1-P_g^{pc}) = 1. \tag{3}$$

Hence it follows that $P_g^{ccp} = P_g^{cb}$. Based on the assumptions made, the P_g^{Σ} operational friction parameter is determined by the formula:

$$P_g^{\Sigma} = \prod_{i=1}^{i=k} P_{g.i}^{mb} \prod_{j=1}^{j=m} P_{g.j}^{cb}, \tag{4}$$

The indicator is P_g^{Σ} used for a comparative assessment of engines with identical numbers of connecting rod and crankshaft main bearings. To evaluate engines with different numbers of bearings, an "equivalent crankshaft bearing" model is proposed, which has a generalized assessment of the lubrication process in connecting rod and main bearings. For quantitative assessment, the parameter is used E_g - "integral degree of existence of the lubricating layer", the value of which is determined by the formula:

$$E_g = \sqrt[k+m]{\prod_{i=1}^{i=k} P_{g.i}^{mb} \prod_{j=1}^{j=m} P_{g.j}^{cb}}. \tag{5}$$

The value of the parameter E_g changes from the maximum value $(E_g)_{\max} = 1$, which characterizes the steady state of liquid lubrication in all crankshaft bearings, to the minimum value $(E_g)_{\max} = 0$, at which at least one bearing operates in the mode of boundary lubrication or dry friction. Intermediate values of the parameter $0 < E_g < 1$take place under the conditions of a transient lubrication process with successive alternation of liquid and boundary lubrication in time.

On fig. 4 shows the dependences of tribological parameters P_g^{Σ} and E_g on the speed of the crankshaft.

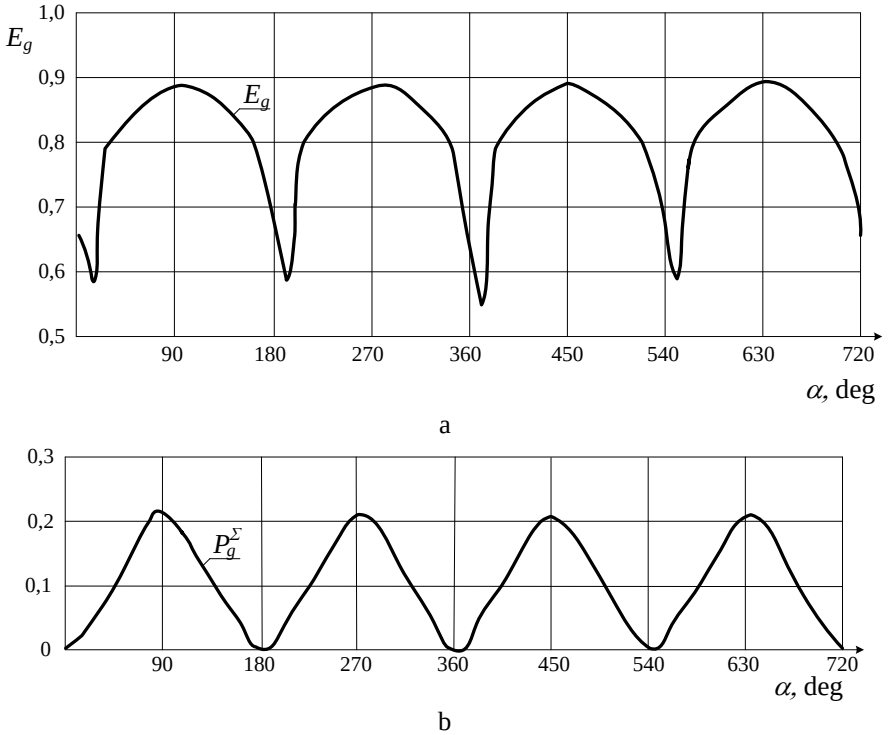

Fig. 4. Scheme of formation of parameters E_g (a) and P_g^{Σ} (b)

It is determined that under operating conditions the value of the parameter E_g depends on a number of factors:

$$E_g = E_g(l_b, d_b, M, n, \mu(T_M), T_{MP}, p_P, h_{кр}, \Delta, ...). \quad (6)$$

The factors involved in the model (6) change according to various patterns:

– bearing length l_b and bearing diameter d_b remain practically unchanged;

– the dynamic viscosity of the oil μ is determined by the viscosity-temperature properties of the oil $\mu(T_M)$ according to SAE, due to the aging of the base base, dilution with fuel, and the operation of additives;

– the crankshaft speed n and torque M vary over a wide range depending on the load and speed modes of the engine;

– the critical thickness of the lubricating layer $h_{кр}$ depends on the roughness and other micro- and macrogeometric parameters of the friction surfaces, is formed initially during manufacture and installation, decreases during running-in, changes insignificantly during the period of steady (normal) wear, and increases during accelerated wear;

– the diametrical clearance Δ is formed during manufacture and installation, increases due to wear of the journals and liners of the crankshaft, both at the running-in stage and during periods of steady (normal) and accelerated wear;

– oil pressure is p_P determined by the design and characteristics of the elements of the main oil line and the lubrication system, increases with increasing crankshaft speed, oil viscosity, and decreases with increasing oil filter contamination, wear of the oil pump and crankshaft bearings, overheating and dilution by fuel;

– the oil temperature T_M depends on the thermal state of the engine parts, the operation of the engine preheating system; in the starting mode during warm-up increases, while driving it depends on the load-speed mode of the engine and on the factors of warming and cooling the engine.

Thus, the integral degree of existence of the lubricating layer E_g in the crankshaft bearings depends on the oil temperature and the load-speed mode, and these dependencies have their own characteristics at the stages of running-in, steady-state (normal) and accelerated wear.

During the running-in of bearings, the factors $h_{кр}$ and are variables Δ.

Under the same factors, the conditions of the load-speed mode of operation, the thermal state of the engine and the properties of the engine oil, the values of the factors M, n, T_{MP} and $\mu(T_M)$ in model (6) are unchanged, which makes it possible to determine the values of the parameter E_g depending on the factors of the technical condition of the bearings using the dependence $E_g = E_g(h_{кр}, \Delta)$.

The operational wear of bearings depends on a variable factor Δ. The validity of diagnosing the crankshaft bearings is determined by the fact that under the same operating modes, the thermal state of the engine and the properties of the engine oil, the values of the parameters M, n, $T_{MП}$, $h_{кр}$ and $\mu(T_M)$ in model (6) are unchanged, and it becomes possible to determine the diametrical clearance using the established dependence $\Delta = \Delta(E_g)$.

When the engine is warming up at idle, the values of the factors Δ and $h_{кр}$, as well as the viscosity-temperature characteristic of the oil $\mu(T_M)$ in model (6) are unchanged, and the factors n, $T_{MП}$ and $p_{П}$ depend on the time τ in the start mode. This allows you to determine the parameter values E_g depending on the values of the crankshaft speed n and oil temperature T_{MP} using the model $E_g = E_g(T_{MP}, n, \tau)$.

When the engine is running, the factors *M* and *n* are variables. With the same thermal and technical conditions of the engine and the properties of engine oil, the values of the parameters T_{MP}, $\mu(T_M)$, Δ and $h_{кр}$ in model (6) are unchanged and it becomes possible to determine the value of the parameter E_g depending on the operating mode factors (M and n) using the model $E_g = E_g(M, n)$.

The basis of experimental studies of the lubrication process in the crankshaft bearings, depending on the load-speed mode of the engine on the stand, is an enlarged model containing input (torque on the crankshaft M, crankshaft speed at idle n) and output (indicator E_g and dependencies $E_g = E_g(M, n)$ and $W_i = W_i(M, n)$ variables.

The test object was the KamAZ-740.14-300 diesel engine, which is used on KamAZ-53212, 43353, 53229, 65115 vehicles, and is identical in design of the lubrication system and crank mechanism with engines

of other modifications KamAZ-740.11-240, 740.13 -260 used on many vehicles. The tests were carried out in the engine testing laboratory of the ERM department. The engine was installed on the stand of the company "AVL" with a hydraulic brake company "SCHENCK". The test engine was run-in, and the operating time at the time of testing was about 1200 moto-hours.

When testing the engine, coolant temperatures were maintained from 80ºC to 85ºC and oil from 75ºC to 80ºC. Steady operating modes were sequentially set at crankshaft speed n = 1000, 1400, 1800, 2200 and 2400 min $^{-1}$ with a stepwise change in torque M at each frequency from 100 to 1000 N·m with a step of 100 N·m.

The measurements were carried out in the forward and reverse directions. The duration of measurement in each mode was 30 s after an exposure of 30 s.

The results of parameter measurements E_g in each operating mode were averaged. The obtained load and speed characteristics of the engine in terms of the parameter E_g made it possible to draw the following conclusions:

– with an increase in the load on the engine at a constant crankshaft speed, the parameter decreases, which indicates a progressive deterioration of the liquid lubrication (fig. 5);

– with an increase in the shaft rotation frequency at a constant torque, the dependence of the parameter has a parabolic form (fig. 6) with a maximum characterizing the best lubrication conditions in the frequency range from 1250 to 1550 min $^{-1}$.

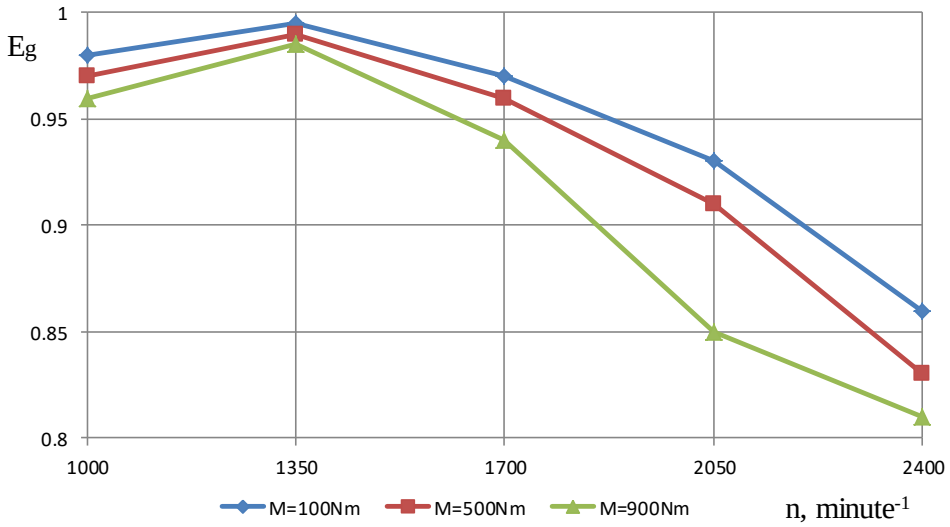

Fig. 5. Motor speed characteristics by parameter E_g (*n*)

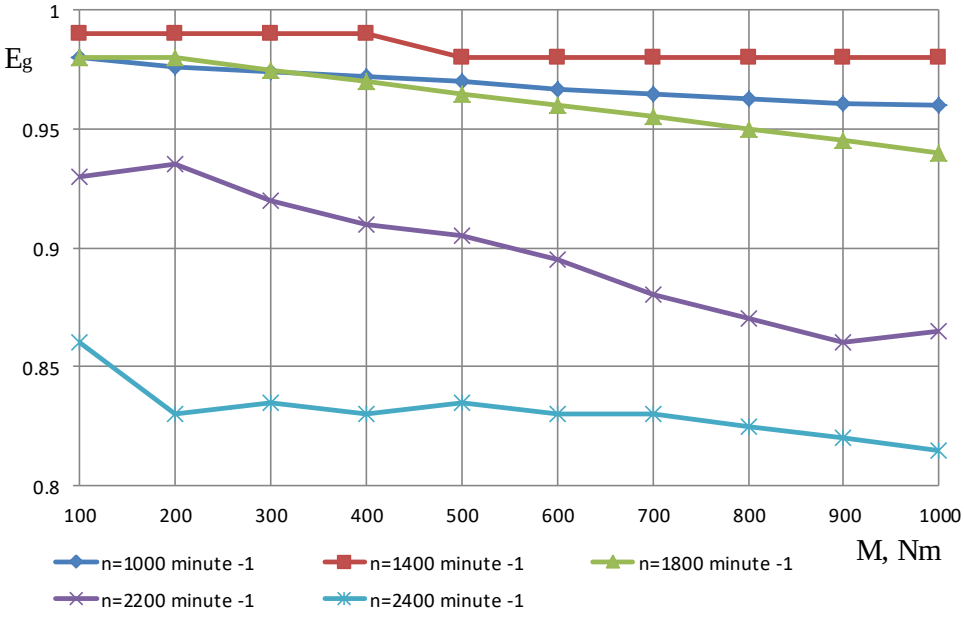

Fig. 6. Engine load characteristics by parameter E_g (*M*)

For further analysis of the lubrication process in KamAZ engines, the values of rotational speed and torque were recalculated into relative values according to the formulas:

$$n_0 = 100(n_x / n_{nom}), \quad (7)$$

$$M_0 = 100(M_x / M_{nom}), \quad (8)$$

where M_0 and n_0 are the relative values of torque and crankshaft speed, %: n_{nom}=2600 min $^{-1}$ and $M_{ном}$=1000 Nm are the maximum absolute values of the indicators.

The experimental data $E_g(M,n)$ were approximated using PC applications, and a polynomial model of the form was obtained:

$$E_g = a + bn_0 + cM_0 + dn_0^2 + eM_0^2 + fn_0M_0, \quad (9)$$

where *a*, *b*, *c*, *d*, *e*, *f* – the coefficients of the model, the values of which are: *a* = 0.6966; *b* = 0.01107; *c* = 0.0004430; *d* = -0.0001012; *e* = -2.2734 10 $^{-6}$; *f* = -9.3841 10 $^{-6}$.

The coefficient of determination of the model was r^2 = 0.974, the standard error was 0.0104, which indicates a sufficient quality of the approximation.

Using model (9), the multifactorial characteristics of the engine were built according to the parameter of the integral degree of existence of the lubricating layer E_g in the crankshaft bearings (fig. 7 and 8).

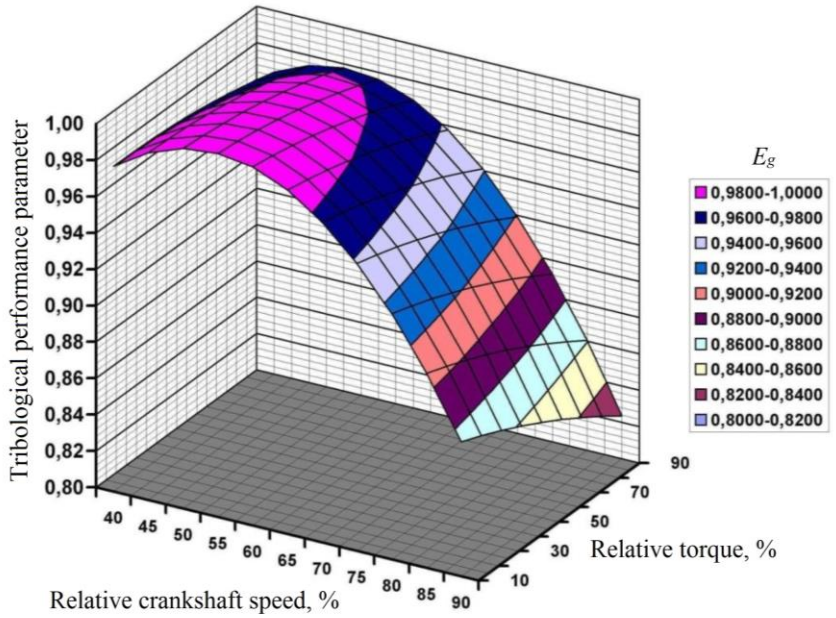

Fig. 7. Graphical interpretation of equation (9) by parameter E_g in the field of load-speed mode of engines of the KamAZ series

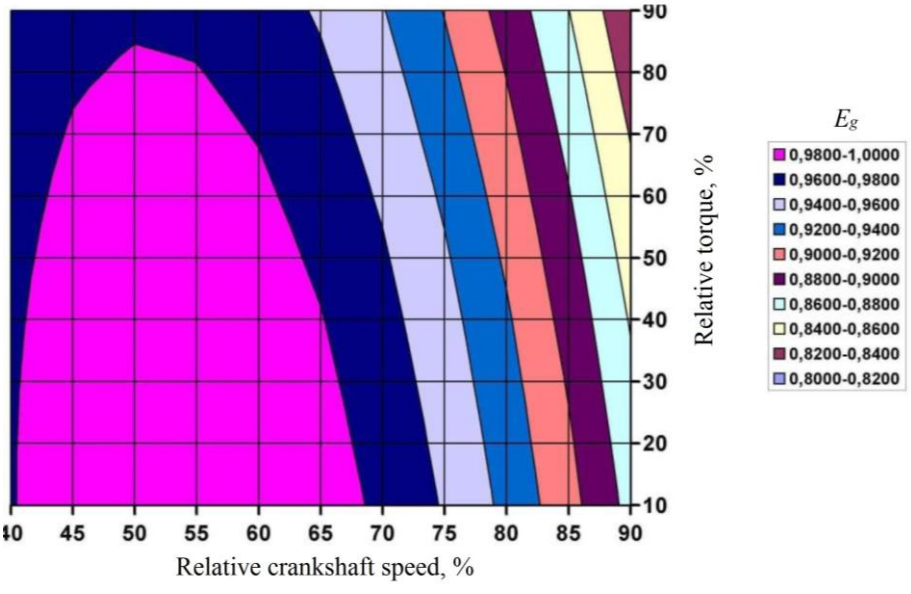

Fig. 8. Areas of parameter levels E_g in the field of the load-speed mode of the KamAZ engine

The analysis of the multifactorial characteristics of the engine by the parameter E_g makes it possible to determine the areas of the load-speed mode of operation, in which the lubrication mode of the crankshaft bearings with different levels of the parameter values is provided E_g. It can be seen that the area of the load-speed mode with a high level of parameter values $E_g \geq 0{,}98$ is: for the crankshaft speed from 40% to 65% and torque from 10% to 50%; crankshaft speed from 45% ... 60% and torque from 50% to 80%.

Model (9) and multifactorial characteristics give an idea of the suitability of the engine to the operating mode in terms of the parameter of the integral degree of existence of the lubricating layer E_g in the crankshaft bearings.

Of practical interest is the assessment of the suitability of the engine to the operating mode in terms of the integral wear resistance W_{I} of the crankshaft bearings. The multifactor characteristic of the engine (fig. 9) shows the distribution of parameter values W_{I} in the areas of the load-speed mode.

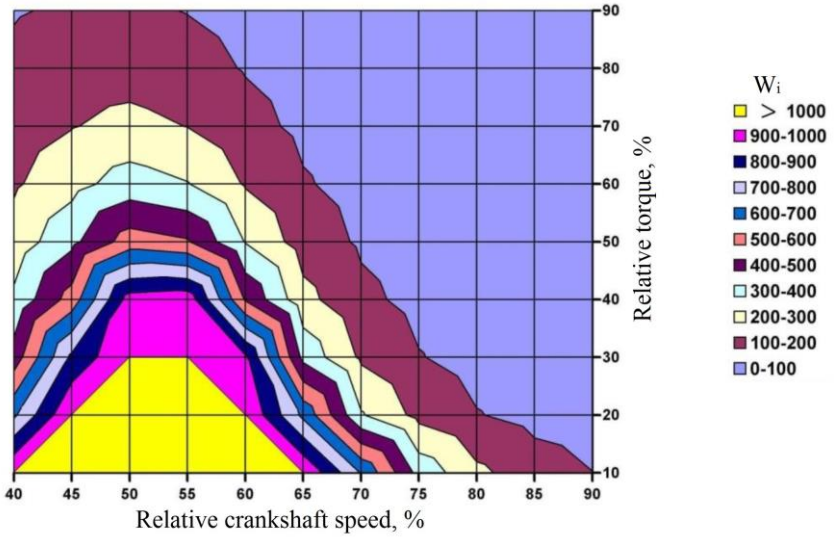

Fig. 9. Multifactorial characteristic of the engine by parameter W_{I} in the areas of load-speed mode

The resulting graphical display shows that: high wear resistance of the crankshaft bearings is $W_{\text{I}} > 1000$ provided in the region of relative speed from 45% to 60% and relative torque from 10% to 30%. As the load-speed mode expands, the relative torque equal to 30% or more and the relative speed of 65% or more reduce the wear resistance of bearings. The speed range of 45% to 60% corresponds to an average piston speed in the range of 4.7 to 6.2 m/s. These values are close to the speed range of 5...7 m/s, which provide "wear-free" speeds of the crankshaft of the engine.

Conclusions

1. A technique has been developed for the experimental study of the lubrication process in the bearings of the crankshaft of an automobile engine during bench tests.

2. The regularities of the parameter of the integral degree of existence of the lubricating layer in the crankshaft bearings from the load-speed mode of operation of the KamAZ-740.14-300 engine have been established, which made it possible to find the regularities of the wear resistance index of the crankshaft bearings also from the load-speed mode of the engine.

3. It was revealed that the maximum wear resistance of the bearings is provided in the region of the relative value of the crankshaft speed from 45% to 60% and the relative value of the torque from 10% to 30%; and it is on average 20...25 times higher compared to wear resistance in other modes; as the load-speed mode expands from a relative torque of 30% and from a relative crankshaft speed of 65%, the wear resistance of the bearings decreases sharply.

References

1. Aulin V.V., Hrynkiv A.V. (2016). Problemy i zadachi efektyvnosti systemy tekhnichnoi ekspluatatsii mobilnoi silskohospodarskoi ta avtotransportnoi tekhniky [Visnyk Zhytomyrskoho derzhavnoho tekhnolohichnoho universytetu. Seriia tekhnichni nauky. №2 (77)]. S.36-41.

2. Priest, M. and C.M. Taylor, 2000. Automobile engine tribology - approaching the surface. [Wear, 241(2)] 193-203.

3. Khruliev O.E., Saraiev O.V. i Saraieva I.Iu. (2021). Vplyv vidtsentrovykh syl na zmashchuvannia

pidshypnykiv kolinchastoho vala v avariinykh rezhymakh roboty dvyhuna avtomobilia. [Visnyk mashynobuduvannia ta transportu. 12, 2]. S.112–121.

4. Saraieva I.Iu., Khruliev, O.E. i Vorobiov, O.M. (2021). Ekspertna otsinka tekhnichnoho stanu tsylindro-porshnevoi hrupy dvyhuna avtomobilia [Visnyk mashynobuduvannia ta transportu. 13, 1] S.133–139.

5. Aulin V.V., Dykha O.V., Lysenko S.V., Hrynkiv A.V. (2018). Vplyv ekspluatatsiinykh faktoriv na rezhym zmashchuvannia i znosostiikist detalei dyzelnykh dvyhuniv avtomobiliv [Problems of tribology. №4] S.41-53.

6. Stelmakh O., Fu H., Guo Y., Wang X., Zhang H., & Dykha, O. (2022). Adhesion-Deformation-Hydrodynamic model of friction and wear [Problems of Tribology, 27(3/105)] S.49–54.

7. Aulin V.V. [ta in.] (2016). Trybofizychni osnovy pidvyshchennia nadiinosti mobilnoi silskohospodarskoi ta avtotransportnoi tekhniky tekhnolohiiamy trybotekhnichnoho vidnovlennia: monohrafiia [Kropyvnytskyi : Lysenko V. F.] 303 s.

8. Kuzmenko A. H., Dykha O.V. (2005). Doslidzhennia znosokontaktnoi vzaiemodii zmashchenykh poverkhon tertia : monohrafiia [Khmelnytskyi : KhNU] 184 s.

9. Kuzmenko A.G., Dyiha A.V. (2007). Kontakt, trenie i iznos smazannyih poverhnostey : monografiya [Hmelnitskiy: HNU] 342 s.

10. Kuzmenko A.G., Dyiha A.V., Babak O.P. (2011). Kontaktnaya mehanika i iznosostoykost smazannyih tribosistem: monografiya. [Hmelnitskiy: HNU] 248 s.

11. Dykha O.V., Sorokatyi R.V., Babak O.P. (2011). Rozrakhunky ta vyprobuvannia na nadiinist mashyn i konstruktsii : navch. posib. [Khmelnytskyi: KhNU] 151 s.

12. Shayler P.J., Baylis W.S., Murphy M. (2002). Main bearing friction and thermal interaction during the early seconds of cold engine operation [Presented at ASME 2002 internal combustion engine division fall technical conference, New Orleans, USA].

13. Zammit, J-P., Shayler P.J., Gardiner R., Pegg I. (2012). Investigating the potential to reduce crankshaft main bearing friction during engine warm-up by raising oil feed temperature [SAE Int J Engines 2012; 5(3) paper 2012-01-1216].

14. Hudz, H. S., Herys, M. I., Kotsiumbas, O. Y., & Ostashuk, M. M. (2022). Vplyv pokaznykiv olyvy v avtomobilnomu dvyhuni na temperatury vkladok pidshypnykiv kolinchastoho vala. [Naukovyi visnyk NLTU Ukrainy, 32(3)] S. 66-72.

15. Dykha O. V. (2018). Rozrakhunky trybotekhnichnoi nadiinosti pidshypnykiv kovzannia. [Tekhnichnyi servis ahropromyslovoho, lisovoho ta transportnoho kompleksiv. № 13] S. 20-26.

16. Aulin V.V., Hrynkiv A.V., Holub D.V., Ahaponenko M.I. (2018). Rozrobka kryteriiu vdoskonalennia systemy tekhnichnoi ekspluatatsii zasobiv transportu z vrakhuvanniam neobkhidnoi diahnostychnoi informatsii [Mizhvuzivskyi zbirnyk "Naukovi notatky". – Lutsk: Lutskyi NTU №62] S.17-20.

17. Hrynkiv, A., Rogovskii, I., Aulin, V., Lysenko, S., Titova, L., Zagurskiy, O., Kolosok, I. (2020). Development of a system for determining the informativeness of the diagnosing parameters for a cylinder-piston group in the diesel engine during operation [Eastern-European Journal of Enterprise Technologies, 3 (5-105)] pp. 19-29.

18. Podoliak O.S., Malinina Yu.V. (2015). Doslidzhennia znoshuvanosti dvyhuniv vnutrishnoho zghoriannia pry ekspluatatsiinykh rezhymakh roboty [Mashynobuduvannia No16] S. 30-33.

19. Podolyak O. S., Melnichenko A. A. (2008). Issledovanie modeli izmeneniya resursa silovogo agregata avtomobilnogo krana metodom iteratsii [Vostochno-evropeyskiy zhurnal peredovyih tehnologiy. Vyip. 6 (36)] S. 27–30.

20. Moschenok V.I., Glushkova D.B., Nesterenko E.A. (2007). Tehnologicheskie metodyi povyisheniya rabotosposobnosti podshipnikov [Visnyk Kharkivskoho natsionalnoho avtomobilno-dorozhnoho universytetu №38] S. 54-56.

21. Ronen S., Goltsberg R., Etsion I. (2017). A comparison of stick and slip contact conditions for a coated sphere compressed by a rigid flat. [Friction 5(3)]. S. 326–338.

22. Balytskyi O. I., Kolesnikov V. O., Khmel Ya., Lopatkin I. O., Cherniakhov P. I. (2016). Doslidzhennia znosostiikosti materialiv dlia detalei transportu [Problemy ta perspektyvy rozvytku avtomobilnoho transportu : Materialy IV-yi Mizhnarodnoi naukovotekhnichnoi internet-konferentsii. Vinnytsia] S. 60-64.

23. Voytov V.A., Stadnichenko N.G. (2005). Tehnologii tribotehnicheskogo vosstanovleniya. Obzor i analiz perspektiv [Problemyi tribologii N 2] S. 86 - 93.

24. Chihos H. (1982). Sistemnyiy analiz v tribonike [Per. s angl. S.A. Harlamova. – M.: Mir] 352 s.

25. Dykha O.V. (2013). Vuzly tertia mashyn. Rozrakhunky na znosostiikist: navch. posib. [Khmelnytskyi : KhNU] 147 s.

Аулін В.В., Лисенко С.В., Гриньків А.В., Ляшук О.Л., Гупка А.Б., Лівіцький О.М. Параметри мастильного процесу при експлуатаційному зношуванні підшипників колінчастого валу автомобільних двигунів

У статті розглядається динаміка мастильного процесу при експлуатаційному зношуванні підшипників колінчастого валу автомобільних двигунів. Проаналізовано всі режими змащення та процеси зношування. Основна увага приділена режимам змащення підшипників колінчастого валу, що встановився і не встановився. Характер динаміки зміни режимів змащення обґрунтовується через експлуатаційні трибологічні параметри, які характеризують інтегральний ступінь існування мастильного шару. Запропоновано модель зв'язку цих параметрів з цілого ряду факторів, а також обґрунтовано характер їх змін із зміною частоти обертання колінчастого валу двигуна автомобіля.

Наведено результати стендових випробувань дизелів серії КамАЗ, швидкісних та навантажувальних характеристик двигуна за трибологічними експлуатаційними параметрами. Дано графічну інтерпретацію трибологічного параметра в полі навантажувально-швидкісного режиму двигунів серії КамАЗ.

Ключові слова: автомобільний двигун, підшипники колінчастого валу, режим змащення, трибологічний параметр, швидкісні та навантажувальні характеристики